UNIVERSIDAD MAYOR
para espíritus emprendedores

Vicerrectoría de Investigación
DOCTORADO EN NEUROBIOLOGÍA

H3K9ME3 DECREASE PREVENTS THE AGE-ASSOCIATED DECLINE IN OLFACTORY FUNCTION THROUGH MAINTENANCE OF THE MITOCHONDRIAL UNFOLDED PROTEIN RESPONSE CAPACITY IN *DROSOPHILA*.

Thesis submitted to the Universidad Mayor in fulfillment of the criteria to qualify for Doctor of Philosophy in Neurobiology.

FRANCISCO MUÑOZ-CARVAJAL Ph.D (c).

Thesis director: Felipe Court P.hD.

Thesis co-director: Mario Sanhueza P.hD,

November 29, 2022

2. Doctoral Thesis Defense Certificate.

Ph.D candidate: Francisco Muñoz Carvajal

Date: November, 29. 2022.

Thesis commission members: **Signature:**

1. Dr. Claudio Hetz (External) _____

2. Dra. Ute Woehlbier (Internal) _____

3. Dr. Julio Cesar Cárdenas (Internal) _____

4. Dr. Felipe Court (Director) _____

5. Dr. Mario Sanhueza (Co-director) _____

6. Dra. Melissa Calegaro N (President) _____

7. Dr. René Vidal (PhD Program Director) _____

3. Topic Index.

4. Figure Index.

5. Abbreviations

A53T: α Synuclein mutation A53T

ABCB10: ATP Binding Cassette B 10

AD: Alzheimer's Disease

AKT: Serine Threonine Kinase

AL: Antennal Lobe

ALS: Amyotrophic lateral sclerosis

APP: Amyloid precursor protein

ATF5: Activated Transcription Factor 5

ATP: Adenosine Triphosphate

AUC: Area Under the Curve Score

Aβ: Amyloid-β

BAZ2: Bromodomain Adjacent To Zinc Finger Domain 2B

BCA: Bicinchoninic acid

BDNF: Brain-derived neurotrophic factor

BDSC: Bloomington *Drosophila* Stock Center

CHOP: C/EBP homologous protein-10

CO2: Carbon Dioxide

COX: Cytochrome c oxidase

Crc: Cryptochepal (UPR^{MT} activator)

DAM: *Drosophila* Activity Monitor

dve: Defective proventriculus

$EH^{MT}1$: Euchromatic histone-lysine N-methyltransferase 1

$EH^{MT}2$: Euchromatic histone-lysine N-methyltransferase 2

ER: Endoplasmic reticulum

ETC: Electron Transport Chain

GFP: Green Fluorescent Protein

H2A: Histone 2 A

H3: Histone 3

H3K27: Histone 3 Lysine 27

H3K9: Histone 3 Lysine 9

H3K9ME3: Histone 3 Lysine 9 Trimethylated

HTRA2: Serine Protease 2

IMS: Inner Membrane Space

KDM2: Lysine demethylase 2

JMJC: Demethylase Jumonji C Domain

LH: Lateral Horn

Me: Methyl/Monomethyl

Me2: Dimethyl

Me3: Trimethyl

mPTP: mitochondrial permeability transition pore

MPTP: 1-methyl-4-phenyl-1,2,3,6-tetrahydropyridine

MRI: Magnetic Resonance Imaging

^{MT}DNA: Mitochondrial DNA

OPN: Olfactory Projection Neurons

OXPHOS: Oxidative Phosphorylation

PD: Parkinson's Disease

PGAM5: PGAM Family Member 5, Mitochondrial Serine/Threonine Protein Phosphatase

PGC: Peroxisome proliferator-activated receptor-gamma coactivator (PGC)-1alph

PINK1: PTEN-induced kinase 1

PITRM1: Pitrilysin Metallopeptidase 1

ROS: Reactive Oxygen Species

SDS: Sodium dodecyl sulfate

SER: Smooth endoplasmic reticulum

SET: Methyltransferase Domain Su (var)3-9, Enhancer-of-zeste and Trithorax

SIRT3: Sirtuin 3

SOD: Super Oxide Dismutase

SOD1G93A: Super Oxide Dismutase in G93A

TCA-Cycle: tricarboxylic acid cycle

TRIP: Transgenic RNAi Project

UAS: Upstream Activation Sequence

Ubl: Ubiquitin-like protein 5 (UPR^{MT} activator)

UPR^{ER}: Endoplasmic reticulum unfolded protein response

UPR^{MT}: Mitochondrial unfolded protein response.

UTX: Lysine Demethylase 6 linked to the X chromosome

6. Resume.

Aging is one of the main risk factors for the onset and severity of neurodegenerative diseases. Progressive accumulation of dysfunctional mitochondria is particularly harmful in post-mitotic cells such as neurons, contributing to aging phenotypes including neurodegeneration. The mitochondrial unfolded protein response (UPR^{MT}) is a stress-triggered cellular mechanism to cope with mitochondrial dysfunction and is associated with the transcriptional activation of speficic mitochondrial chaperones, proteases and antioxidant enzymes. The activation of the UPR^{MT} requires an open chromatin state characterized by the dimethylation of H3K9. In contrast, age-associated trimethylated H3K9 generates a closed chromatin state that impairs the transcriptional activation of the UPR^{MT}. Whether the decline in the adaptive capacity of the UPR^{MT} caused by age-associated H3K9 trimethylation contributes to neurodegeneration and impairment of nervous system function has just begun to be elucidated. Here, using *Drosophila melanogaster,* we demonstrate that the age-associated functional decline of olfactory function is associated with an increase in H3K9 trimethylation and a decrease in UPR^{MT} activation in olfactory neurons, leading to mitochondrial dysfunction and neurodegeneration. Remarkably, reducing H3K9Me3 levels by knockdown of the methyltransferase dSetdb1 in olfactory neurons of aged organisms enhances the response capacity of the UPR^{MT}, ameliorating age-associated neurodegeneration and mitochondrial abnormalities, and rescuing the decrease in olfactory function. In addition, downregulation of the UPR^{MT} transcriptional modulators in young flies mirrored the impaired functional phenotype observed in aged animals. This data demonstrates that the UPR^{MT} acts as a hormetic surveillance pathway regulating mitochondrial homeostasis and function in olfactory projection neurons. Significantly, this stress-response pathway is epigenetically regulated and contributes to the age-associated loss of neuronal function.

7. Introduction.

7.1. Aging.

Aging is defined as the time-dependent functional deterioration that increases susceptibility to various forms of stress and finally results in the organism's demise (Pessin et al., 2014). The repercussions of aging are most severe for organs made primarily of post-mitotic cells, such as heart and brain. Greater life expectancy is a substantial risk factor for the emergence of neurodegenerative illnesses and the overall loss of fitness, as seen by the distinctive sensorimotor and cognitive declines associated with human aging (Schroeder and Salthouse, 2004). Age-related degradation suggests that the brain undergoes time-dependent repressive changes that impede its optimal function, as indicated by functional MRI studies of normal human aging, in which the brain displays atrophy (Haug, 1978; Gur et al., 1991; Wang et al., 2017). In an effort to intervene and prevent aging, new studies on aging have created crucial concerns about the physiological factors that induce tissue damage along aging, the compensatory cellular responses that restore homeostasis after the damage, and the interaction between these two processes. Recent research on aging has identified seven cellular hallmarks of aging, each of which meets three main criteria: it must manifest in normal aging, its experimental aggravation must accelerate aging, and its experimental amelioration must delay the normal aging process and, thus, increase healthy lifespan (Pessin et al., 2014). These hallmarks of aging include regeneration, proteostasis, macromolecular damage, epigenetic alterations, and adaptations to stress (López-Otín et al., 2013). Multiple lines of research have demonstrated that mitochondrial dysfunction contributes considerably to the aging process and affects tissues across the organism, suggesting that mitochondrial dysfunction is a common component connecting multiple of these hallmarks. It has been recognized that aging in model organisms is accompanied by a decrease in mitochondrial function, contributing to the age-related decline in tissue function (Chistiakov et al., 2014; Kim et al., 2018). Indeed, aging is the major risk factor for the onset of neurodegenerative diseases. Thus, maintaining mitochondria function is indispensable to prevent the accumulation of cellular damage and age-associated diseases. Therefore, mitochondrial quality control mechanisms are prime candidates for understanding the onset of age-related disorders and developing potential therapies.

7.2 Mitochondria as a regulator of aging-causing damage.

Mitochondria are the primary generators of energy within the cell. Mitochondria produce ATP through oxidative phosphorylation (OXPHOS), a metabolic pathway that coordinates the breakdown of fatty acids and glucose. In addition to being the energy source for the entire organism, mitochondria are also responsible for regulating many pathways of intermediate metabolism, which allows them to manage the levels of a wide variety of essential metabolites for various cellular processes (Nunnari and Suomalainen, 2012). Only 37 genes, two ribosomal RNAs, 22 transfer RNAs, and 13 proteins are part of the mitochondrial OXPHOS complexes encoded in the mitochondrial DNA (Wallace et al., 2014). Click or tap here to enter text.The rest of the 6000 proteins located in the mitochondria are encoded in the nuclear genome. Mitochondrial function depends on the coordination of nuclear and mitochondrial genomes; indeed, transcription and translation of both genomes are coregulated. Coregulation is especially evident for the OXPHOS complexes, composed of stoichiometrically-assembled protein subunits encoded in the nuclear and mitochondrial genome (Couvillion et al., 2016). Anterograde regulation (from mitochondria to nuclei) promotes mitochondrial biogenesis and regulates mitochondrial activity to match cellular demands (Cui et al., 2006; Kaarniranta et al., 2018). However, mitochondria can regulate metabolism due to a retrograde mechanism of communication that enables them to affect the expression of nuclear genes. This mechanism involves signals from mitochondria to the nucleus and allow mitochondria to control metabolism. These bidirectional mechanisms of communication help to stabilize a gene network responsible for cellular homeostasis and regulate how the cell responds to different types of mitochondrial stressors (Quirós et al., 2016; Matilainen et al., 2017; Bárcena et al., 2018). Therefore, the mitochondrial stress response against the different forms of damage contributing to the aging process could represent the link between adaptation to stress and the other hallmarks of aging.

7.3 The mitochondrial Unfolded protein response (UPR^{MT}).

The mitochondrial unfolded protein response (UPR^{MT}), one of the mitochondrial quality control pathways, is activated to recover homeostasis during mitochondrial dysfunction, such as ETC impairments, impaired mitochondrial dynamics, or accumulated unfolded proteins within the mitochondrial matrix (Zhao et al., 2002; Pimenta de Castro et al., 2012; Runkel et

al., 2013). In the mitochondria, the homeostasis of the protein folding environment is constantly challenged by reactive oxygen species (ROS) and deficits in the functioning of the electron transport chain. These challenges can induce unfolded protein stress sensed in an organelle-specific manner. In contrast to the endoplasmic reticulum UPR (UPR^{ER}), the mechanisms underlying the UPR^{MT} are poorly understood. UPR^{MT} was observed originally in mammalian cells, where mitochondrial stress was induced by $_{mt}$DNA deletions (Martinus et al., 1996) and by aggregation of mutant ornithine transcarboxylase (ΔOTC)(Zhao et al., 2002). Both stimuli upregulated the expression of mitochondrial chaperones Hsp60 and Hsp10 under the control of the transcription factor CHOP (Aldridge et al., 2007; Horibe and Hoogenraad, 2007). Already known UPR^{MT} activators include impairments of Electron Transport Chain (ETC), altered mitochondrial dynamics, accumulated unfolded proteins within the mitochondrial matrix (Zhao et al., 2002; Pimenta de Castro et al., 2012; Runkel et al., 2013), $_{mt}$DNA deletions, inhibition of mitochondrial chaperones or proteases, OXPHOS impairments, and increased reactive oxygen species (ROS) levels (Yoneda et al., 2004; Nargund et al., 2012, 2015; Schulz and Haynes, 2015; Lin and Haynes, 2016; Qureshi et al., 2017).

Three nuclear components were identified in *C. elegans* as UPR^{MT} regulators: ATFS-1, *DVE*-1, and UBL-5. ATFS-1, a leucine zipper protein, carries a nuclear localization sequence and a mitochondrial targeting sequence. These transcriptional activators compose the now to known as UPR^{MT}-ATF5 axis (Deng and Haynes, 2017; Fiorese et al., 2015). Under mitochondrial stress, the continuous transport of ATFS-1 towards mitochondria is blocked, translocating to the nucleus where it interacts with *DVE*-1 and UBL-5 (Nargund et al., 2012, 2015). *DVE*-1 is a DNA binding protein that, together with its coregulator UBL-5, interacts with chromatin regions to maintain an ATFS-1-dependent active transcription of UPR^{MT}-related genes (Benedetti et al., 2006; Haynes et al., 2007; Tian et al., 2016). The coordinated action of these three proteins upregulates the expression of specific mitochondrial chaperones hsp-60, hsp-6, and the mitochondrial protease clpp-1 (Haynes and Ron, 2010). In mammals, the CHOP target ATF5 was identified as the functional ortholog for ATFS-1, which also contains targeting sequences for mitochondria and nuclei (Teske et al., 2013; Fiorese et al., 2016; Deng and Haynes, 2017). The ATFS-1/ATF5 dependent response, also referred to as

the UPR^{MT}-ATF5 axis, is the most characterized UPR^{MT} pathway (Papa and Germain, 2011, 2014; Mouchiroud et al., 2013; Riar et al., 2017; Gomez and Germain, 2019; Ji et al., 2020).

Two other pathways have been associated with this stress response. Following the accumulation of proteins in the mitochondrial intermembranous space, the UPR^{MT}-ERα axis, a pathway dependent on the activation of the estrogen receptor α (ERα), was described.(Papa and Germain, 2011). Accumulattion of proteins in the IMS, additionally increase mitochondrial ROS production and trigger the phosphorylation of the protein kinase AKT and, consequently, the activation of ERα. After ERα activation the transcription of protease HTRA2 and the mitochondrial biogenesis regulator NFR1 are upregulated, which translates into an increased proteasome activity, which is independent of the UPR^{MT}-ATF5 axis (Papa and Germain, 2011). Finally, the UPR^{MT}-SIRT3 axis is based on the activation of Sirtuin 3 by increased levels of mitochondrial ROS production. When proteotoxic stress cannot be resolved increased levels of mitochondrial ROS are unavoidable, in this escanerio SIRT3 is required for FOXO3A activity which in turn modulates the expression of antioxidant machinery SOD1, SOD2, and catalase (Chen et al., 2011; Papa and Germain, 2014; Kenny and Germain, 2017; Kenny et al., 2017). The UPR^{MT}-SIRT3 axis has been characterized in worms and mammalian cells, supporting the high evolutionary conservation of the pathway (Mouchiroud et al., 2013). Notably, ERα and SIRT3 UPR^{MT} axes work independently of CHOP (Papa and Germain, 2011, 2014), upholding the idea of three parallel paths coordinating the mitochondrial quality control through stress responses .

Chromatin remodeling has been shown to play a central role in UPR^{MT} epigenetic regulation. Histone 3 is a target for methylation catalyzed specifically by methyltransferase MET-2 in *C.elegans* (ortholog of human SETDB1). Activation of UPR^{MT} requires the dimethylation of lysine 3 of histone 3 (H3K9), which translates into a compacted and overall silenced chromatin state. At the same time, other chromatin portions remain loose, favoring the binding of UPR^{MT} regulators such as *DVE*-1 (Tian et al., 2016). Also required for UPR^{MT} activation are the conserved demethylases JMJD-3.1 and JMJD-1.2, which reduce the chromatin compaction removing methylation from H3K9 and H3K27 (Merkwirth et al., 2016; Sobue et al., 2017). Interestingly, chromatin remodeling acts independently of ATFS-

1, as its downregulation does not affect the nuclear localization of *DVE* (Merkwirth et al., 2016; Tian et al., 2016). All described pathways composed the relatively new mitochondrial stress response known as UPR^{MT}, which is ssummarized in Figure 1.

Activation of the UPR^{MT} also promotes an increase in glycolysis and amino acid catabolism genes together with the repression of TCA-cycle and OXPHOS encoding genes, probably to relieve mitochondrial stress by repairing and recovering defective mitochondria, promoting cell survival (Nargund et al., 2015). It is not clear whether UPR^{MT} can activate other forms of mitochondrial quality control, such as stimulating mitochondrial fission or the elimination of damaged mitochondria through mitophagy; however, activation of mitophagy can occur under the same stimuli as UPR^{MT} (Nargund et al., 2012; Jin and Youle, 2013; Runkel et al., 2013; Burbulla et al., 2014; Lin et al., 2016).

Unlike other cells, damaged neurons are rarely replaced through lifespan and are more prone to the accumulation of malfunctioning mitochondria (Terman et al., 2009). The relationship between the molecular mechanism that regulates the UPR^{MT} and the functional decay of neurons during aging is poorly understood. UPR^{MT} as a hormetic surveillance pathway has been observed when mitochondrial stressors such as paraquat, rotenone, or antamicyn are presented in low doses to animals (Yoneda et al., 2004; Runkel et al., 2013). Mitochondrial function decline is a hallmark of aging (López-Otín et al., 2013) and multiple studies suggest that increased UPR^{MT} activation can prolong or recover mitochondrial function in various tissues and promote longevity (Jensen et al., 2017). Thus, this pathway has an underlying potential for promoting healthy cellular homeostasis, especially in response to environmental or genetic challenges.

On the other hand, experimental evidence indicates a potential toxic role for the UPR^{MT}, which shortens lifespan and promotes de accumulation of malfunctioning mitochondria (Martinez et al., 2017). Recently, it has been reported that the overactivation of the UPR^{MT} by expressing an active form of *ATFS-1* in worm's dopaminergic neurons can lead to cell death in aged animals, an effect that was increased by the overexpression of mutated α-synuclein A53T (Martinez et al., 2017). These studies show that the duality of UPR^{MT} needs more investigation on cellular health (which, in an activated state, is beneficial, but surpassed a certain threshold, it triggers cell death), especially in diseases with a strong involvement

with mitochondrial dysfunction where there is no knowledge of how the overactivation of this pathway would affect already damaged neurons. Therefore, understanding how the regulation of UPR^{MT} in neurons will affect achieving healthy aging is still unclear.

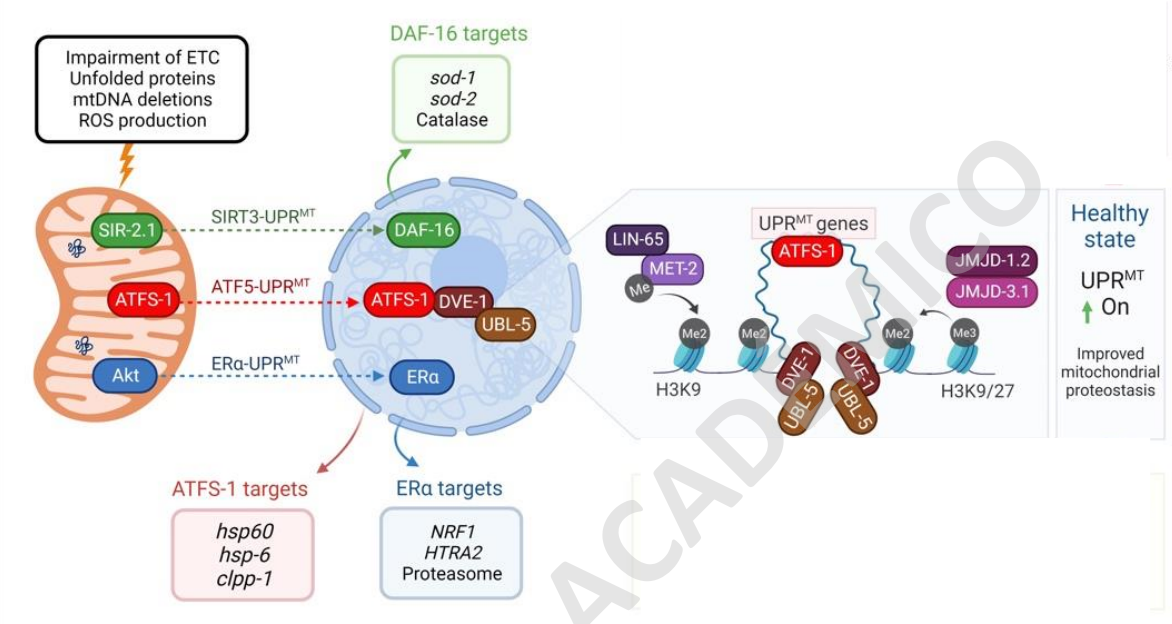

[Muñoz-Carvajal., 2020]

Figure 1. Mitochondrial unfolded protein response (UPR) and its regulation. Insults to mitochondria (top left) activate three different axes of the UPR^{MT} program. The SIRT3-UPR^{MT} axis (green arrow) increases the transcription of superoxide dismutases and catalase after the activation of DAF-16/FOXO3 by the deacetylase SIR-2.1/SIRT3. In the ATF5-UPR^{MT} axis (red arrow), the transcription factor ATFS-1/ATF5 relocalizes from mitochondria to the nucleus to upregulate mitochondrial proteostasis-related genes (red box) after the interaction with the chromatin stabilizers DVE-1 and UBL-5. In the ERα-UPR^{MT} axis (blue arrow), the estrogen receptor is activated by the kinase Akt to increase the expression of the protease HTRA2 and mitochondrial biogenesis regulator NRF1. In a healthy state (center right), ATF5-UPR^{MT} activation requires chromatin reorganization. Dimethylation of Histone 3 by MET-2, and the presence of demethylases JMJD-1.2 and JMJD-3.1, allow the binding of DVE to facilitate the ATFS-1-dependent expression of UPR^{MT} genes and improve mitochondrial proteostasis. In neurodegenerative states triggered by accumulation of Aβ42 (AD), α-syn (PD) ,or SOD1G93A (ALS, top right), UPR^{MT} could be persistently activated, affecting mitochondria proteostasis and neuron viability. In aging cells (bottom right), Histone 3 is preferentially trimethylated, which blocks DVE and ATFS-1 binding to compacted DNA. Lack of expression of UPR^{MT}-related genes decreases mitochondrial response to aging-causing damage. All protein names are taken from C. elegans, except the ones from the ERα axis, which has only been described in mammalian cells. Figure adapted from Muñoz-Carvajal., 2020.

7.4 The role and regulation of UPR^{MT} in aging.

Evidence indicates that mitochondrial dysfunction is a common factor for these events, suggesting a potential role of mitochondrial reparative machinery in aging progression. Furthermore, it is accepted that aging in model organisms is functionally associated with mitochondrial decline, contributing to time-dependent tissue malfunction (Chistiakov et al., 2014; Kim et al., 2018). Therefore, activation of UPR^{MT}, one of the mitochondrial mechanisms against other aging-causing damage, could partially be bridging the adaptation to stress and other pillars of aging as proteostasis and epigenetics (Quirós et al., 2016). Current evidence highlights an age-dependent effect of UPR^{MT} on lifespan. Activation of UPR^{MT} triggered by the downregulation of ETC complexes I and IV promotes longevity (Dillin et al., 2002; Durieux et al., 2011; Mouchiroud et al., 2013). Histone demethylases JMJD-1.2 and JMJD-3.1 mediate in part that extension, as their overexpression is sufficient to extend the lifespan of worms (Merkwirth et al., 2016)On the other hand, reducing the expression of nuclear effectors ATFS-1, UBL-5, and DVE-1, or demethylases JMJD-1.2 and JMJD-3.1, suppress the lifespan extension (Durieux et al., 2011; Houtkooper et al., 2013; Merkwirth et al., 2016; Cooper et al., 2017; Lan et al., 2019) It is interesting that UPR^{MT} activation after exposure to mitochondrial stress is strongly responsive only during development and not in later stages of the lifespan (Dillin et al., 2002; Copeland et al., 2009; Durieux et al., 2011; Houtkooper et al., 2013). UPR^{MT} appears less active in adult organisms, so there is not an increase in lifespan as a response to mitochondrial stressors, as observed in developmental stages in worms and flies (Dillin et al., 2002; Owusu-Ansah et al., 2013; Jensen et al., 2017).

Decreased chromatin accessibility of target UPR^{MT} genes in aged organisms is a potential explanation for the differential UPR^{MT} activation. Indeed, this was recently confirmed in a study where the methyltransferase SET-6 and the neuronal epigenetic reader BAZ-2 mediated an age-dependent regulation of UPR^{MT}. When overexpressed in aged worms, both proteins increased the levels of H3K9Me3, thus inhibiting UPR^{MT} activation in the H3K9-protected loci. Loss of function of SET-6 or BAZ-2 increased healthspan but not longevity, a phenotype that was inhibited downregulating UBL-5 or ATFS-1 in worms, cultured neurons, and mice (Yuan et al., 2020). Histone 3 methylation appears then as a critical epigenetic mediator for UPR^{MT} throughout the lifespan (Merkwirth et al., 2016; Tian et al.,

2016; Ono et al., 2017; Sobue et al., 2017) Longitudinal studies have proved that H3K9Me3, the triple methylated state of the protein, increases during aging in mice hippocampus, and inhibition of this state is sufficient to inhibit age-associated cognitive decline in mice (Petrosyan et al., 2016). However, the relevance of H3K9Me3 in the control of UPRMT during neuron degradation has yet to be investigated.

7.5 UPR^{MT} in aging neurons and disease.

In the nervous system, mitochondrial dysfunction affects neuronal function and their ability to respond to different forms of stressors. Substantial evidence points to the mitochondria as an important executor of neurodegenerative processes. To cope with mitochondrial dysfunction, cells activate the UPR^{MT} to restore mitochondrial homeostasis. Therefore, the mitochondrial stress response against the different aging triggers could represent the link between adaptation to stress and the other pillars of aging (Obashi and Okabe, 2013). , Evidence shows that mitochondria located at nerve terminals are more sensitive to age-related dysfunction and oxidative damage than non-synaptic mitochondria (Lores-Arnaiz et al., 2016). Synaptic mitochondria showed a higher level of peroxide production, higher susceptibility to calcium insult, less basal respiration, and increased leakage of protons when compared to non-synaptic mitochondria (Lores-Arnaiz and Bustamante, 2011; Lores-Arnaiz et al., 2016). It is important to note that the distinction between these two populations of mitochondria appears to get more pronounced with age (Borrás et al., 2003, 2010; Lores-Arnaiz and Bustamante, 2011; Lores-Arnaiz et al., 2016). It is essential to emphasize that neurons are differentiated cells that do not divide and have a lifespan comparable to that of the complete organism (Terman et al., 2009). This fact highlights the significance of homeostatic responses in preserving neuronal integrity and survival. When compared to mitotic cells, neurons are more susceptible to the accumulation of oxidative damage and more likely to have an accumulation of defective mitochondria along aging (Kirkwood and Kowald, 2000; Terman et al., 2009). Mitochondrial dysfunction contributes to the age-related loss in the functional capacity of the nervous system, for instance, by restricting the amount of energy that can be used, decreasing the capacity of the OXPHOS system, increasing the amount of damaged mtDNA, and causing structural damage to cells by the generation of an excessive amount of reactive oxygen species (ROS) (Sastre et al., 1998; Federico et al., 2012;

Niemann et al., 2017). Neurodegenerative disorders share essential mechanisms such as the presence of misfolded or aggregated proteins, neuroinflammation, impaired mitophagy, oxidative stress, and aberrant mitochondria, even if they have varied clinical and pathological aspects (Franco-Iborra et al., 2018), which are also observed, but to a lesser extent, in the aged brain of healthy individuals (Lucas-Sánchez et al., 2014; Salvadores et al., 2017; Franco-Iborra et al., 2018; Hussain et al., 2018).

Mitochondria are constantly challenged by harmful stimuli, which accumulate damage in a time-dependent fashion. Under this context, mitochondrial quality control mechanisms such as mitochondrial dynamics, mitophagy, and the UPR^{MT} have arisen as critical candidates for adequately understanding and possible development of treatments of age-related diseases. These mitochondrial quality control mechanisms respond to alteration of mitochondria homeostasis by changing the protein expression, eliminating damaged organelles, or activating cellular death pathways (Ristow and Zarse, 2010; Larsen et al., 2017; Misgeld and Schwarz, 2017). One possible hypothesis for the decline in mitochondrial function during aging is that mitochondria cannot be repaired due to a decrease in the activation of proteins involved in the mitochondrial quality control machinery, which could contribute to a structural and functional decay of the nervous system.

Moreover, mitochondria interact with many specific proteins involved in genetic forms of neurodegenerative diseases (Casley et al., 2002; Mattson, 2007; Newman and Shadel, 2018; Gomez and Germain, 2019). We can find different forms of mitochondrial dysfunction in neurogenerative diseases. For instance, in Alzheimer's disease (AD), which is the most common neurodegenerative disease caused mainly by the abnormal accumulation of the amyloid-β (Aβ) peptide (reviewed in Masters et al., 2015), there is evidence that oxidative damage and mitochondrial dysfunction have a role in the pathogenesis of this disease. In transgenic cells and mice, the overexpression of the Amyloid-β precursor protein (APP) causes mitochondrial dysfunction. Amyloid-β also inhibits the ketoglutarate dehydrogenase complex and reduces the activity of cytochrome-c-oxidase (COX), where reduced energy activity due to inhibition of complex I and COX promote tau phosphorylation.

Additionally, an essential role of Amyloid-β has been described in modulating proteins involved in mitochondrial dynamics (reviewed in Masters et al., 2015). Evidence indicates

that oxidative damage and mitochondrial dysfunction are critical in AD pathogenesis. However, the relationship between UPR^{MT} and AD has only been recently explored. Aβ accumulation activates UPR^{MT} in human cells and mice (Shen et al., 2020). In *C.elegans*, the sirtuin-activator resveratrol reduced the Aβ-induced toxicity in a Ubl-5-dependent manner, decreasing the amount of Aβ aggregates (Regitz et al., 2016). Further characterizations of these observations could provide clues to a potential connection between the different UPR^{MT} axes and AD.

Amyotrophicamyotrophic lateral sclerosis (ALS) is the most common motor neuron disease. A relevant link between ALS and mitochondrial dysfunction is associated to mutations in the superoxide dismutase SOD1, the first discovered causative gene for the disease (Rosen et al., 1993). Post-mortem samples of ALS patients show an altered activity of ETC complexes (Bowling et al., 1993), while SOD1 overexpression in transgenic mice causes dysregulated ETC activity and increases ROS production, which diminishes mitochondrial Ca^{2+}-buffering (Mattiazzi et al., 2002a; Brookes, 2004). Studies have located SOD1 and its mutant forms in the mitochondria, where SOD1 aggregates in the mitochondrial outer membrane, blocking proteins and promoting aberrant ROS production and oxidative damage (Mattiazzi et al., 2002a; Vijayvergiya, 2005). Mutant $SOD1^{G93A}$ localizes in the mitochondria IMS, which is sufficient to activate two axes of UPR^{MT} *in vivo* (Gomez and Germain, 2019). CHOP, part of one of these axes, is transiently activated in mice spinal cord, followed by Akt-dependent phosphorylation of ERα and upregulation of NRF1 and the proteasome activity (Riar et al., 2017; Gomez and Germain, 2019). This regulation is consistent with recent reports showing that UPR^{MT} activation precedes the onset of ALS, and its activity increases throughout the disease progression (Pharaoh et al., 2019). Dysregulation of TDP-43, another ALS causative gene, impairs mitochondrial function in ALS patients, suppressing ETC complex I activity, and activating the UPR^{MT} in *in vitro* and *in vivo* models. Downregulation of the UPR^{MT} protease LonP1 increased TDP-43 levels, mitochondrial damage, and neurodegeneration (Wang et al., 2019). A third ALS-linked mitochondrial protein is CHCHD10. Mutant CHCHD10 aggregates in the mitochondria, causing proteotoxic stress, mitochondrial dysfunction, and upregulation of the UPR^{MT} regulators CHOP and ATF5 (Anderson et al., 2019). These reports suggest that the accumulation of ALS-associated mutant proteins in the

mitochondria persistently activates the UPR^{MT}, which could trigger detrimental effects on already stressed neurons.

Parkinson's disease (PD) is another age-related neurodegenerative disorder where mitochondrial dysfunction has been widely characterized (Schapira, 2008; Moisoi et al., 2014; Franco-Iborra et al., 2018). Many observations suggest that mitochondrial dysfunction is involved in the pathogenesis of PD and the degeneration of dopaminergic neurons (Sonntag et al., 2017). Substance nigra samples from Parkinson's disease patients show decreased activity in the complex I of the electron transport chain, the NADPH dehydrogenase. Interestingly, complex I inhibitors cause neurological changes similar to those observed in PD patients (Schapira, 2008). The first evidence that linked mitochondrial dysfunction to PD was the discovery that 1-methyl-4-phenyl-1,2,3,6-tetrahydropyridine (MPTP), an inhibitor of mitochondrial electron transport chain complex I (NADH/ubiquinone oxidoreductase), causes parkinsonism in humans. Later, sporadic PD patients were reported to present reduced complex I activity, not only in the dopaminergic circuits of substantia nigra, but also in other brain areas and peripheral tissues (Beal, 2003; Bender et al., 2006). Identification of genes related to the familial forms of PD boosted the role of mitochondrial dysfunction in this process. In cell lines, PINK1 deficiency reduces mitochondrial respiration, ATP generation, and neuronal loss in response to stress caused by the accumulation of unfolded protein within the mitochondrial matrix and genetic deletion of PINK1 itself (Moisoi et al., 2014). Therefore, mitophagy and other mitochondrial quality control mechanisms, such as the UPR^{MT}, have arisen as prime candidates for the understanding and development of possible treatments for neurodegenerative diseases with a robust component of mitochondrial dysfunction, such as PD or PD-like pathologies. PD pathomechanism is strongly connected to mitochondrial dysfunction and, recently, to UPR^{MT} (Franco-Iborra et al., 2018; Chen et al., 2019). Two proteins encoded by PD-causative genes, serine-threonine kinase PINK1 and E3 ubiquitin ligase Parkin, work together to unclutter dysfunctional mitochondria through mitophagy. PINK1 or Parkin downregulation induces decreased mitochondrial respiration and ATP synthesis, degeneration of dopaminergic neurons, locomotor defects, and reduced lifespan (Zhu et al., 2013; Choi et al., 2015; Moisoi et al., 2014; Tufi et al., 2014). In *C.elegans*, the downregulation of their orthologs (*pink-1* and *pdr-1*) activates UPR^{MT} as a mitigation mechanism. Without atfs-1-dependent UPR^{MT} activation, lifespan decreases and

dopaminergic neurons degenerate (Cooper et al., 2017). PINK1 also interacts with the UPR^{MT} target HTRA2, mediating its phosphorylation and activation (Plun-Favreau et al., 2007). Interestingly, mutant alleles of HTRA2 were found in PD patients (Strauss et al., 2005).

PD pathogenesis is strongly connected to the accumulation of α-synuclein and mutations in its encoding gene (Poewe et al., 2017). αSyn^{A53T} preferentially accumulates in mitochondria and interacts with the UPR^{MT}-regulator ClpP, suppressing its peptidase activity. Overexpression of the protease is sufficient to decrease αSyn^{A53T}-associated pathology in mice (Hu et al., 2019). Despite the previous evidence, reports suggest a toxic role of UPR^{MT} overactivation. Expression of an active form of ATFS-1 lacking the mitochondrial targeting sequence in dopaminergic neurons mimics stress conditions with a constant nuclear expression of UPR^{MT} targets. The overactivation of UPR^{MT} shortens lifespan and promotes faulty mitochondria accumulation. This condition is exacerbated by the synergistic overexpression of mutant Syn^{A53T} (Martinez et al., 2017). From the epigenetic point of view, a study showed that α-synuclein expression in *Drosophila* led to an upregulation of the dimethyltransferase EHMT2, with an overall H3K9 dimethylation effect (Sugeno et al., 2016). It would be interesting to study whether chromatin remodeling linked to H3K9Me2 in this PD model modifies UPR^{MT} activation, as previously reported.

8.6 Proposed regulation of UPR^{MT} by histone methylation in aging.

Current evidence highlights an age-dependent effect of UPR^{MT} on lifespan. Activation of UPR^{MT} triggered by the downregulation of ETC complexes I and IV promotes longevity (Dillin et al., 2002; Durieux et al., 2011; Mouchiroud et al., 2013). Histone demethylases JMJD-1.2 and JMJD-3.1 mediate in part that extension, as their overexpression is sufficient to extend lifespan in worms(Merkwirth et al., 2016) On the other hand, reducing the expression of nuclear effectors ATFS-1, UBL-5, and *DVE*-1, or demethylases JMJD-1.2 and JMJD-3.1, suppress lifespan extension (Durieux et al., 2011; Houtkooper et al., 2013; Merkwirth et al., 2016; Cooper et al., 2017; Lan et al., 2019). Interestingly, UPR^{MT} activation after exposure to mitochondrial stress shows beneficial effects only if induced in developmental stages(Dillin et al., 2002; Copeland et al., 2009; Durieux et al., 2011; Houtkooper et al., 2013). Decreased chromatin accessibility for target UPR^{MT} genes in aged

organisms is a potential explanation for the differential UPR^{MT} activation along aging. This was recently confirmed in a study where the methyltransferase SET-6 and the neuronal epigenetic reader BAZ-2 were shown to mediate a specific age-dependent regulation of UPR^{MT}. When overexpressed in worms, both proteins increased the levels of H3K9Me3, thus inhibiting UPR^{MT} activation in the H3K9-protected loci. Loss of function of SET-6 or BAZ-2 increased healthspan, but not longevity, a phenotype inhibited downregulating UBL-5 or ATFS-1 in worms, confirming UPR^{MT} participation in the increment of healthspan by decreasing H3K9Me3 (Yuan et al., 2020). Histone 3 methylation appeared then as a critical epigenetic mediator for UPR^{MT} throughout lifespan (Merkwirth et al., 2016; Tian et al., 2016; Ono et al., 2017; Sobue et al., 2017). Longitudinal studies have demonstrated that H3K9Me3 increases during aging in mice hippocampus but not cerebellum, and inhibition of this state is sufficient to delay the age-associated cognitive decline in mice(Petrosyan et al., 2016). H3K9Me3 growth has been observed in the brains of aged flies(Wood et al., 2010; Petrosyan et al., 2016). Furthermore, modulation of epigenetic factors SET-6 and BAZ2 activated UPR^{MT} and improved mitochondrial performance by reducing H3K9Me3 in aging and Alzheimer's disease in *C. elegans*. Additionally, H3K9Me3 reduction increased dopamine-dependent pharyngeal pumping ages animals (Yuan et al., 2020). Nevertheless, age-associated changes in UPR^{MT} activity were not evaluated along aging, and age-associated changes by BAZ2 and SET6 were associated with dopamine and serotonin maintenance, but not neurodegeneration.

Recently, Hussain et al. found that olfactory projection neurons (OPNs) in adult *Drosophila*'s antennal lobe (AL) show an age-related reduced odor response accompanied by defects in neuronal integrity and reduction in synaptic proteins. This neurodegeneration was prevented by genetically inhibiting oxidative stress (Hussain et al., 2018). As *Drosophila* OPNs show, age-dependent neurodegeneration correlated with functional changes (Hussain et al., 2018). Therefore, we aim to determine if epigenetic regulation of UPR^{MT} is related to neurodegeneration of the olfactory system during aging in *Drosophila*. These findings could aid in developing specific anti-aging medicines for neural function.

In this work, we utilized behavioral, molecular, and morphological methodologies to demonstrate that dSetdb1 regulates H3K9Me3, whose repressive epigenetic regulation on

UPR^{MT} during aging causes mitochondrial morphological abnormalities and mitochondrial oxidation. This regulation contributes to the conserved age-associated olfactory loss of function and OPNs degeneration, particularly in somas located in the antennal lobe and the presynaptic connections of the lateral horn of the *Drosophila* brain. Surprisingly, genetic inhibition of H3K9Me3 by dSetdb1 knockdown, specifically in OPNs, restored H3K9Me3 to youthful levels, allowing UPR^{MT} activation capacity to restore mitochondrial oxidation. UPR^{MT} activation also prevented age-associated OPN changes by inhibiting neurodegeneration, measured by the maintenance of the number of neurons, axonal volume and presynaptic connections. Importantly, maintenance of UPR^{MT} in aging led to increased healthspan and the maintenance of olfactory function in aged organisms, but not locomotor or circadian activity. Furthermore, the olfactory function, locomotor, and circadian activity were impaired by genetically increasing the H3K9Me3 levels or by inactivating UPR^{MT} by the downregulation of its transcriptional activators in young animals. These data argue in favor of the therapeutical potential of target repressive epigenetic regulators of UPR^{MT} but raise the warning on specific differential epigenetic regulation on different behaviors governed by different neuronal types.

8. Hypothesis and General aim.

There have been no changes in the hypothesis since the corrections from May 21th, 2021.

8.1 Hypothesis

"Age-associated H3K9 trimethylation reduces the mitochondrial unfolded protein response capacity leading to neurodegeneration and functional impairment of the olfactory system." (Fig. 2)

8.2 General Aim

Characterize the UPR^{MT} activation during aging and its regulation by the age-associated H3K9 trimethylation in the neurodegeneration observed in the *Drosophila* antennal lobe.

8.3 Specific Aims

8.3.1 To characterize the UPR^{MT} during aging in the *Drosophila* antennal lobe.

8.3.2 To determine methylation state levels of H3K9 and UPR^{MT} activation during aging in the *Drosophila* antennal lobe.

8.3.3 To study whether modification of UPR^{MT} activity modulates age-associated neurodegeneration in the *Drosophila* antennal lobe.

8.3.4 To evaluate whether modulation of the UPR^{MT} by altering the methylation levels of H3K9 modifies the age-related neurodegeneration of the *Drosophila* antennal lobe.

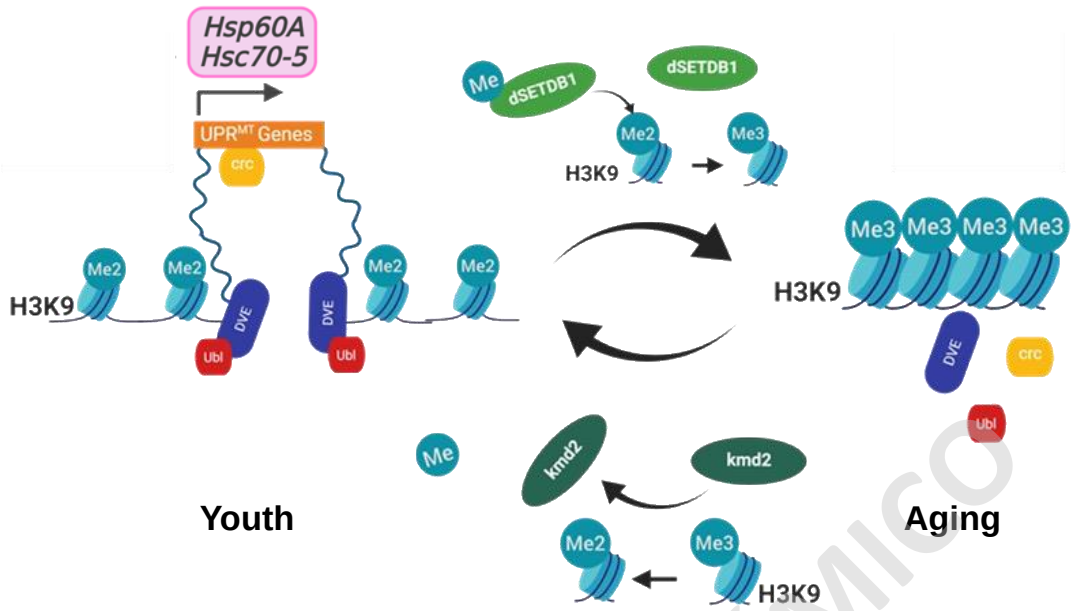

Figure 2. Proposed regulation of UPR^{MT} by age-associated histone trimethylation in Olfactory Projection Neurons. During youth, mitochondria are challenged by various insults that lead to the accumulation of mitochondrial dysfunction, causing damage and activating a retrograde response from the mitochondria to the nucleus. Ubl, crc and DVE are translocated to the nucleus, and DVE maintains an open chromatin state, allowing the binding of transcriptional modulators of the UPR^{MT}. This event activates the transcription of chaperones and proteases to recover mitochondrial homeostasis and oxidation exclusively on a mono/dimethylated state of H3K9. During aging, trimethylation of H3K9 is a mark of heterochromatin associated with the repression of transcription.

9. Materials and Methods.

9.1 *Drosophila* Strains and Culture.

Strains carrying the following transgenes were obtained from the Bloomington *Drosophila* Stock Center (BDSC) from Indiana University: UAS-Mito-GFP (BL#8443, encodes the 31 amino acid mitochondrial import sequence from human cytochrome C oxidase subunit VIII fused to the N-terminus of the Green fluorescent protein), UAS-MitoTimer (BL#57323, encodes a mitochondrial targeting sequence with a roGFP which turns its fluorescence from green to red when oxidized), elav-Gal4 (BL#485), actin-Gal4 (BL#9431), GH146-Gal4 (BL#1104), GH146-Gal4,UAS-GFP (BL#36500); RNAi lines for crc (BL# 25985), dve (BL#26225), ubl (BL#65893), dSetdb1 (BL# 31352), Utx (BL#34076), and Kdm2 (BL#33699); dSetdb1 loss of function (BL#30566), wild-type flies used as controls are Canton S (BL#64349), and RNAi Control flies from the Transgenic RNA Interference Project (TRIP) (BL#35787). Only female flies were used for all experiments to avoid males' genetic variation and aggressive behavior. All fly stocks were maintained on a standard *Drosophila* medium which consisted of 112.5g of Molasses, 35g of dry yeast, 90g of corn flour, 9g of agar, 2.5g of Tegosept diluted in 10ml of ethanol 95%, and 6ml of propionic acid per 1L of water; at 25ºC and under a circadian cycle of 12h of light and 12h of darkness.

9.2 Treatment with Mitochondrial Stressor Paraquat.

Experiments requiring mitochondrial stressor paraquat (Sigma, 36541) were performed by supplementing standard *Drosophila* medium with 100µl of paraquat diluted in dH_2O at 10µM. After PQ addition, vials must be airdried before use. Groups of flies had been exposed to a paraquat-supplemented medium for 48hrs before experiments were conducted.

9.3 Aging and recording of survival.

One hundred flies were maintained in a standard *Drosophila* medium and divided into four vials of 25. Flies were flipped to new vials containing fresh *Drosophila* medium every second day for up to no flies remained alive. For lifespan recordings, dead flies were counted when moved to vials with a fresh medium. As flies have not been recrossed for more than ten generations, it is crucial to emphasize that conclusions on lifespan may be influenced by genetic background, etc. The main purpose of the survival tests was to correlate the longevity of each genetic group of flies with its specific behavioral, physiological, or anatomical

characteristics. Survival analyses were performed using a Kaplan-Meier Curve in GraphPad Prism 9.0 and the Gehan-Breslow-Wilcoxon test. The significance of differences between survival curves was calculated using the log-rank test. **** P-value < 0.0001, ns p-value> 0.05.

9.4 Climbing Protocol.

To measure the locomotor activity of flies with different genotypes, we utilized the *Drosophila* activity monitor system (DAM System, trikinetics) (Pfeiffenberger et al., 2010). DAM system consists of 3 rings of infrared laser emitters and detectors; each detects the passage of individual flies through their respective ring. The rings are located at three different heights, 3, 6, and 9 centimeters, respectively (Fig.3A). In this study, we measured the number of flies that crossed the 9 cm ring of detectors. *Drosophila* possesses negative geotaxis, so when placed in a cylinder-shaped sealed vial and taped down, they tend to go up. Briefly, the system records locomotor activity from individual flies maintained in sealed vials placed in the activity monitors. An infrared beam directed through 3 different heights measures an "activity event" each time a fly crosses the beam. The optimal number of files we observed with no significant dropouts was an n of 10 (Fig. 3B). This allows us to correlate the alterations of the nervous system of the flies with locomotor performance. The experiment was conducted under the following protocol: flies were collected in groups of 10 and placed in *Drosophila* narrow vials. One duplicate per genotype plus a backup to replace dead or escaped flies. Flies were changed to new vials every 2 – 3 days. Flies need to be trained three times before a climbing assay begins, tapping them to the bottom of the vial and letting them climb. Flies can be used only for this experiment because every assay is performed with an independent batch of flies. Thus, an independent set of flies with their respective backups was aged for aging experiments. The system software was configured to take a read every 10 seconds. In a way, flies are softly tapped down in the bottom of the vials by tapping in softly in the odd number reads displayed by the software, and then in the even number reads, the number of flies that cross the 9 cm beam will be quantified. One climbing assay per genotype corresponds to 10 reads, technical replicates of the experiment, on which averages were plotted. Thus, an n corresponded to a population of ten flies per genotype.

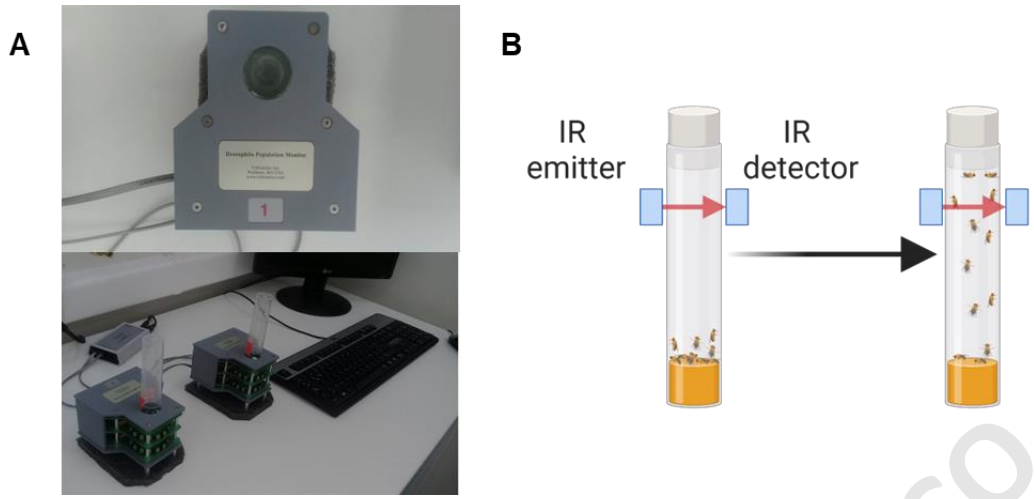

Figure 3. *Drosophila* Activity Monitor System for measuring locomotor activity using negative geotaxis of *Drosophila*. A) *Drosophila* activity monitor consists of 3 rings of infrared emitter/detector, each detecting the passage of individual flies through their respective ring. The first rings are at three different highs, 3, 6, and 9 centimeters, respectively. In this study, we measured the number of flies that cross the third ring of infrared detectors at the 9 centimeters mark. The lower panel image shows the DAM System monitor installed next to an analysis computer. B) Schematics of quantification of *Drosophila* locomotor activity when flies interrupt the infrared signal between emitter and detector.

9.5 Olfactory functional assay.

Olfactory T-maze was used to perform the olfactory behavioral test based on Hussain et al. 2018. Briefly, 15 flies are presented with an abrasive odor of 0.1M of Hydroxychloroquine, 0.1M of 3-octanol (Sigma, W358118), or a pleasant odor of 0.1M of 2.3-butanedione (Sigma, B85307) at the end of one arm of the T-maze and the end of the opposite arm flies are exposed to control solution (vehicle only). Flies have 60 seconds to discriminate between odors and go to an arm of the T-maze. An image is acquired at the end of the 60 seconds, and flies in both arms are counted. The olfactory preference index consists of ((Flies in Experimental Odor – Flies in Vehicle Odor) / (Total flies in the experiment)) (Fig. 4). The olfactory preference index is calculated for every trial, and every n in the graph corresponds to the mean of 5 trials of 15 flies each. For statistical analysis when comparing genotype and treatment, two-way ANOVA tests were performed with analysis of variance and Bonferroni's multiple comparisons for more than two groups using GraphPad Prism 9. P-value: *** $p < 0.001$; ** $p < 0.01$, * $p<0.05$ and ns > 0.05.

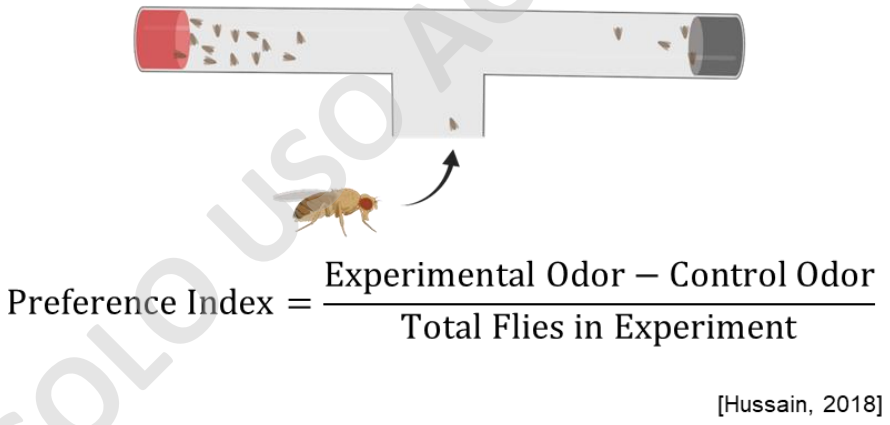

Figure 4. Olfactory T-maze paradigm. Schematics of a T-shaped maze in one arm contain the experimental odor, which can be pleasant or abrasive for flies. The population of flies has 60 seconds to choose one arm of the maze. Olfactory sensitivity is quantified by subtracting the number of flies in the control odor arm tfromthe number of flies in the experimental odor arm. The resulting number is normalized by the total number of flies population used for the experiment.

9.6 Circadian Activity.

Circadian activity and sleep measurements were analyzed as performed previously (Gilestro and Cirelli, 2009). Briefly, three vials with 15 flies each per genotype and age were introduced in narrow vials and placed on a *Drosophila* activity monitor of 32 slots. DAM system detector was placed in an incubator with a controlled temperature at 25°C, 60% humidity, and a 12h/12h light-dark circadian cycle. System Software was programmed to take reads every 1 minute. The activity was counted as read, and a sleep event was considered when zero reads were detected in the 5 min window or more (Fig. 5). Activity, number of sleep events, and length of sleep events were quantified using software PySolo data, tabulated in circadian activity, sleep events, and length of sleep events, and plotted using GraphPad Prism 9. The significance of the interaction between genotypes and time was calculated by a two-way ANOVA test with Bonferroni's multiple comparisons using GraphPad Prism 9. P-value: *** $p < 0.001$; ** $p < 0.01$, * $p<0.05$ and ns > 0.05.

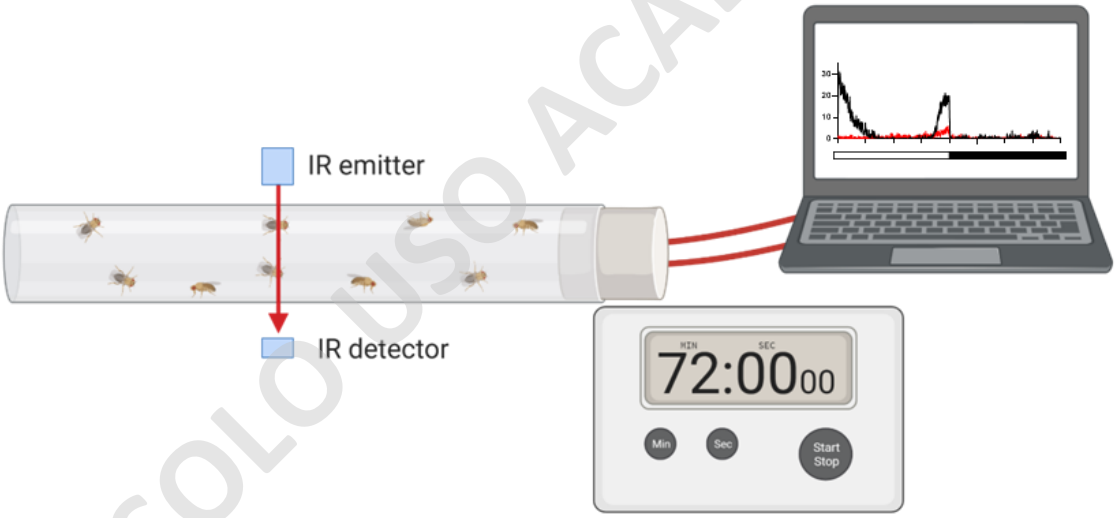

Figure 5. Scheme of circadian activity setup using *Drosophila* activity monitor System. The population of flies is introduced in a DAM system placed horizontally for three days, where each day represents a technical replicate. Each day consists of 12 hours in light and 12 hours in the dark. Spontaneous activity is quantified when flies interrupt the infrared laser from the emitter and detector. Sleep is defined as 5 minutes time window where no read is detected.

9.7 Protein Quantification and western blotting.

For immunostaining of H3K9Me3, samples were prepared as described previously (Chu and Tao, 2018). Briefly, samples were frozen in liquid nitrogen and ground to a fine powder using a pestle fitted to a 1.5ml Eppendorf Centrifuge tube filled with RIPA buffer, which included 50nM Tris, 150 mM NaCl, 1 mM EDTA, 0.1% of Nonodet P-40 (NP-40), 0.25% of Sodium Deoxycholate, and 0.02% of sodium azide in ddH_20. RIPA buffer was supplemented with phenylmethylsulphonyl fluoride (PMSF – Sigma) and a protease inhibitor cocktail (Sigma, P8340). Homogenized samples were incubated at 4°C for 1h and sonicated by a sonicator (QSonica) at 40% of equipment maximal amplitude with three pulses in 1 min. Sonicated Samples were centrifuged at 500g to pellet the debris, and all supernatant was transferred to a new tube and then centrifuged for 14 min at 13000g at 4C. The upper soluble phase was transferred to a new 1.5ml Eppendorf for membrane and plasma proteins and pellet, and 200µl of liquid phase was kept for nuclear proteins. Pellet was dissolved in the liquid phase by pipetting. Quantification of samples was performed using the Pierce BCA Protein Assay Kit (Thermo Scientific, 23225) under the manufacturer's instructions. Samples were boiled in SDS sample buffer for 15 min, separated on an SDS-PAGE gel, transferred, and revealed using BioRad TransBlot and ChemiDoc, respectively. Primary antibodies used were rabbit anti-H3K9Me3 1:2000 (Abcam, ab8898) and loading control anti-Tubulin 1:1000 (Thermofisher, MA1-744). Secondary antibodies were anti-rabbit conjugated with Horse Radish Peroxidase (HRP) 1:1000 (Thermofisher). The stained membranes were briefly incubated in luminol and scanned using ChemiDoc (BioRad). One biological replicate corresponded to a homogenized solution of 20 fly heads minimum. The normalized H3K9Me3 levels were calculated by normalizing the ratio of H3K9Me3 and loading control to that of young control samples. The significance of the interaction between genotypes and time was calculated by a one-way ANOVA test with Dunnet multiple comparisons or two-way ANOVA with Bonferroni's multiple comparisons test using GraphPad Prism 9. P-value: *** $p < 0.001$; ** $p < 0.01$, * $p<0.05$ and ns > 0.05.

9.8 Dissection of adult *Drosophila* brains and quantification.

Flies of the desired genotype were collected in groups of 15 and placed in vials containing *Drosophila* medium. Flies were anesthetized using a CO_2 pad. Using Dumont forceps #5, flies were held from the thorax and dipped in the sylgard petri dish filled with cold PBS. Brains were isolated by removing the exoskeleton from the fly´s head and carefully removing the esophagus and air sacs of the flies' brains as previously described(Wu and Luo, 2006). For live imaging of endogenous fluorescence, brains were fixed in 2% paraformaldehyde with 0.1% Triton X-100 (Sigma, T9284) for 20 minutes and then changed to a 4% paraformaldehyde, 0.1% Triton X-100 solution, then washed for 10 min 3 times in PBS Triton X-100 at 0.1% followed by three quick washes with PBS only. Brains were mounted in VectaShield (Sigma) for later visualization in an SP8 confocal microscope. For all experiments, all brains were imaged on the same day. For immunostaining, brains were dissected as described previously (Hartl et al., 2011). Brains were fixed for 1h at room temperature in 4% PFA with 0.5% Triton X-100, washed three times for 10 minutes with PBS with 0.5% Triton X-100, and blocked for 1h with Normal goat Serum (NGS) (Cell Signaling, 5425S) at 5% in PBS, 0.5% Triton X-100 and stained overnight at 4ºC with primary and after three washes in PBS, 0.5% Triton X-100 with secondary antibodies using the same conditions. The secondary antibody was washed six times for 10 min each with PBS, 0.5% Triton X-100 a three quick washes in PBS before mounting. Washed brains are placed in a stripe of 15 to 20 µl of Vectashield antifade mounting medium (Vector, H1000) on cover glass (Deltalab, D10004), and imaging was performed in confocal microscope SP8 using the 63x objective with digital zoom necessary for desired resolution. Fluorescence intensity for each channel was adjusted using control flies to the point that no saturation was observed, then the same parameters were used for all images. Images of antennal lobe sections of *Drosophila* brains and OPNs were taken at a depth of 10µm using a Z stack separation of 0.6µm. Primary antibodies used were anti-GFP (Invitrogen, 1:1000), rabbit anti-H3K9Me3 (Abcam, ab8898; 1:500), and secondary antibody donkey anti-Rabbit 555 (Thermofisher, 1:1000) or goat anti-mouse (Thermofisher, 1:1000). For image quantification of fluorescent signal, 3D reconstruction of labeled structures was performed in Imaris Software. The surface of the desired signal was rendered, and mean intensity values were obtained. To account for the volume variability where the mean intensity signal was measured, integrated density was calculated by multiplying the mean intensity per volume

(μm^3) (Fig. 6B and C). For quantification of the specific signal in Olfactory Projection Neurons, a surface of GFP-labeled OPNs was rendered, then To-Pro3 labeled nuclei signal was masked. The surface rendered, and finally, the signal for H3K9Me3 in the nuclei of OPNs was quantified as described previously (Fig. 6D). Mitochondrial Morphology was analyzed by rendering the surface of mitochondrial reporter mitoGFP expressed specifically in the OPNs. Total mitoGFP volume (μm^3), mitoGFP puncta number, mitoGFP fragmentation index, which corresponds to volume (μm^3) per area, (μm^2) mitoGFP sphericity index, mitoGFP average size (μm^3), and integrated density were analyzed (Fig. 7B). Mitochondrial Oxidation analysis was performed as described previously (Hernandez et al., 2013; Laker et al., 2014). Neuronal Integrity was analyzed by rendering the surface of labeled OPNs in AL, the distal part of the axon, and axonal terminals in the LH. Volume and Integrated density were analyzed (Fig. 8C). Data were plotted and analyzed using GraphPad Prisms 9 Software. To compare the interaction between age and genotype/treatment, two-way ANOVA and for more than two groups, analysis of variance with Bonferroni's multiple comparisons was performed using GraphPad Prism 9. P-value: *** $p < 0.001$; ** $p < 0.01$, * $p<0.05$ and ns > 0.05.

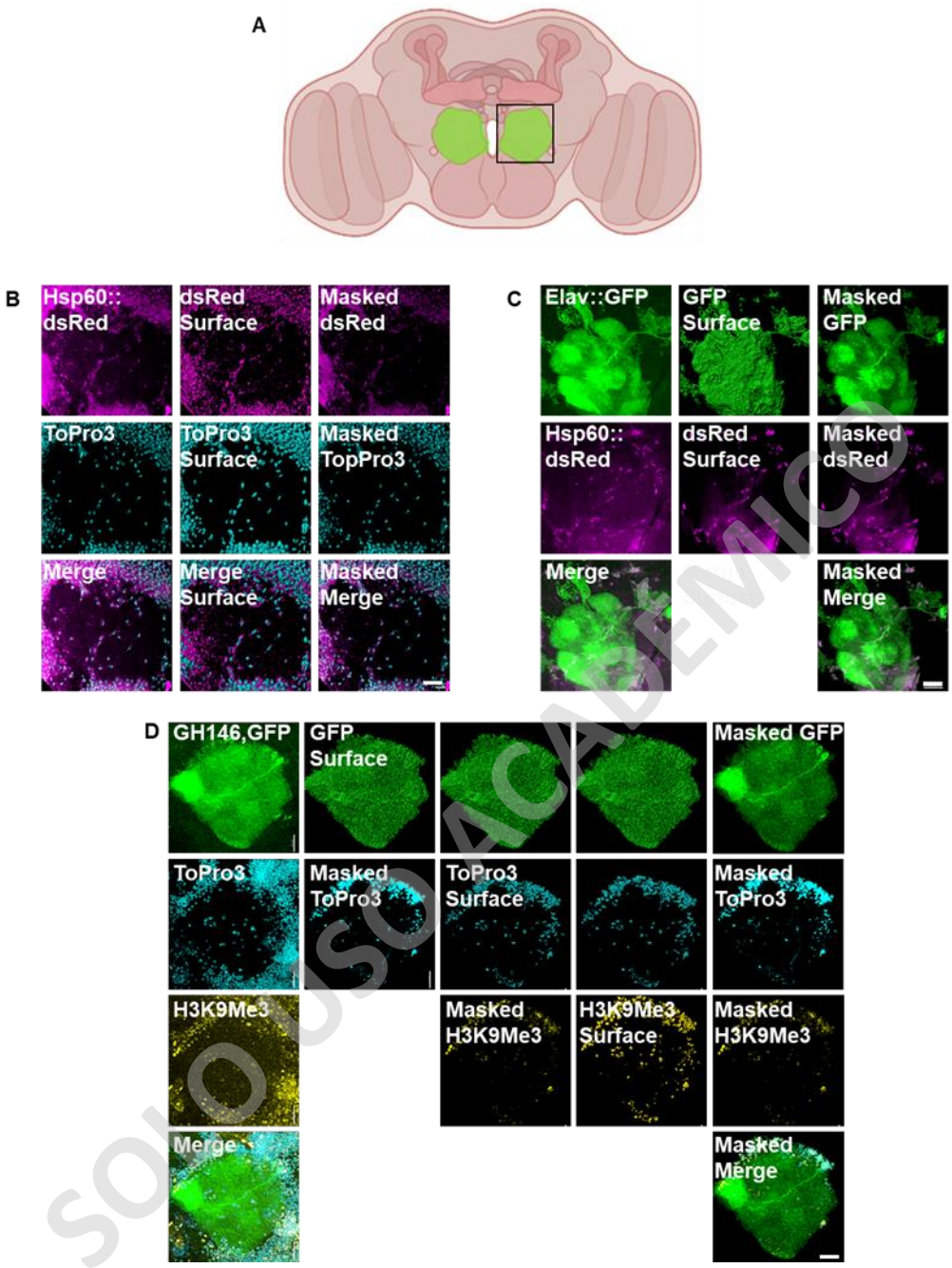

Figure 6. Quantification of the fluorescent signal using 3D reconstructed surface in the Antennal Lobe of *Drosophila* brain. A) Schematics of field imaged B) Quantification of fluorescent signal within the Antennal Lobe. C) Quantification of fluorescent signal within GFP-labeled neurons in the Antennal Lobe. D) Quantification of fluorescent signal within ToPro3-labeled nuclei within GFP-labeled neurons in the Antennal Lobe. Scale Bar 10 µm.

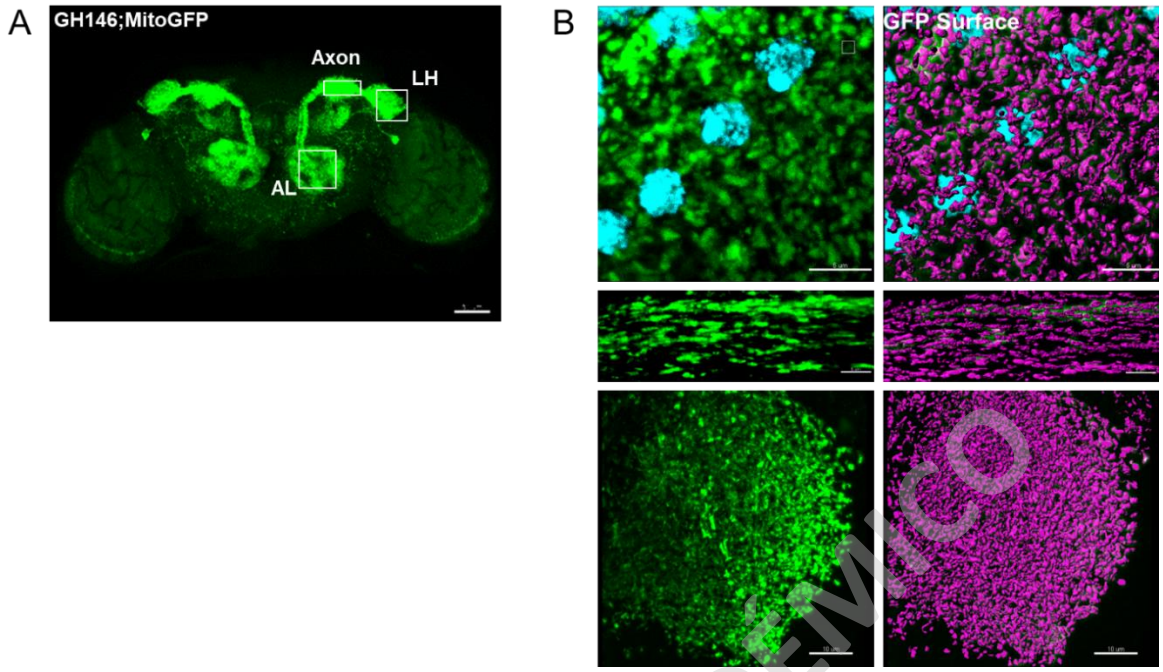

Figure 7. Quantification of fluorescent signal within GFP-labeled mitochondria expressed in OPN in the Antennal Lobe, axons, and Lateral Horn. A) Representative 20X image of GFP-labelled mitochondria, specifically in olfactory projection neurons. White squares show the Antennal Lobe (AL), the axon, and the Lateral Horn (LH). B) Representative images at 63X magnification of GFP-labeled mitochondria in the AL (upper panel), distal part of the axon in the middle panel, and in LH (lower panel). Images in the left panel show GFP signal coming from the mitochondria, and the right panels showthe high-resolution 3D surface reconstruction of GFP s,ignal which were used to quantify mitochondrial morphology. Scale Bar in A 50 µm, and, for B Scale bar is 5 µm.

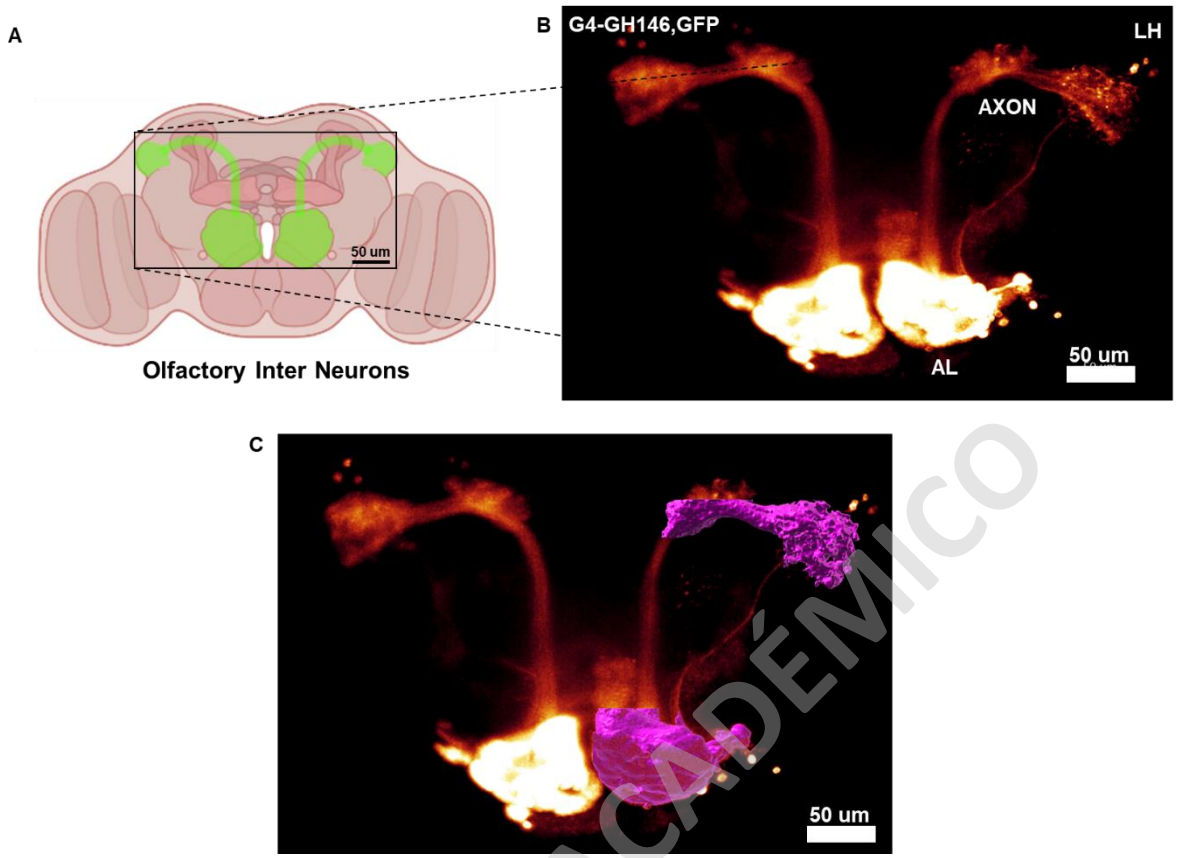

Figure 8. Quantification of neuronal integrity of OPN in the antennal lobe, the distal section of the axon, and lateral horn. A) Schematics of OPN GFP-labeled circuit in the *Drosophila* brain. OPN somas are located in the antennal lobe, where its axonal projection goes from anterior to posterior to innervate the Lateral Horn of the mushroom body, where axonal terminals of OPN are located, and the LH is enriched in presynaptic connections. B) High-resolution image at 20X magnification of GFP-labeled olfactory projection neurons in the *Drosophila* brain, AL, shows the antennal lobe, the distal part of the axon, and the lateral horn as LH. C) High-resolution 3D reconstruction of AL, axon, and LH, which were used for quantification of neuronal integrity. The scale bar is 50 µm.

9.9 RNA extraction, RT-PCR, and qPCR.

Total RNA was extracted from 2 whole flies or 20 heads using a standard trizol extraction following these steps: tissue was placed on a 1.5 ml Eppendorf tube, and 300 µl of trizol reagent was added before homogenization with a plastic pestle 60 times. At this point, the sample can be stored at -80ºC. 700 µl of trizol were added, and samples were centrifuged at 13000 rpm for 10 min at 4ºC to pellet the tissue debris. The supernatant was transferred to a fresh 1.5 tube. 300ul of chloroform was added, and samples were shaken vigorously by hand 15 times. Then incubation of the samples at room temperature for 5 min. Samples were centrifuged at 13,000 rpm for 15 min at 4ºC. The upper phase was carefully transferred to a new RNAse-free tube without touching the interphase. 700uL of isopropanol was added to precipitate the RNA, and samples were incubated for 5 minutes at room temperature or 1 hour at -20ºC. Centrifuge at 12,000 rpm for 15 min at 4ºC. The supernatant and RNA pellet was washed with 1 ml of ethanol 70% prepared with miliQ quality H_2O. Centrifuge at 13000 rpm for 10 min at 4ºC. Air dry the pellet briefly and resuspend the pellet in an appropriate volume of MiliQ water (20 to 50 µl). The RNA concentration was measured for each sample in duplicate using a NanoQuantMultiskan spectrophotometer, and the purity of the sample was evaluated using the 260/280nm absorbance ratio.

Reverse transcriptase-PCRs (RT-PCR) were carried out using the iScript RT Kit for cDNA synthesis (BioRad, 1708841). The final mix included 1 µg of RNA sample and 5µL of iScript RT-PCR mix with reverse transcriptase, and the final mix was carried to a final volume of 20ul. The cDNAs obtained were then used as a template for real-time PCRs using the Eva Green qPCR Master Mix (SolisBioDyne, 08242510.6) in a StepOne Plus Machine (Applied Biosystems). The final PCR mixture (20ul) contained 1ul of cDNA, 4 µl of 5xFirePol MasterMix, and 0.2 µmoles of each primer and was carried out to the final volume of 20ul. The thermal profile used for the reaction included a 2-minute heat activation of the enzyme at 95ºC, followed by 35 cycles of denaturation at 95ºC for 15 seconds and annealing/extension at 58ºC for 60 seconds, followed by melt analysis ramping at 58-90ºC. Negative control was conformed of water instead of cDNA and was included in each plate. Relative transcript levels were assessed using the Comparative CT method, and expression values were normalized to 28S ribosomal expression, used as an internal control. One biological replicate corresponded to a homogenized solution of 20 fly heads minimum. For

statistical analysis when comparing genotype and treatment, two-way ANOVA tests were performed with analysis of variance and Bonferroni's multiple comparisons for more than two groups using GraphPad Prism 9. P-value: *** $p < 0.001$; ** $p < 0.01$, * $p<0.05$ and ns > 0.05.

9.10 Data reporting and statistics.

No statistical methods were used to predetermine the sample size. The sample sizes in our experiments were determined from related published analyses, and the experiments were not randomized. All *Drosophila* strains were synchronized and at 25 °C under the same dietary conditions. Behavioral and lifespan experiments were repeated at least three times, and investigators were blinded to the genotypes or treatments. Flies were picked at 0 days post eclosion (dpe) and raised to a range of ages of 45 dpe, chosen unbiasedly for behavioral, lifespan, and imaging assays.

We used GraphPad Prism 9 (GraphPad Software, Inc.) for statistical analyses. We used an unpaired Student's t-test to analyze differences between two groups; one-way analysis of variance (ANOVA) followed Dunnett's correction test to analyze differences between multiple groups with one variable; two-way ANOVA to analyze differences between multiple groups with two variations with Bonferroni's multiple comparison test, and a two-sided log-rank Survival curve comparison with Gehan-Breslow-Wilcoxon test results to analyze lifespan statistics. The variance of all plots and graphs is represented as means ± s.e.m.; n refers to the number of animals, the population of animals, independent experiments, or for single-cell expression analysis, n is the number of cells analyzed. The significance of statistical differences is indicated as: P-value: *** $p < 0.001$; ** $p < 0.01$, * $p<0.05$ and ns > 0.05. All statistical analyses are tabulated in detail and cand be found in Annex 1 organized by its corresponding figure.

10. Results.

10.1 Hsp60::dsRed reporter activation depends on *Drosophila* UPR^{MT} transcriptional activators and shows an age-related decline in the AL of *Drosophila*.

To study the modulation of the UPR^{MT} along aging in *Drosophila*, we first generated a reporter based on the expression of the fluorescent protein dsRed under the promotors of chaperones hsp60 and hsp-6, which in worms specifically responds to UPR^{MT} stimuli (Benedetti et al., 2006). As olfactory function decreases in aged organisms, we focused on the antennal lobe (AL), the homolog region to the vertebrate olfactory bulb, in which olfactory projection neurons processes sensory inputs. In young flies, a low-intensity signal of the Hsp60::dsRed reporter was detected in AL in control conditions, which robustly increased by the mitochondrial stressor paraquat (PQ, Fig. 9A and B). This increase in the Hsp60::dsRed signal is not induced by other cellular stressors such as tunicamycin, which inhibits protein glycation at the endoplasmic reticulum (ER), inducing unfolded protein accumulation, and activating the ER-stress specific reporter Xbp1::GFP45 (Fig. 9A-E). To further test the specificity of the Hsp60::dsRed reporter for the UPR^{MT}, the response of the sensor to PQ was evaluated in the AL of flies knocking down the key UPR^{MT} nuclear activators dve, ubl, and crc. Indeed, pan-neuronal knockdown of each of these nuclear UPR^{MT} activators reduces the fluorescent response to PQ of the Hsp60::dsRed reporter compared to control flies (Fig. 10A and B), with similar results using the second hsp-6 reporter (Supplementary Fig. 1), demonstrating that activation of these reporters by specific stimuli depends on key UPR^{MT} nuclear activators in *Drosophila*.

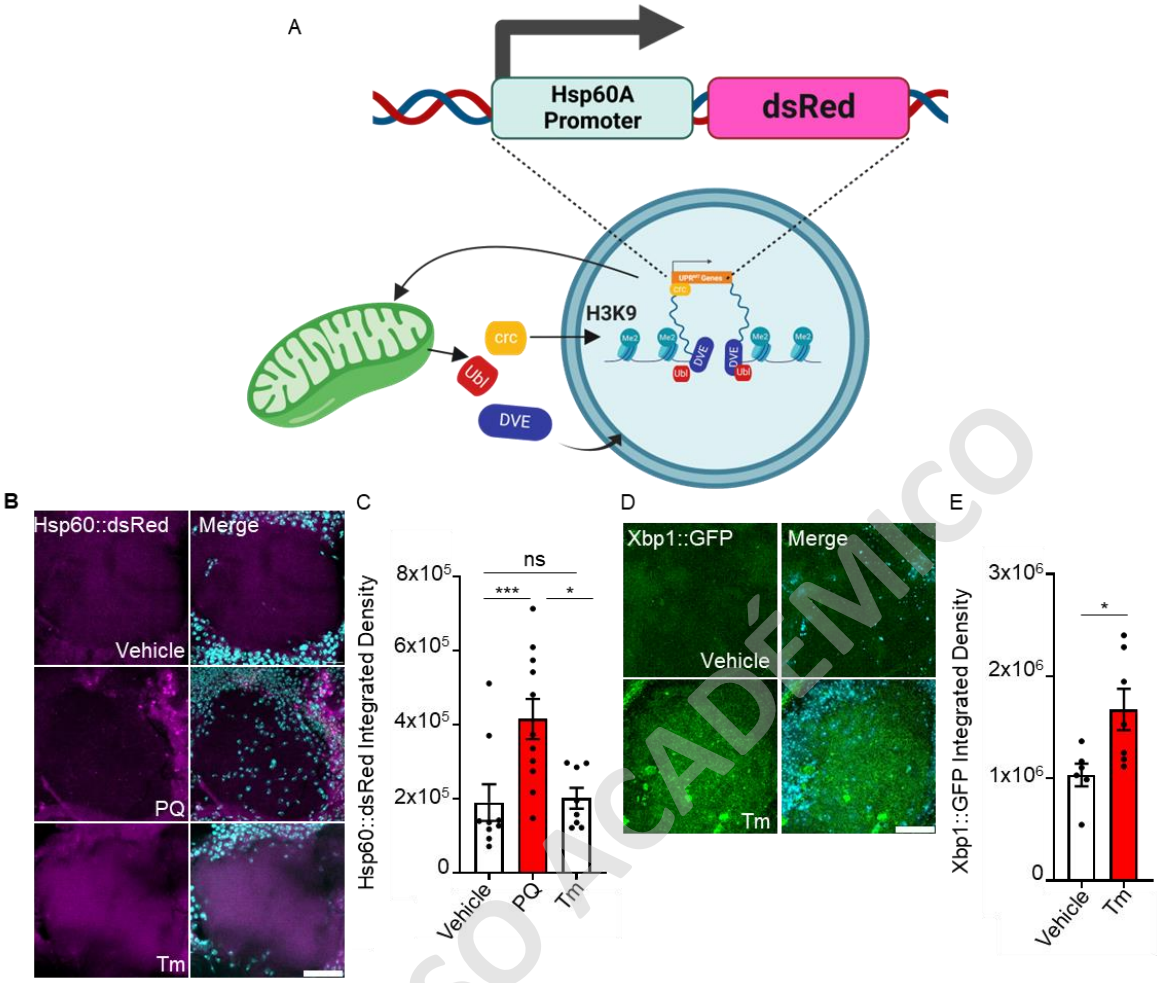

Figure 9 UPR^{MT} reporter responds to the mitochondrial stressor PQ, but not ER stressor tunicamycin. A) Representative images of AL of UPR^{MT} reporter flies treated with PQ or Tm. Magenta is Hsp60::dsRed and Cyan is DAPI. B) Hsp60::dsRed integrated density of images shown in A. C) Representative images of AL of Xbp1::GFP flies treated with Tunicamycin. Xbp1::GFP is in green, and DAPI is in cyan. D) Integrated density of Xbp1::GFP signal of images shown in C). Scale Bar is 10µm. Unpaired student t-test and One-way ANOVA statistical analysis with Dunnett's multiple comparisons test between different treatments were performed. P-value: **** $p < 0.0001$; *** $p < 0.001$; ** $p < 0.01$, * $p<0.05$ and ns > 0.05 (Table 1 and 2).

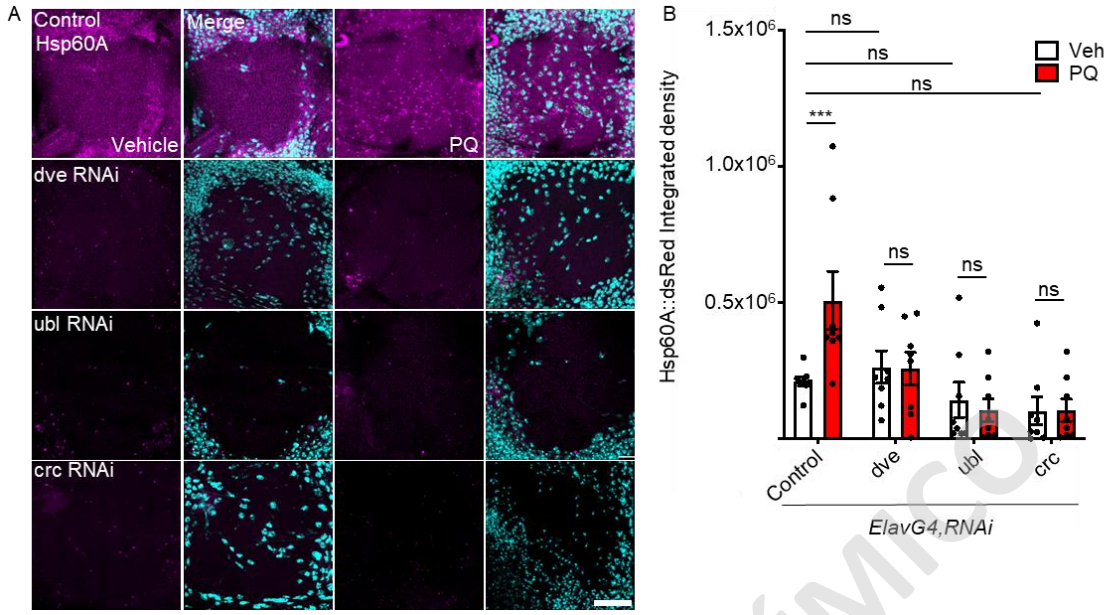

Figure 10. UPR^{MT} reporter activation depends on *Drosophila* UPR^{MT} transcriptional activators. A) AL of Hsp60::dsRed reporter flies in together with the pan-neuronal RNAi-mediated knockdown of dve. Hsp60A-dsRed in magenta and DAPI in cyan. Scale bar 10µM. B) Quantification of integrated density vehicle in white and PQ in red. Scale Bar is 10µm. Two-way ANOVA statistical analysis was performed with Bonferroni's multiple comparisons between different genotypes with the same treatment and treatments in the same genotype. P-value: *** $p < 0.001$; ** $p < 0.01$, * $p<0.05$ and ns > 0.05 (Table 3).

To define if the endogenous expression of the UPR^{MT}-associated chaperones Hsp60 and Hsc70-5 were also modified by age, we took advantage of Scope, a single-cell repository of brain cells from *Drosophila* at different ages (http://scope.aertslab.org). Three major groups of neurons can be found in the *Drosophila* brain, cholinergic, glutamatergic ,and GABAergic neurons, expressing vAChT, vGlut, and Gad11, respectively (Fig. 11A). The antennal lobe is mainly composed by cholinergic neurons, which are also the major neuronal component of the *Drosophila* brains (Fig. 11A). For cholinergic neurons, single cells data demonstrate that both Hsp60A and Hsc70-5 expression levels decrease in aged flies at 50 dpe compared to young animals at 0 dpe (Fig. 11B and C). Interestingly, this is also true for glutamatergic but not for GABAergic neurons, suggesting that neuronal types have different susceptibility to an age-dependent decrease in the UPR^{MT} activation.

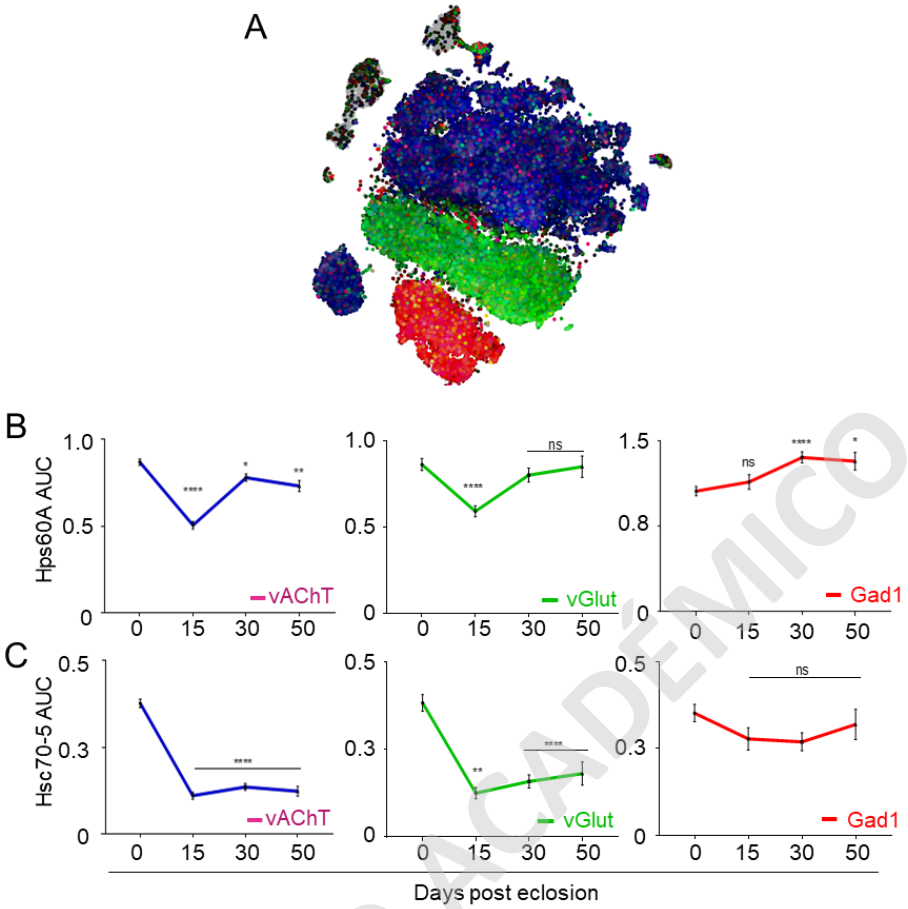

Figure 11. UPR^{MT} activation decreases with aging in the AL and vAChT but not in the vGlut and Gad1 neurons. A) Dot plot showing analysis of UPR^{MT} activation through the aging brain using single-cell RNA seq data in Scope. B and C) AUCell scores given by Scenic[11] showing the expression levels of Hsp60 (upper panel) and Hsc70-5 (lower panels) in cholinergic neurons (vAChT), glutamatergic neurons (vGlut), and GABAergic neurons (Gad1) through aging. One-way ANOVA statistical analysis with Dunnet's multiple comparisons against time control 0 dpe. P-value: *** $p < 0.001$; ** $p < 0.01$, * $p<0.05$ and ns > 0.05 (Tables 4 to 9).

Equipped with the Hsp60::dsRed reporter, we evaluated UPR^{MT} activity throughout aging in the *Drosophila* AL. To analyze UPR^{MT} in neurons, we used flies expressing GFP under a neuronal promoter (ElavGFP), and the Hsp60::dsRed signal was measured only in the GFP-positive signal from the AL (Fig. 12A). Compared to the robust signal triggered by PQ in young flies (0 dpe), no increase in the Hsp60::dsRed reporter signal was observed in AL neurons from aged flies (45 dpe, Fig. 12A, and C). Importantly, no significant changes in the GFP volume were found in aged vs young flies or after PQ treatment at both ages (Fig. 12B). Using this newly developed UPR^{MT} reporter, our data suggest that aging strongly decreases the UPR^{MT} activation capacity in neurons of the antennal lobe.

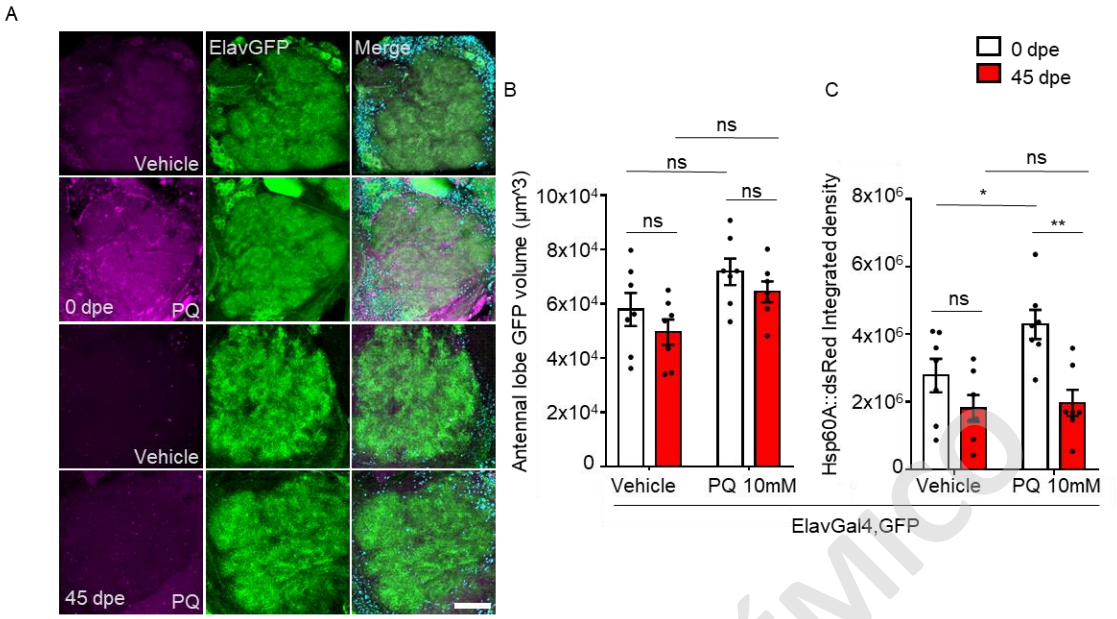

Figure 12. UPR^{MT} activation decreases with aging in the AL, which is required for correct olfactory function. A) Representative images of GFP neurons in the AL of *Drosophila*. Hsp60::dsRed in magenta, Pan-neuronal GFP in green, and DAPI in cyan. B) AL volume of young in white and old flies in red treated with PQ or vehicle. C) Integrated density of UPR^{MT} reporter in the AL of young in white and aged flies in red treated with PQ or vehicle. D) Olfactory preference index in flies with pan-neuronal downregulation of UPR^{MT} transcriptional modulators dve, ubl, and crc mirrored the impaired olfactory function of aged control flies. Scale Bar is 10µm. Two-way ANOVA statistical analysis with Bonferroni's multiple comparisons between different genotypes of the same age or treatment and different ages or treatments in the same genotype was performed. P-value: *** $p < 0.001$; ** $p < 0.01$, * $p<0.05$ and ns > 0.05 (Tables 10 to 12).

To evaluate if reduction of UPR^{MT} activation capacity in aging was contributing to the age-associated loss of olfactory function, we used the olfactory T-maze. Flies were presented with 2,3-butanedione as pleasant and 3-octanol or hydroxychloroquine as an abrasive odor. As flies age, they become less sensitive to discriminate between odors and at 45 dpe, and cannot distinguish between the experimental and control odor (Fig. 13A). We then evaluated olfactory function in flies bearing the pan-neuronal downregulation of UPR^{MT} transcriptional activators dve, ubl and crc (Fig. 13A). Remarkably, 0 dpe flies bearing the knockdown for nuclear activators of UPR^{MT} presented a decreased olfactory capacity to discriminate an abrasive odor compared to wild type animals (Fig. 13A). Animals at 45 dpe do not show a difference with age-matched controls, or when compared to young flies from the same genotype (Fig. 13A). This suggests that the knockdown of these UPR^{MT} nuclear activators mirrored the impaired functionality of the olfactory nervous system of wildtype flies at 45 dpe (Fig. 13A). It has been previously demonstrated that trimethylation of H3K9 (H3K9Me3) increases during *Drosophila* aging (Wood et al., 2010), a phenomenon that has also been linked to activation of the UPR^{MT} (Merkwirth et al., 2016; Tian et al., 2016; Yuan et al., 2020). Indeed, the decline of olfactory function in aged animals (Fig. 13B) correlates with increased trimethylation of H3K9 in the fly brain (Fig. 13C).

Taken together this data suggests that UPR^{MT} epigenetic regulation by H3K9 methylation also ocurrs in the neurons of AL in *Drosophila*. Where H3K9Me3 increases and neuronal UPR^{MT} activation decreases which is required for correct olfactory function in vivo.

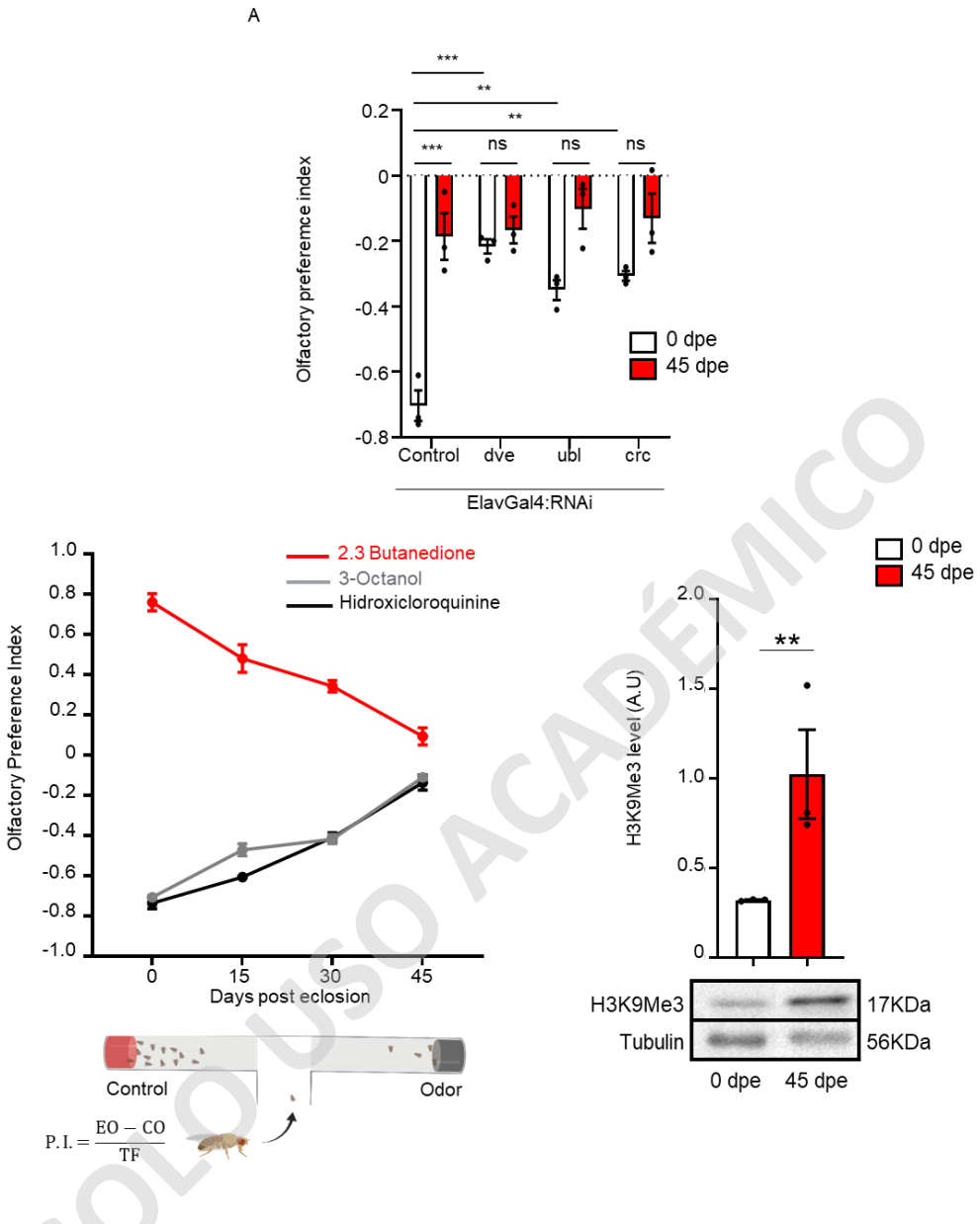

Figure 13. The age-associated decline in olfactory function correlates with increased H3K9Me3 in the *Drosophila* Olfactory preference index showing the age-associated functional decline in the olfactory system. Olfactory T-maze was used to perform the olfactory behavioral test. Flies are presented to an experimental odor or vehicle. Flies have 60 seconds to discriminate between odors and go to an arm of the T-maze. At the end of the time, an image is acquired, and the preference index is calculated for every trial; every dot corresponds to 10 trials of 20 flies each. B) Western blot of Trimethylation of H3K9 in young in white and old flies in red. Unpaired student t-test and one-way ANOVA statistical analysis with Dunnet's multiple comparisons against time control 0 dpe. P-value: **** $p < 0.0001$; *** $p < 0.001$; ** $p < 0.01$, and ns > 0.05 (Tables 13 and 14).

10.2 Epigenetic regulation on UPR^{MT} by dSetdb1 in the AL of *Drosophila*.

To demonstrate that the UPR^{MT} is mediated by chromatin condensation in the AL of flies, we used the Hsp60::dsRed reporter with EMS-generated loss of function of dSetdb1 (dSetdb1 lof), a specific H3K9Me3 methyltransferase. Loss of function of dSetdb1 is caused by a nonsense mutation, which introduces a stop codon in the fourth intron of the mRNA (Clough et al., 2014). We evaluated fluorescent reporters for Hsp60A and Hsc70-5 in the AL of 0 dpe dSetdb1 lof flies (Fig. 14). The basal fluorescence intensity of Hsp60::dsRed reporter in aged dSetdb1 lof flies was significantly higher than in age-matched control and young dSetd1 lof flies (Fig. 14B and C). The fluorescence intensity of Hsc70-5::dsRed reporter in young dSetdb1 lof antennal lobe was significantly higher than that of young control flies (Fig. 14E and F). Remarkably dSetdb1 pan-neuronal knockdown did not present an age-associated increase of H3K9 trimethylation compared to 45 dpe control flies which showed a significant increase in the H3K9Me3 levels in aging (Fig. 14D). These results demonstrate that dSetdb1 negatively regulates UPR^{MT} in the AL neurons through H3K9Me3.

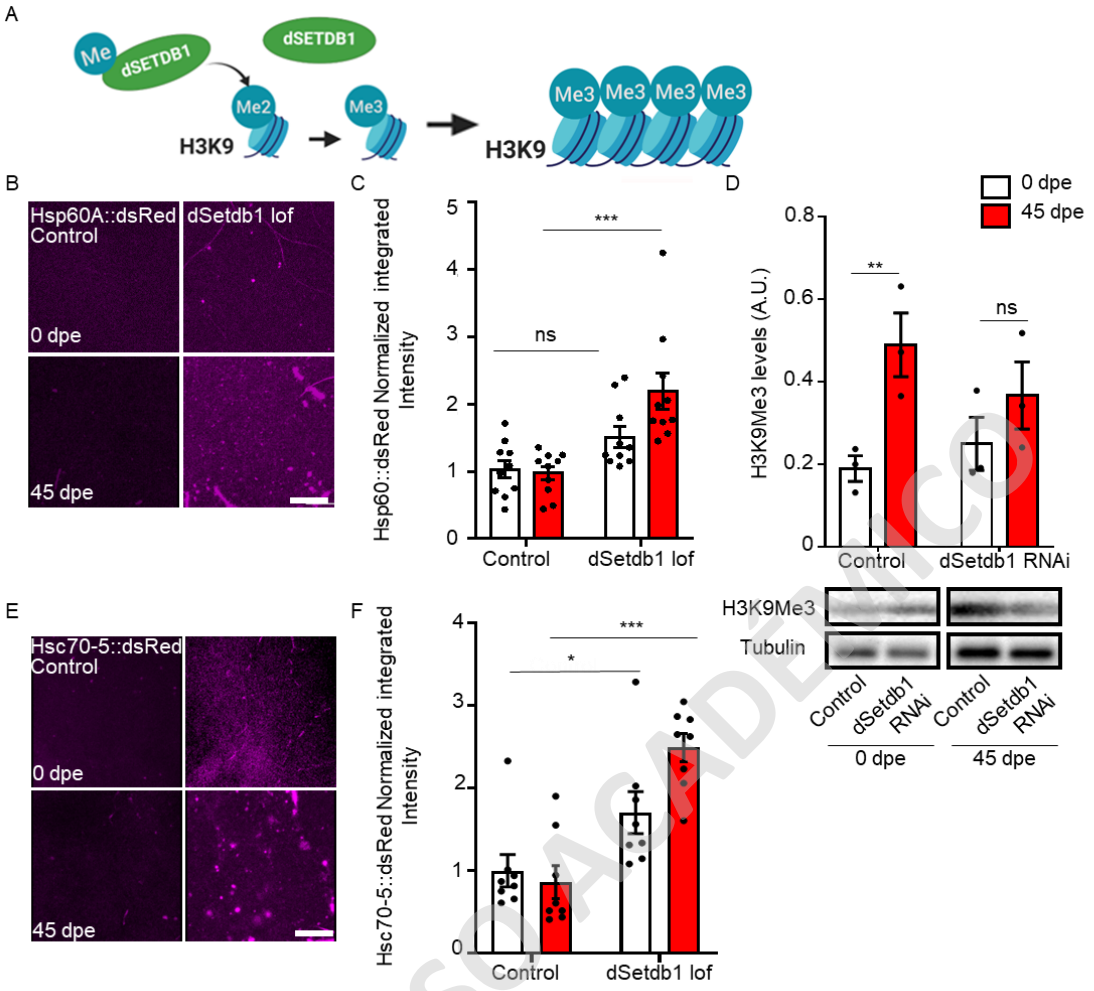

Figure 14. dSetdb1 negatively regulates Hsp60::dsRed reporter along aging through increasing H3K9Me3 levels in AL of *Drosophila*. B) Representative images of *Drosophila* AL sections of UPR^{MT} reporter flies with the dSetdb1. Hsp60A::dsRed in magenta. C) Quantification of the normalized integrated density of Hsp60A::dsRed in A. dSetdb1 loss of function induces UPR^{MT} activation in the *Drosophila Olfactory lobe*. E) Representative images of *Drosophila* olfactory lobe in anterior protocerebrum sections of UPR^{MT} sensor flies with the loss of function of methyltransferase dSetdb1. Hsc70-5::dsRed in magenta. F) Quantification of normalized mean fluoresce intensity for D. Scale bar 10µM. n=10. D) Western blot showing protein levels of H3K9Me3 in young and aged flies with pan-neuronal downregulation of dSetdb1. Scale Bar is 10µm. Two-way ANOVA statistical analysis with Bonferroni's multiple comparisons between different genotypes of the same age and different ages in the same genotype was performed. P-value: **** $p < 0.0001$; *** $p < 0.001$; ** $p < 0.01$, * $p<0.05$ and ns > 0.05 (Tables 15 to 17).

Additionally, using single-cell expression analysis with SCope, we evaluated the expression levels of H3K9 methyltransferase dSetdb1 and utx and kdm2, genes reported to be involved in UPR^{MT} regulation (Merkwirth et al., 2016). In vAChT neurons, dSetdb1 expression shows a non-significant increase with age (Fig. 15B). The specific H3K9 demethylase kdm2 shows an age-associated decrease at 30 and 50 dpe, as the expression decreases compared to young flies (Fig. 15D). Utx is a nonspecific demethylase that acts not only in H3K9 but also demethylates H3K27 (Herz et al., 2010; Merkwirth et al., 2016). Nevertheless, the expression levels of utx do not show changes throughout aging (Fig. 15C). This age-associated change in expression between histone methylase dSetdb1 and demethylase kdm2 argues in favor of the hypothesis that an increase in age-associated trimethylation of H3K9 participates in the decrease of UPR^{MT} activity during aging (Fig. 12), which in turn is contributing to the functional decline that comes with aging in the olfactory circuit in *Drosophila* nervous system (Fig. 13). However, this is only the case for vAChT neurons, since UPR^{MT} reporters and H3K9Me3 regulating enzymes behave differently in vGlut and Gad1 neurons (Fig. 11 and 15). These last results suggest that UPR^{MT} may have different epigenetic regulation in different neuronal types.

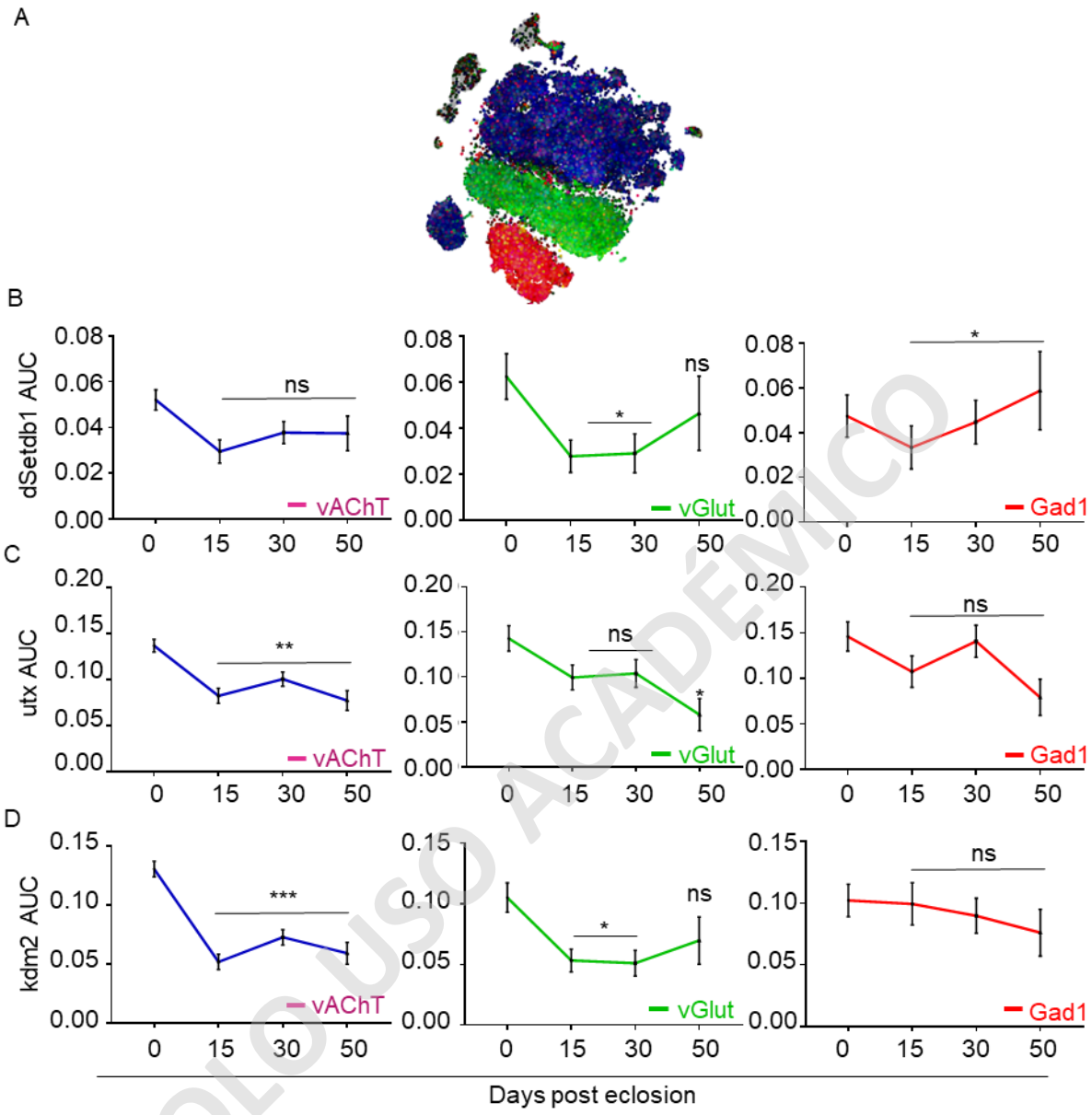

Figure 15. Decreased expression of utx and kdm2 could contribute to the age-associated increase in H3K9Me3, contributing to the decrease of UPR^{MT} in vAChT, but not vGlut and Gad1 neurons of aged flies. A) Dot plot of Scope single-cell expression analysis showing vAChT neurons in blue, vGlut neurons in green, and Gad1 positive neurons in red. B, C, and D) Expression levels of dSetdb1, kdm2, and utx in AUCell scores given by Scope and scenic show different expressions in different neuronal types vAChT, vGlut, and Gad1 positive neurons. One-way ANOVA statistical analysis with Dunnet multiple comparisons against time control 0 dpe. P-value: **** $p < 0.0001$; *** $p < 0.001$; ** $p < 0.01$, * $p<0.05$ and ns > 0.05 (Tables 18 to 26).

10.3 Pan-neuronal downregulation of dSetdb1 preserved olfactory function in aging and did not affect locomotor performance, circadian activity, and sleep homeostasis.

To further investigate the role of epigenetic regulation of H3K9Me3 in neuronal functionality, we generated flies with pan-neuronal knockdown of the H3K9 methyltransferase dSetdb1 and demethylases kdm2 and utx. We evaluated functions that are known to be impaired during aging by neuronal decay such as survival, locomotor performance, olfactory function, and circadian activity (Rhodenizer et al., 2008; de Nobrega and Lyons, 2020). In support of the hypothesis that epigenetic modulation plays a critical role in preserving healthspan and longevity, we found that pan-neuronal downregulation of dSetdb1 caused a significant extension in lifespan since half of this population survived at 78 dpe. In contrast, control flies presented a median survival at 68 dpe (Fig. 16D). Downregulation of utx and kdm2 did not show significant differences in survival and median survival compared to control flies (Fig. 16D). Possibly reflecting the fact that, for lifespan, dSetdb1 contributes to H3K9Me3 increase, which is harmful in aging. Moreover, young flies bearing the knockdown of dSetdb1 did not show a difference in H3K9Me3 levels. However, the flies' brain mutants for H3K9Me3 demethylases utx and kdm2 showed an increase in H3K9Me3 levels (Fig. 16C).

Olfactory function was assessed using the olfactory T-maze. The pan-neuronal knockdown of the specific H3K9 methyltransferase dSetdb1 showed no significant difference with control flies at 0 dpe. Remarkably, aged dSetbd1 knockdown flies showed increased olfactory function compared to age-matched control flies (Fig. 17B), indicating that dSetdb1 knockdown preserved olfactory function in 45 dpe flies. Pan-neuronal knockdown of utx and kdm2 impaired olfactory function in young flies, with a similar discrimination capacity to 45dpe control flies (Fig. 17B). However, since the pan-neuronal driver Elav-Gal4 controls the RNAi-mediated dSetdb1 knockdown, we cannot discard that a non expected effect of the genetic intervention contributes to the observed phenotype.

Moreover, dSetdb1 did not preserve neither locomotor nor circadian spontaneous activity (Fig. 18 and 19), suggesting that dSetdb1 flies do not regulate age-associated loss of locomotor or circadian activity but can be involved in circadian sleep regulation since it

inhibits the increase in sleep events in aged flies and reduces the length of sleep events in young flies (Fig. 20B and C).

Interestingly, we observed that the knockdown of utx and kdm2 did not show a significant difference in the number of sleep events but significantly reduced locomotor performance, circadian activity, and length of sleep events in young flies (Fig. 20B and C). These results indicate that the effect of dSetdb1 on inhibiting age-associated decline of function is specific to the olfactory circuit and that increasing the levels of H3K9Me3 in young animals impaired function resembling the one observed in aged animals. These results imply that the forced demethylation by downregulation of dSetdb1 for H3K9 in aging enabled UPR^{MT} activation, which increased median survival and prevented the age-associated decline of olfactory function and H3K9Me3 increase associated with aging. As the dSetdb1 downregulation specifically ameliorated the age-associated decline in the olfactory function, but no other behaviors affected by an age-related impairment, we focused this work on the olfactory circuits for further investigation.

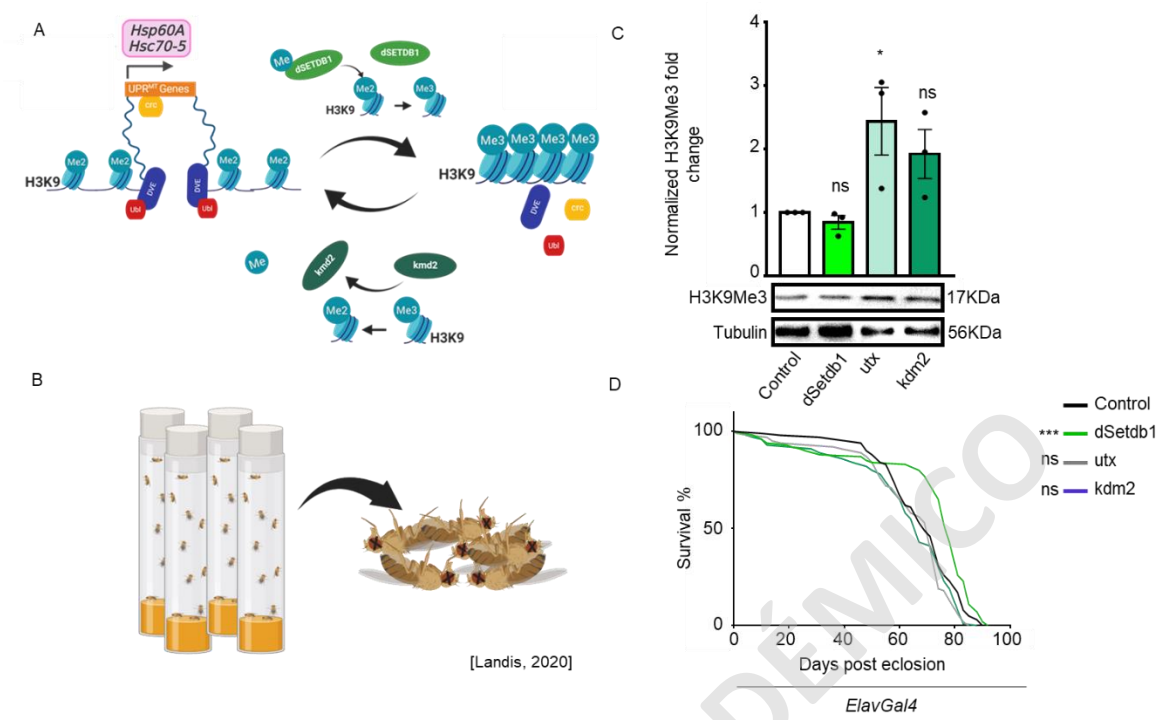

Figure 16. dSetdb1 pan-neuronal downregulation increases healthspan. A) Survival curve of flies bearing pan-neuronal downregulation of dSetdb1 in green, utx in gray, and kdm2 in calypso. B) Western blot of H3K9Me3 in young flies with pan-neuronal downregulation of dSetdb1 in green, utx in gray, and kdm2 in calypso. For survival curve, Gehan-Breslow-Wilcoxon statistical test and grouped experiments. One-way ANOVA statistical analysis with Dunnet multiple comparisons against control genotype was performed. P-value: **** $p < 0.0001$; *** $p < 0.001$; ** $p < 0.01$, * $p<0.05$ and ns > 0.05 (Tables 27 and 28).

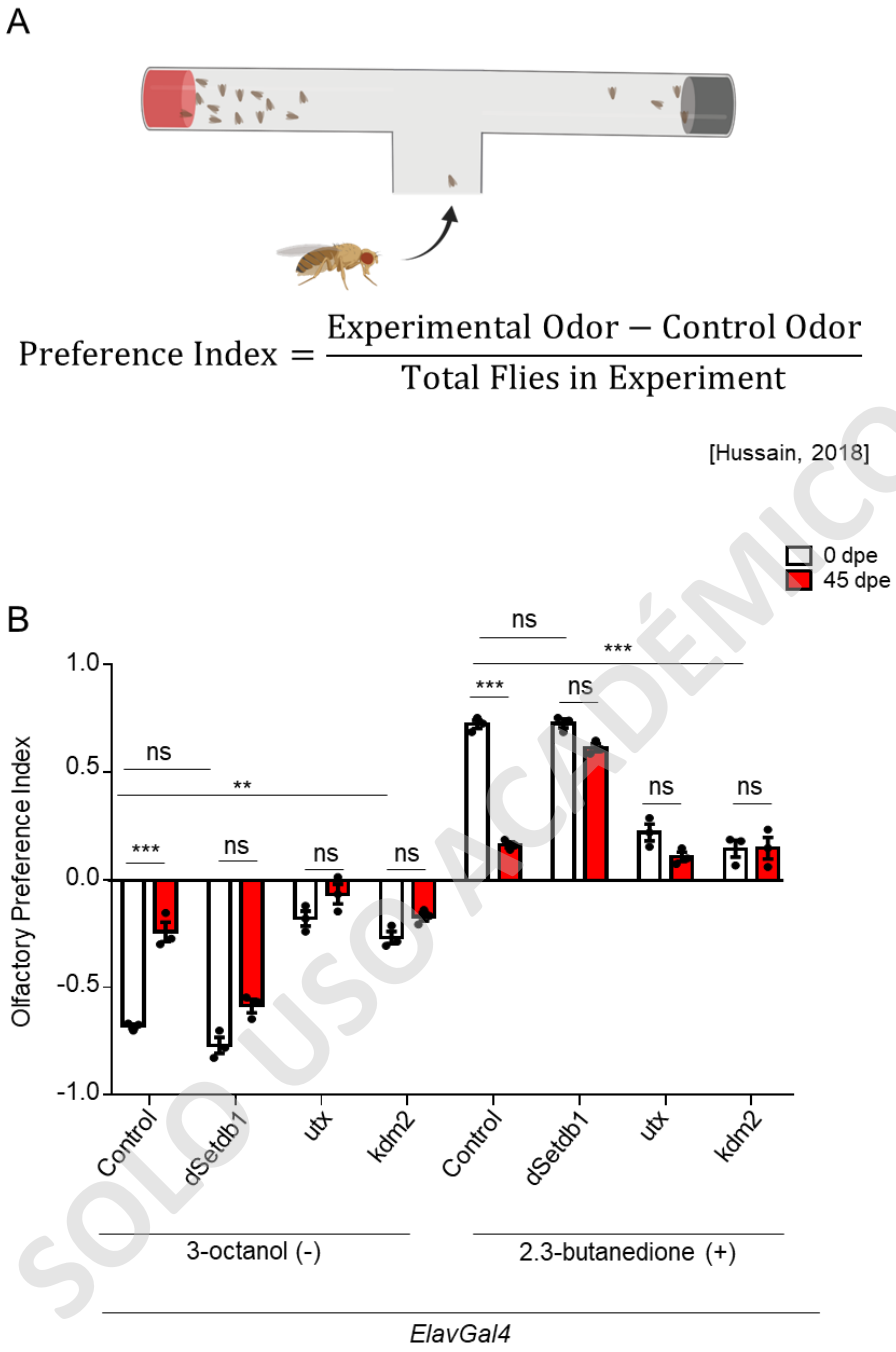

Figure 17. dSetdb1 pan-neuronal downregulation preserves olfactory function. A) Scheme of olfactory paradigm. B) Olfactory preference index for young and aged with the downregulation of *dSetdb1, utx,* and kmd2. Flies were exposed to pleasant odor (+) and abrasive odor (-). Two-way ANOVA statistical analysis with Bonferroni's multiple comparisons between different genotypes of the same age and different ages in the same genotype was performed. P-value: *** $p < 0.001$; ** $p < 0.01$, * $p<0.05$ and ns > 0.05 (Table 29).

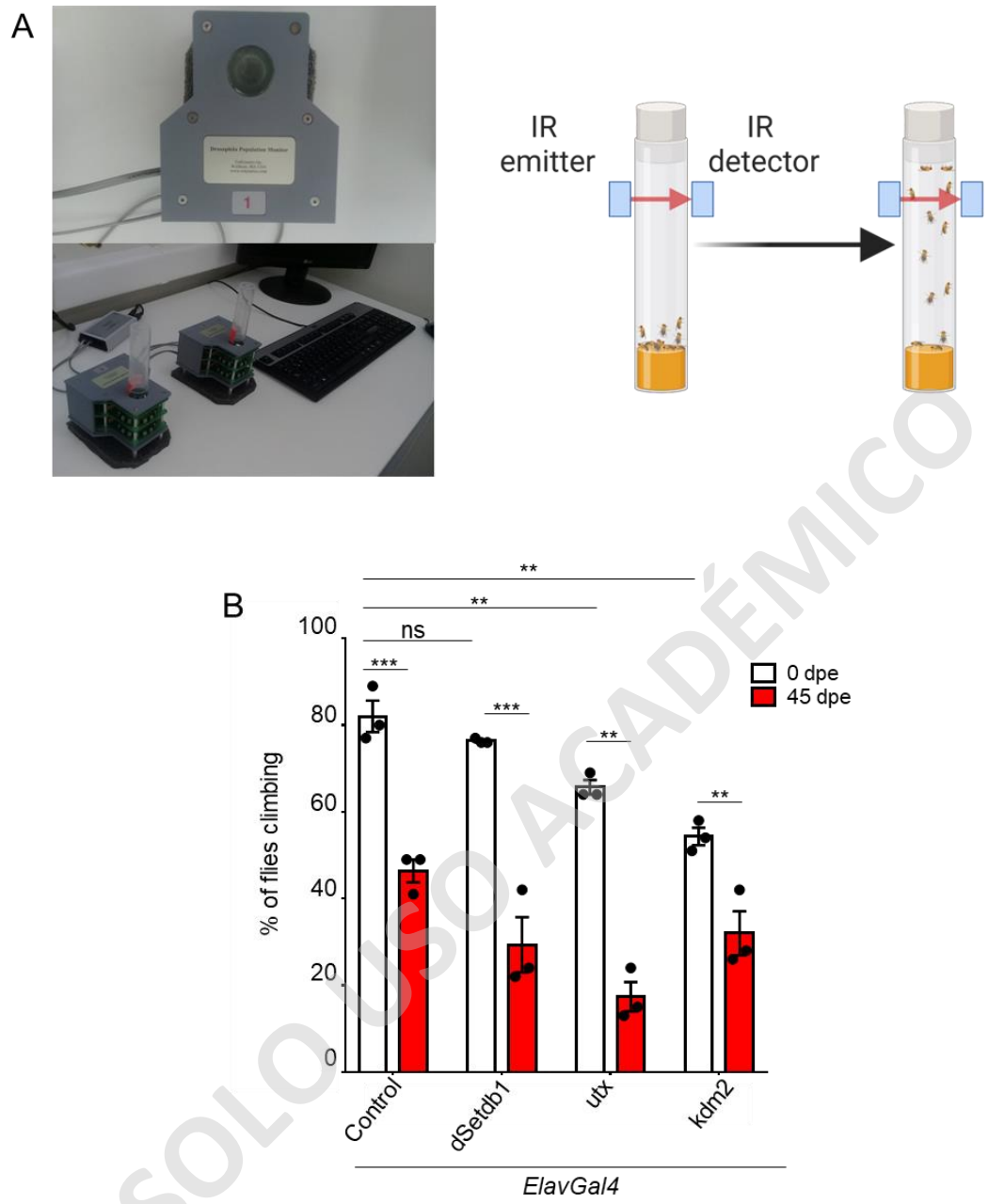

Figure 18. dSetdb1 pan-neuronal downregulation does not affect the age-associated decline in locomotor performance. A) *Drosophila* Activity Monitor System Setup and scheme of reading detection using Infra-Red emitter and receptor. B) Locomotor activity of young and aged flies for the pan-neuronal knockdown of dSetdb1, kdm2, and utx. White bars are 0 dpe flies, and red bars are 45 dpe flies. Two-way ANOVA statistical analysis with Dunnet multiple comparisons between different genotypes of the same age and different ages in the same genotype was performed. P-value: **** $p < 0.0001$; *** $p < 0.001$; ** $p < 0.01$, * $p<0.05$ and ns > 0.05 (Table 30).

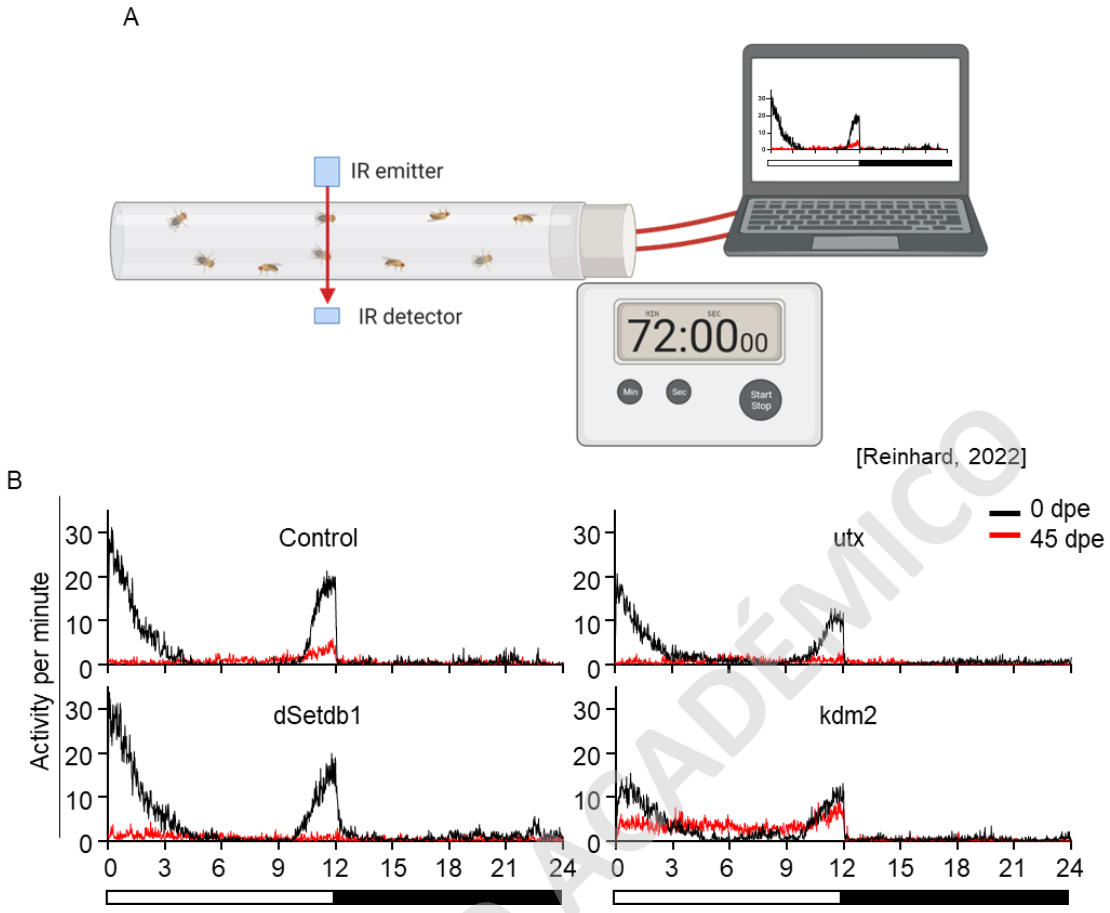

Figure 19. dSetdb1 pan-neuronal downregulation does not affect age-associated impairment in spontaneous activity. A) Scheme of Circadian activity setup by infrared emitter and receptor. B) Activity plots for young flies (black line) and aged flies (red line) for dSetdb1, utx, and kdm2 pan-neuronal downregulation. The X-axis shows Hours. The white and black bar on X-axis denotes the time that flies spend in light in white and the dark in black. The circadian cycle of 12:12 (light: dark). Black lines are 0 dpe flies, and red lines are 45 dpe flies. Two-way ANOVA statistical analysis with Bonferroni's multiple comparisons between different genotypes of the same age and different ages in the same genotype was performed. P-value: *** $p < 0.001$; ** $p < 0.01$, * $p<0.05$ and ns > 0.05.

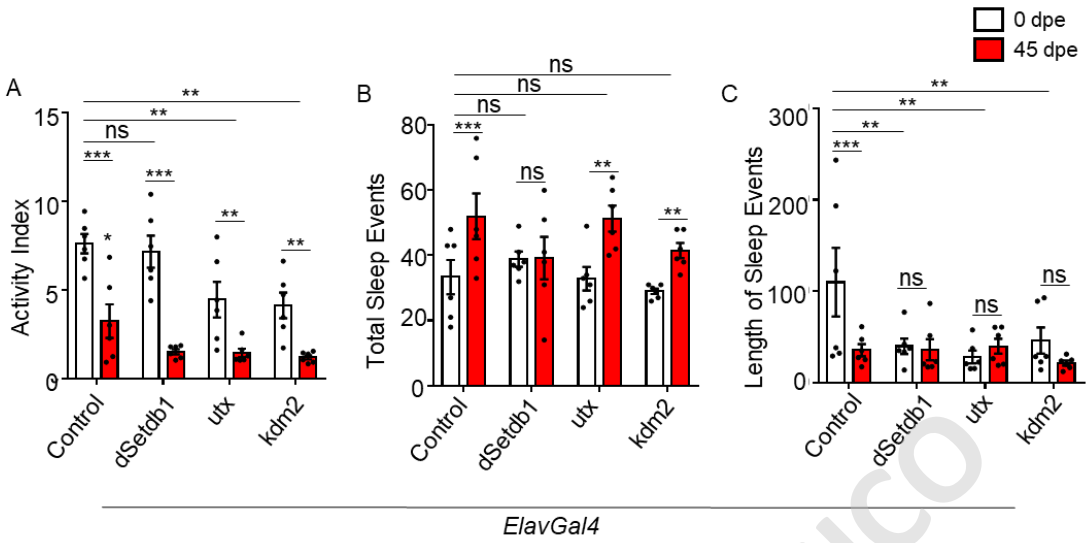

Figure 20. dSetdb1 pan-neuronal downregulation does not affect age-associated impairment in spontaneous activity and sleeps homeostasis. A) Circadian activity index of young and aged flies bearing knockdown for H3K9Me3 regulating enzymes. B) Number of sleep events C) Length of sleep events of young and aged flies bearing the pan-neuronal downregulation of H3K9Me3 regulating enzymes. White bars represent young animals, and red bars are aged animals. Two-way ANOVA statistical analysis with Bonferroni's multiple comparisons between different genotypes of the same age and different ages in the same genotype was performed. P-value: *** $p < 0.001$; ** $p < 0.01$, * $p<0.05$ and ns > 0.05 (Table 31 to 33).

10.4 Downregulation of dSetdb1 in OPNs restores olfactory function in aging through UPR^{MT} activation by decreasing H3K9Me3.

Since it has been reported that OPNs present an age-associated decline in function (Hussain et al., 2018), we inquire whether the regulation of vChAT neurons is conserved in OPNs. Downregulation of dSetdb1 decreases H3K9Me3 in aging, allowing the chromatin opening (Fig. 14D) and enabling the UPR^{MT} nuclear activators such as crc and dve to activate the transcriptional pathway, posibly by binding to the chromatin (Fig. 10). Moreover, pan-neuronal knockdown of UPR^{MT} transcriptional activators reduced UPR^{MT} reporter signal and impaired olfactory function in young flies (Fig. 10 and 12). Thus, we hypothesize that UPR^{MT} inhibition by downregulation of UPR^{MT} transcriptional activators should act downstream of the phenotypes of dSetdb1. To evaluate if the preservation of olfactory function in aged flies bearing the dSetdb1 knockdown was dependent on UPR^{MT} activation, we generated flies carrying the double knockdown of dSetdb1 together with dve or crc, respectively (Fig. 21). Olfactory function was evaluated by presenting young and old flies to pleasant odor 2,3-butanedione. dSetdb1 knockdown alone preserved olfactory function at 45 dpe in contrast to control aged flies. However, the double knockdown of dSetdb1 with dve or crc abolished the preservation of olfactory function in aging, reaching old control levels (Fig. 21B). Moreover, dve and crc knockdown in OPN impaired olfactory function of young flies resembling the performance of 45 dpe control flies. Since its olfactory preference index did not show a significant difference, the crc and dve knockdown phenotype was predominant over dSetdb1 knockdown and abolished the preservation of olfactory function in 45 dpe animals (Fig. 21B). This data demonstrates that dve and crc are downstream of dSetdb1 epigenetic regulation over H3K9Me3 and that preservation of olfactory function in aging partly depends on UPR^{MT}.

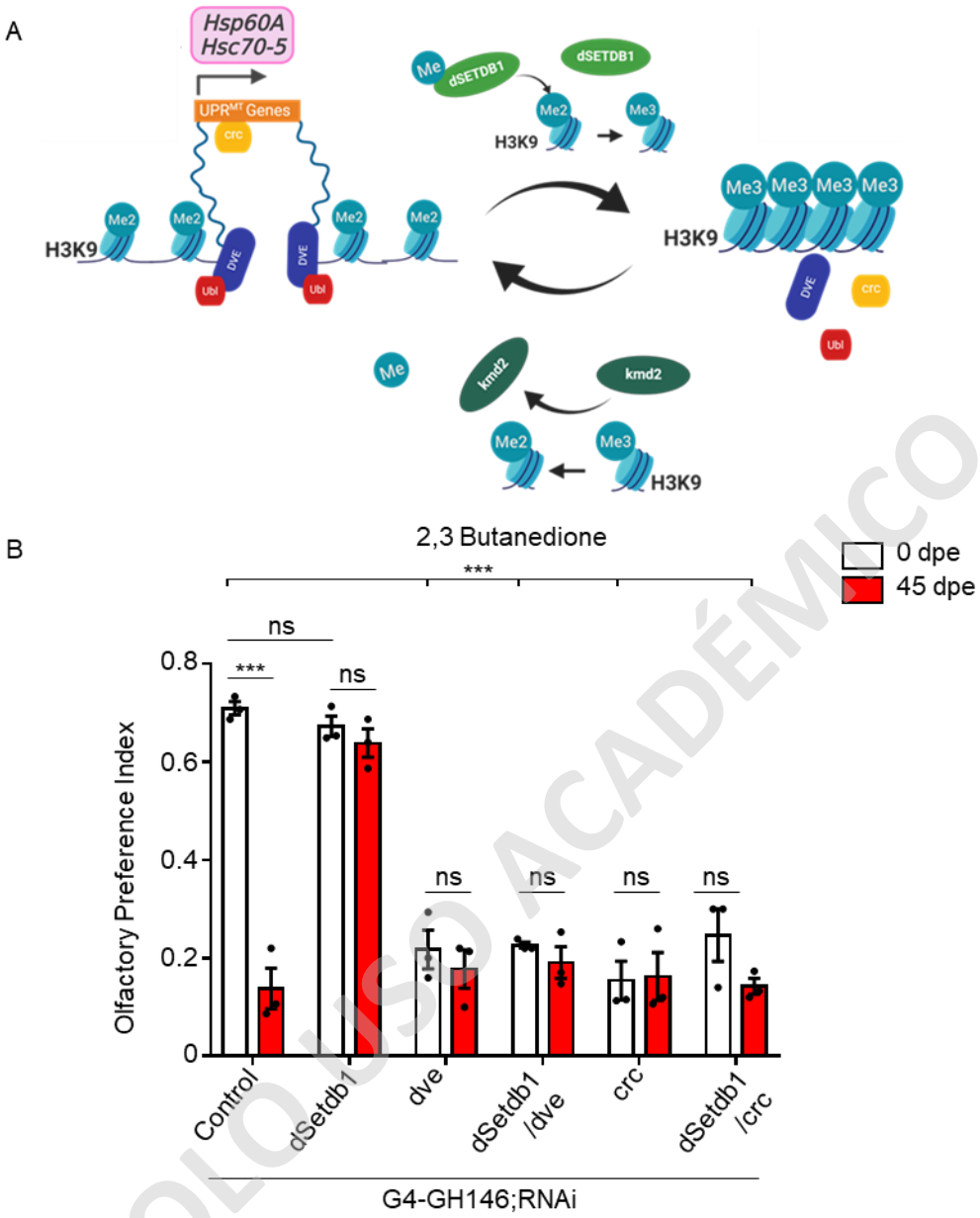

Figure 21. dSetdb1 knockdown in OPNs induces the UPR^{MT} activation in aging and inhibits the age-associated increase of H3K9Me3. A) Scheme of the proposed model for H3K9Me3 regulation on UPR^{MT} in aging. B) Olfactory preference index of flies bearing the GH146 driven knockdown of dSetdb1, dve. crc and the double knockdown of dSetdb1/dve and dSetdb1/crc, respectively. White bars are 0 dpe flies, and red bars are 45 dpe flies. Two-way ANOVA statistical analysis with Bonferroni's multiple comparisons between different genotypes of the same age and different ages in the same genotype was performed. P-value: *** $p < 0.001$; ** $p < 0.01$, * $p<0.05$ and ns > 0.05 (Table 34).

To evaluate if dSetdb1 regulates UPR^{MT} reporter activity in OPNs of the AL in aged *Drosophila*. We tagged OPNs with CD8::GFP and evaluated the Hsp60A::dsRed signal, specifically in GFP-tagged neurons. We observed that UPR^{MT} reporter activity increased in 0 dpe flies treated with the mitochondrial stressor paraquat (PQ) compared to animals treated with vehicle only. However, this response to the mitochondrial stressor was deficient in 45 dpe animals (Fig. 22). Remarkably, RNAi-mediated knockdown of dSetdb1, specifically in OPNs, preserved UPR^{MT} activation marked by the increase in UPR^{MT} fluorescent reporter activity in response to PQ (Fig. 22B). This decrease in UPR^{MT} response capacity correlates with the increase of H3K9Me3 levels, specifically in GH146-positive neurons, marked by the increase in H3K9Me3 integrated density and volume of the signal, specifically in OPNs. This increase in H3K9Me3 volume and integrated density was prevented by dSetdb1 knockdown in OPNs (Fig. 23B and C). This data demonstrated that dSetdb1 negatively regulates UPR^{MT} through H3K9Me3 in aged OPNs.

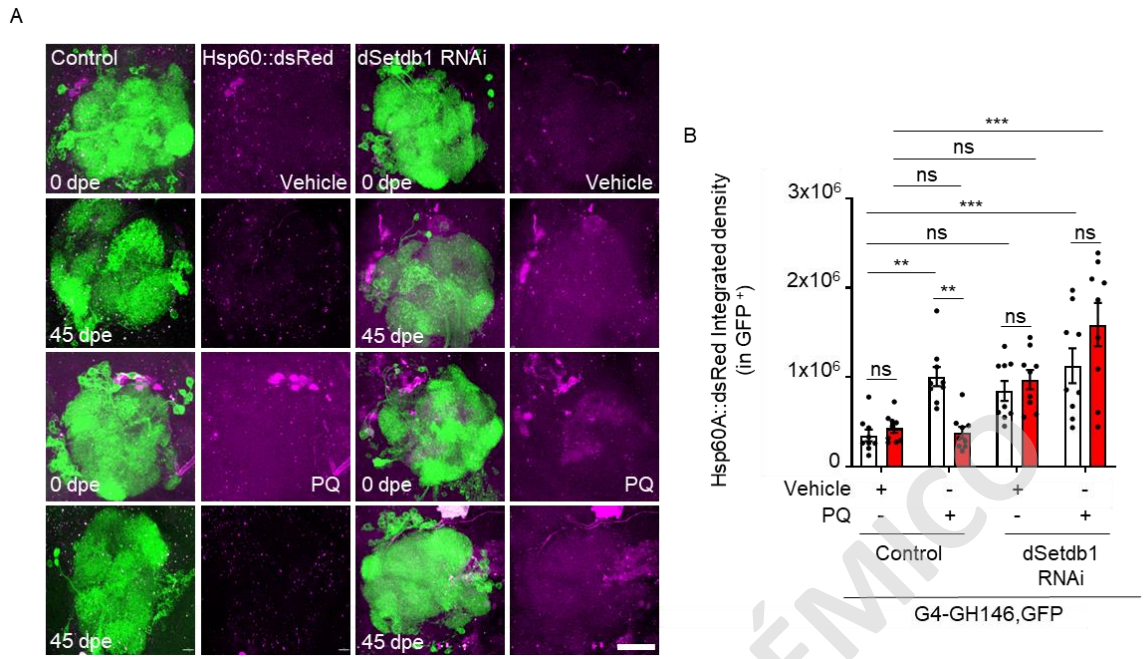

Figure 22. dSetdb1 knockdown in OPNs induces the UPR^{MT} activation in aging. A) Representative images of OPNs labeled with GFP (green) bearing the UPR^{MT} reporter Hsp60::dsRed (magenta) in the AL of young and aged flies treated with PQ or vehicle. D) Integrated density of Hsp60A::dsRed specifically in the GFP labeled neurons in the AL of young and aged flies treated with vehicle or PQ. Scale Bar is 10µm. Two-way ANOVA statistical analysis with Bonferroni's multiple comparisons between different genotypes of the same age and different ages in the same genotype was performed. P-value: *** $p < 0.001$; ** $p < 0.01$, * $p<0.05$ and ns > 0.05 (Table 35).

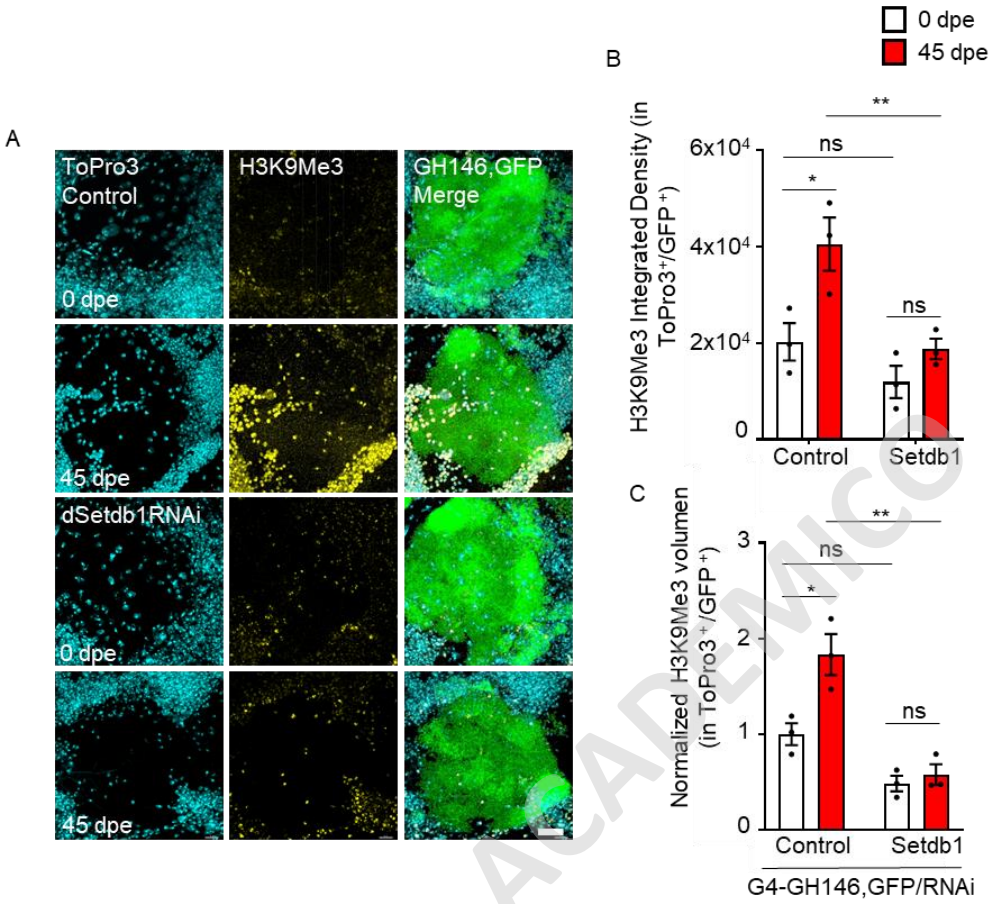

Figure 23. dSetdb1 knockdown in OPNs inhibits the age-associated increase of H3K9Me3. A) Representative images of GFP-tagged OPNs in the AL of young and aged flies bearing the downregulation of dSetdb1 under the control of the GH146 driver. Nuclei are in cyan (ToPro3), H3K9Me3 is in yellow, and the right panel is a merge of three channels with OPNs in green. B) H3K9Me3 integrated density specifically in the nucleus of GFP-tagged OPN of young and aged flies. C) H3K9Me3 volume, specifically in nuclei of GFP signal normalized to control of young and aged flies bearing the downregulation of dSetdb1. Scale Bar is 10µm. Two-way ANOVA statistical analysis with Bonferroni's multiple comparisons between different genotypes of the same age and different ages in the same genotype was performed. P-value: *** $p < 0.001$; ** $p < 0.01$, * $p<0.05$ and ns > 0.05 (Tables 36 and 37).

Additionally, using SCope for single-cell expression analysis, we evaluated the expression of UPR^{MT} reporters and H3K9Me3 regulating enzymes, specifically in OPNs. OPNs presented a decrease in Hsp60 and Hsc70-5 in aging (Fig 24C and D), with constant levels of dSetdb1 and decreased levels of kdm2 (Fig. 24E to G). This data suggests a role for kdm2 in the age-associated increase of H3K9Me3.

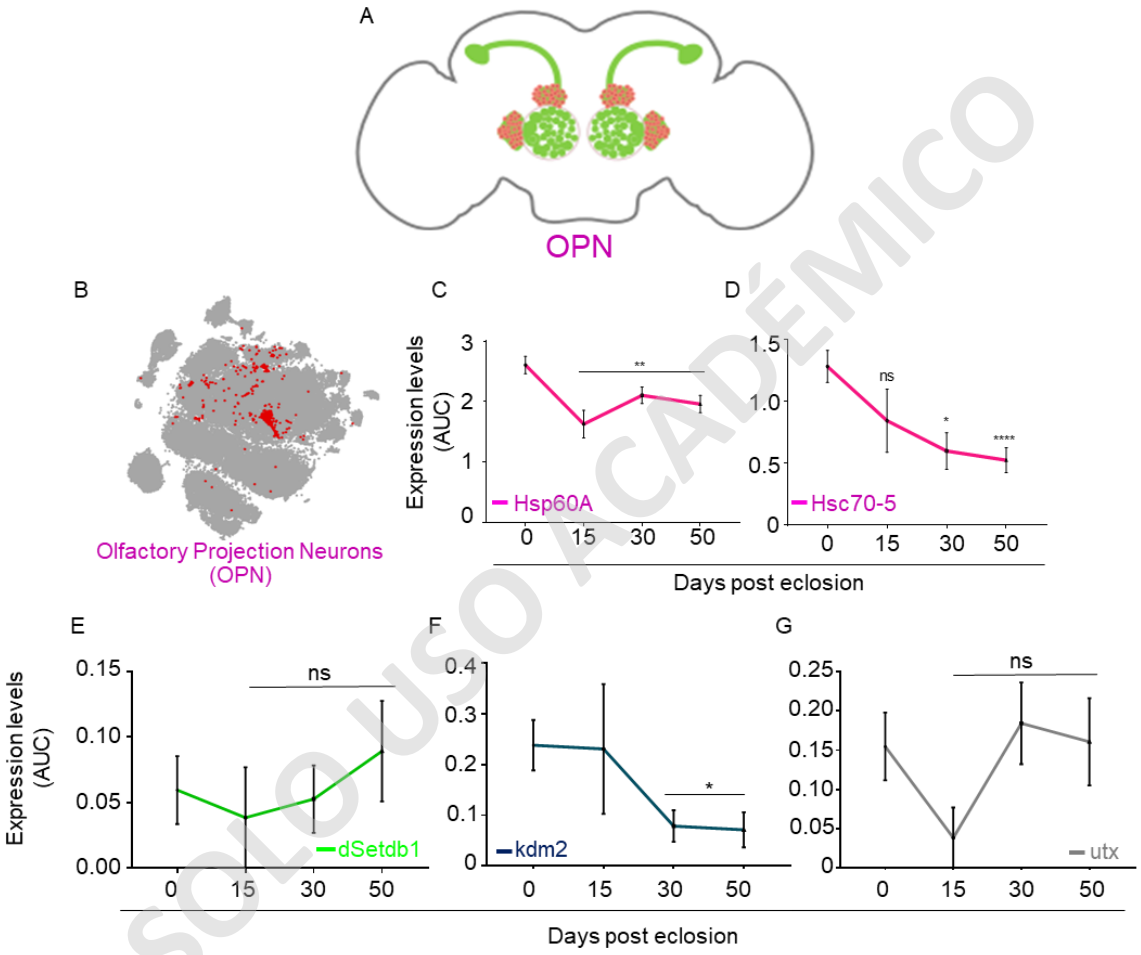

Figure 24. Reduced expression of utx and kdm2 contributes to the age-associated increase in H3K9Me3 in OPNs, which may be related to the decrease of UPR^{MT} in aged flies' cholinergic neurons. A) Scheme of Olfactory Projection Neuron (OPN) circuit in the *Drosophila* brain. B) Dot plot of expression cluster showing specifically OPN cluster in red. C) Hsp60A and D) Hsc70-5 expression levels expressed in AUC values in the olfactory nervous system through aging. E, F, and G) Expression levels of dSetdb1, kdm2, and utx in OPNs through aging. One-way ANOVA statistical analysis with Dunnet multiple comparisons against time control 0 dpe. P-value: **** $p < 0.0001$; *** $p < 0.001$; ** $p < 0.01$, * $p<0.05$ and ns > 0.05 (Tables 38 to 42).

10.5 Downregulation of dSetdb1 in OPNs restores age-associated mitochondrial abnormalities.

Aging has been widely associated to mitochondrial dysfunction, including an increase in mitochondrial ROS that leads to the impairment of mitochondrial redox balance, and morphological parameters such as the reduction of mitochondrial neuronal coverage, mitochondrial swelling, and an increase in mitochondrial fragmentation (Chistiakov et al.; Beal, 2005; Lores-Arnaiz et al., 2016; Arrázola et al., 2019; Rottenberg and Hoek, 2021). Changes in the activation capacity of the UPR^{MT} influence mitochondrial morphology and function (Merkwirth et al., 2016; Yuan et al., 2020; Ng et al., 2021; Zhou et al., 2022). Importantly, changes in mitochondrial morphology have been associated to their functional capabilities and to degenerative mechanisms of neurons (Court and Coleman, 2012; Salvadores et al., 2017; Arrázola et al., 2019).

Therefore, we inquired if activation of UPR^{MT} in aging by downregulation of dSetdb1 could influence mitochondrial morphology and oxidation in OPNs. In order to analyze mitochondrial morphology in OPNs, we expressed the mitochondrial reporter mitoGFP under the control of the GH146-Gal4 driver and analyzed mitochondria from three neuronal compartments of OPNs, first the AL which contains the cell bodies, secondly the distal part of the axonal tract which is projected from anterior to posterior in the *Drosophila* brain, and third, the Lateral Horn (LH) a zone enriched in presynaptic terminals (Fig. 25A). We found that the AL mitochondria presented significant changes in mitoGFP integrated density, total mitoGFP volume, fragmentation index, and sphericity in 45 dpe flies. These age-associated changes were restored to 0 dpe levels by dSetdb1 downregulation in OPNs (Fig. 25B-F). When we evaluated mitoGFP signal in the axonal tract of OPNs, we observed that mitoGFP signal in 45 dpe control axons was significantly reduced in comparison to 0 dpe control axons (Fig. 25G-H). Knockdown of dSetdb1 reduced the age-associated decrease in fluorescence intensity per mitoGFP volume in 0 dpe flies when compared to age-matched controls, but did not present a reduction of mitoGFP signal between 45 and 0 dpe axons (Fig. 25G-H). Lastly, we did not observe significant changes in the age-associated decline in mitochondria located in the LH when comparing *dSetdb1* knockdown flies with age-matched control flies nor between control flies (Fig. 26I-J).

These results indicate that mitochondria of OPNs presents morphological changes in aging such as the decrease in mitoGFP signal in AL and axon, but not in the LH. However, OPN's mitochondrial located in the AL presented and age-associated increase mitochondrial morphological features associated to neurodegeneration such as mitochondrial fragmentation and swelling. Importantly, dSetdb1 downregulation reduced the age-associated degeneration in OPNs of the AL.

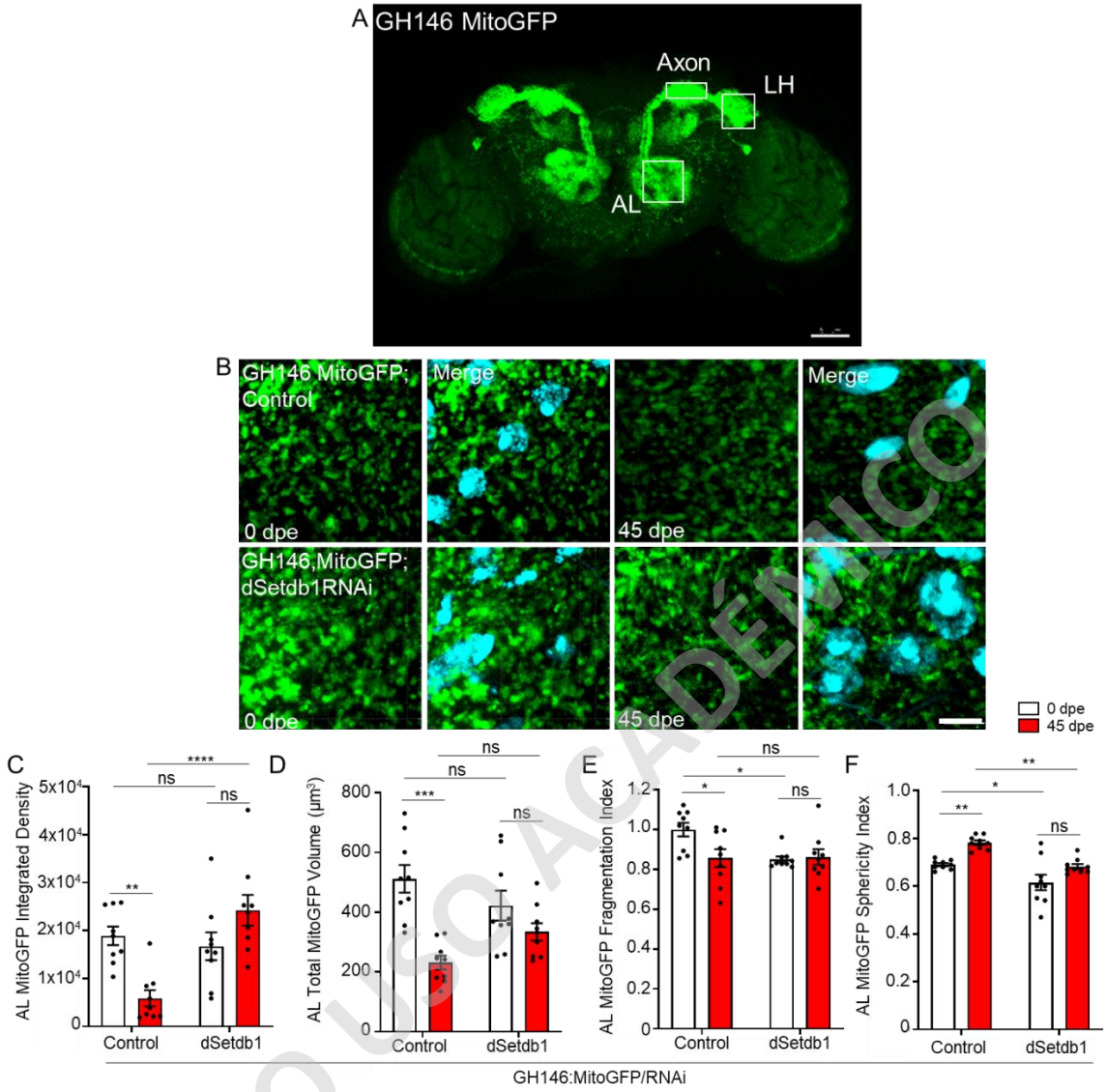

Figure 25. Effect of UPR^{MT} activation by dSetdb1 downregulation in mitochondria of OPNs. A) Upper panel shows schematics of GH146, GFP neuronal circuit, and the lower panel shows mitochondrial GFP reporter expressed in OPNs by the GH146 driver. Neurons possess their soma in the antennal lobe (AL) and project their axons to the synapsis enriched zone, the lateral horn (LH). B) Mitochondria labeled with GFP in the AL of OPNs of young and aged flies bearing the *dSetdb1*. Mitochondria in Green and nuclei in ToPro3. C) Mitochondria from AL integrated density of young and aged flies bearing the knockdown of dSetdb1. D) AL total mitochondrial volume of images showed in B. E) AL mitochondrial fragmentation index of images in B. F) AL sphericity index of mitochondria showed in B. Scale Bar for A is 50µm and for B is 5µm. Two-way ANOVA Bonferroni's multiple comparisons test. P-value: *** $p < 0.001$; ** $p < 0.01$, * $p<0.05$ and ns > 0.05 (Table 43 to 46).

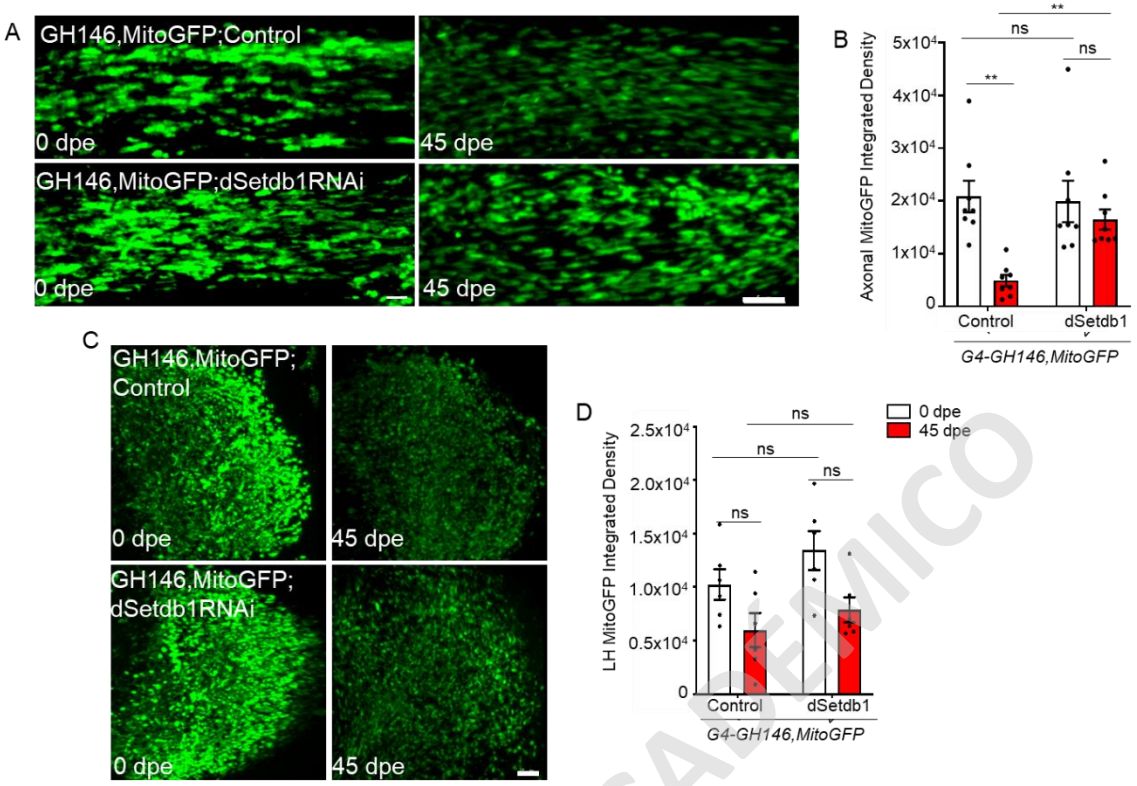

Figure 26. dSetdb1 downregulation in OPN preserves axonal, and LH mitochondrial GFP integrated density. A) Representative images of Axonal mitochondria in the green of young and aged flies bearing the knockdown of dSetdb1. B) Integrated density of axonal mitochondria showed in A. C) Mitochondrial reporter in green in LH of young and aged flies bearing the knockdown of dSetdb1. D) Integrated density of mitochondria showed in I. Scale bars for A and C are 5 and 10µm, respectively. Two-way ANOVA Bonferroni's multiple comparisons test. P-value: *** $p < 0.001$; ** $p < 0.01$, * $p<0.05$ and ns > 0.05 (Tables 47 and 48).

10.6 Downregulation of dSetdb1 restores mitochondrial oxidation in aged OPNs.

To further evaluate the effect of UPR^{MT} activation in aging by dSetdb1 downregulation in mitochondria of OPNs, we assessed mitochondrial capacity to maintain its redox balance in 0 and 45 dpe flies *in vivo* using the mitochondrial oxidation reporter MitoTimer. It encodes a green fluorescent protein which shifts to red fluorescence when oxidized (Laker et al., 2014). Thus, mitochondrial redox balance can be quantified by analyzing the mitochondrial red/green ratio, where oxidized mitochondria will tend to red and healthy mitochondria maintains green. Mitochondria red/green ratio presents an increase in 45 dpe control flies when compared to 0 dpe control flies in the AL, axonal tract and the LH (Fig. 27K-P). Importantly, we observed an increase in Red/Green Ratio of MitoTimer signal in mitochondria from all three neuronal compartments in 45 dpe flies when compared to 0 dpe (Fig. 27). Remarkably, downregulation of dSetdb1 in OPNs preserved mitochondrial red/green ratio levels in 45 dpe flies when compared to age-matched control animals. Mitochondrial red/green ratio levels were preserved in AL, axonal tract and LH (Fig. 27K, M and O). This data indicates that activation of UPR^{MT} in aging by dSetdb1 downregulation in OPNs is sufficient to lessen the age-associated mitochondrial oxidation, which correlates with the impairment of neuronal function in the olfactory system.

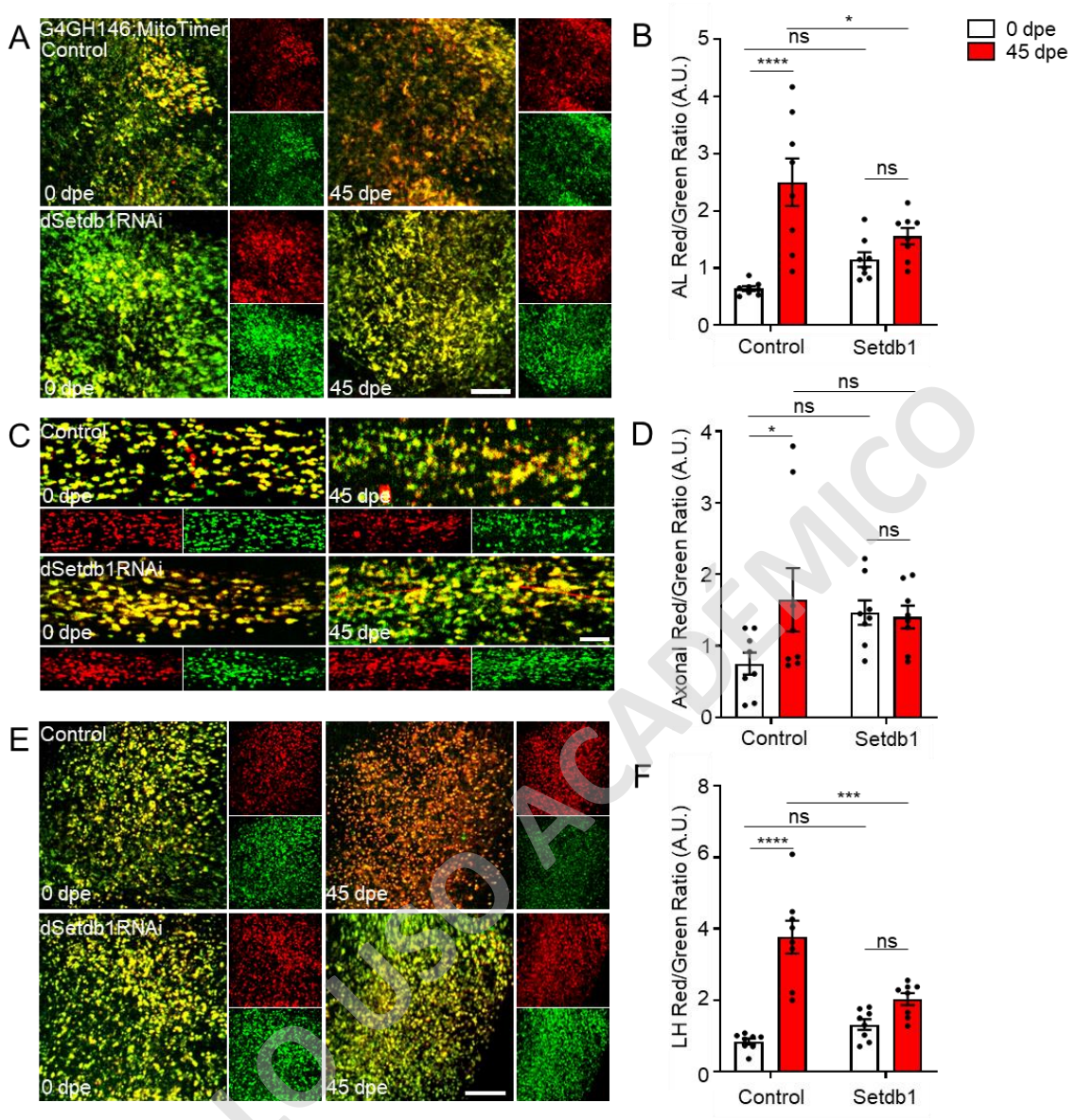

Figure 27. Downregulation of dSetdb1 restores mitochondrial oxidation in aged OPNs. A, C, and D) Representative images of AL, Axonal, and LH showing GH146 GAL4; UAS-MitoTimer, an *in vivo* mitochondrial oxidation reporter at 488 (Green) and 561 (Red) and Merge (Yellow). B, D, and F) Red/Green Ratio of Integrated density of A, C, and D. Scale Bar is 5µm. Two-way ANOVA Bonferroni's multiple comparisons test. P-value: *** $p < 0.001$; ** $p < 0.01$, * $p<0.05$ and ns > 0.05 (Tables 49 to 51).

10.7 Epigenetic regulation of UPR^{MT} by dSetdb1 contributes to the age-associated neurodegeneration of OPNs.

Loss of neuronal function is often associated with degenerative structural changes of the neuronal circuit (Jellinger, 2010; Levenson et al., 2014). Therefore, we inquired if either UPR^{MT} activation by dSetdb1 downregulation or UPR^{MT} inactivation by dve knockdown was due to neurodegeneration of OPNs.

To assess the effect of modulation of UPR^{MT} activation by dSetdb1 or dve downregulation in the neuronal integrity OPNs, we examined OPNs structural integrity by expressing CD8::GFP under the control of the Gal4-GH146 driver, in together with dSetdb1 or dve downregulation. We analyzed three neuronal compartments separately: the AL, the axonal tract, and the LH. To establish changes in neuronal numbers along aging, we counted To-Pro3 positive nuclei specifically in GFP-positive OPNs. As expected, aging leads to a decrease in OPN numbers in control flies, and dSetdb1 knockdown protects from this age-dependent decrease in neuronal numbers (Fig. 28A-B). Knockdown of dve reduced the number of OPN nuclei in young animals to values associated to aged controls (Fig. 6B), in concordance with the effect over olfactory function.

We next evaluated axonal integrity of OPNs by measuring the total axonal tract volume of GFP-labelled OPNs (Fig. 29A). As expected, 45 dpe control flies show a decrease in the axonal integrated density of GFP-labelled OPNs when compared to 0 dpe control flies. Importantly, we found that 45 dpe dSetdb1 knockdown flies maintained axonal integrated density at 45 dpe, which not present significant changes when compared to 0 dpe axons (Fig. 29B-C). Likewise, dve knockdown in OPNs reduced axonal volume, and axonal integrated density in 0 dpe flies compared to age-matched controls animals and did not present significant changes through aging as seen in 45 dpe flies compared to 0 dpe flies (Fig. 29B-C). These results indicate UPR^{MT} activation in 45 dpe flies by the knockdown of dSetdb1 correlates with the maintenance GFP positive nuclei number and axonal integrated density in 45 dpe animals, which in turn correlates with the inhibition of the age-associated decline in olfactory function. Concordantly, UPR^{MT} attenuation by downregulation of dve in 0 dpe flies reduced neuronal number and axonal integrated density, which correlates with the impairment of olfactory function in 0 dpe flies.

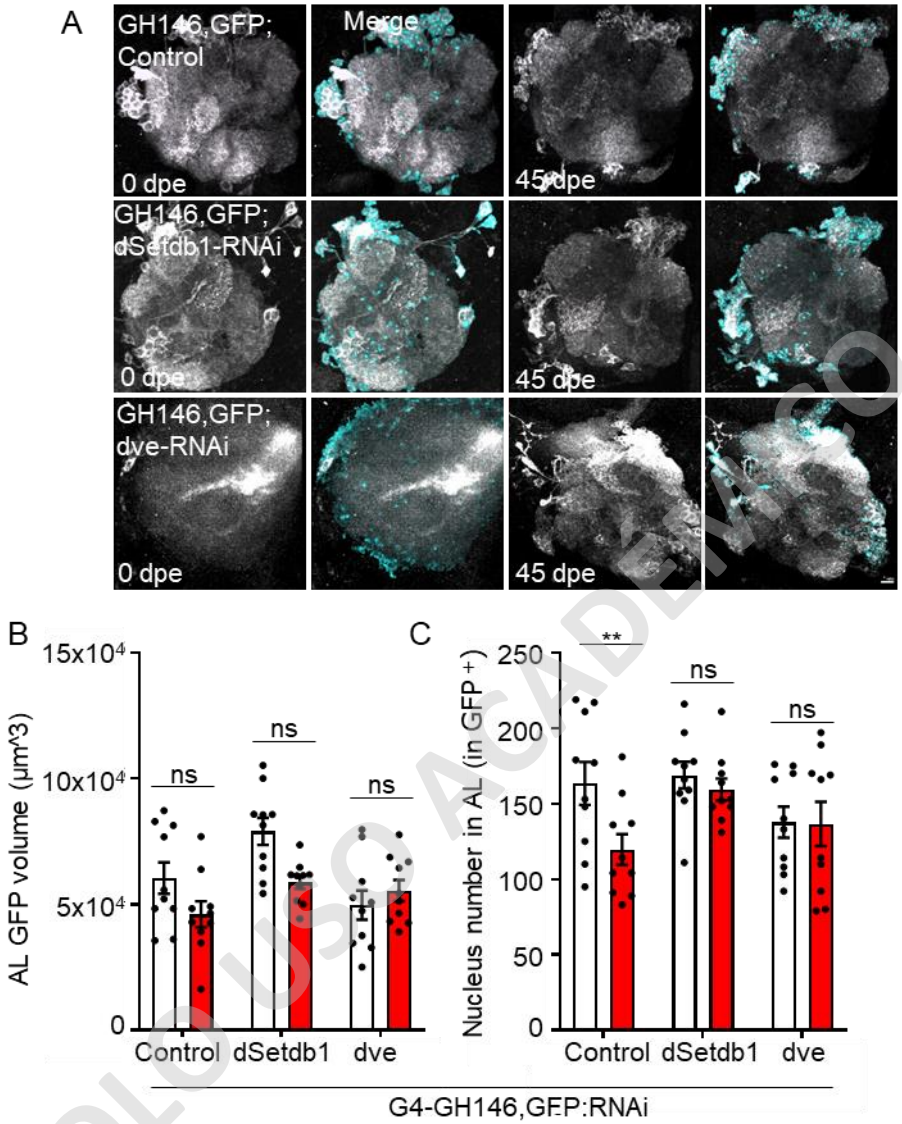

Figure 28. Downregulation of dSetdb1 inhibits the decrease in OPNs nucleus number. A) AL of OPNs tagged with GFP with the knockdown of dSetdb1 and dve. GFP-tagged neurons are gray, and the right panel shows merged channels with nuclei labeled with ToPro3 in cyan, specifically in GH146, GFP neurons. B) AL volume of B. C) Nucleus count specifically in GH146, GFP neurons. Scale Bar is 10µm. Two-way ANOVA statistical analysis with Bonferroni's multiple comparisons. P-value: *** $p < 0.001$; ** $p < 0.01$, * $p<0.05$ and ns > 0.05 (Table 52 and 53).

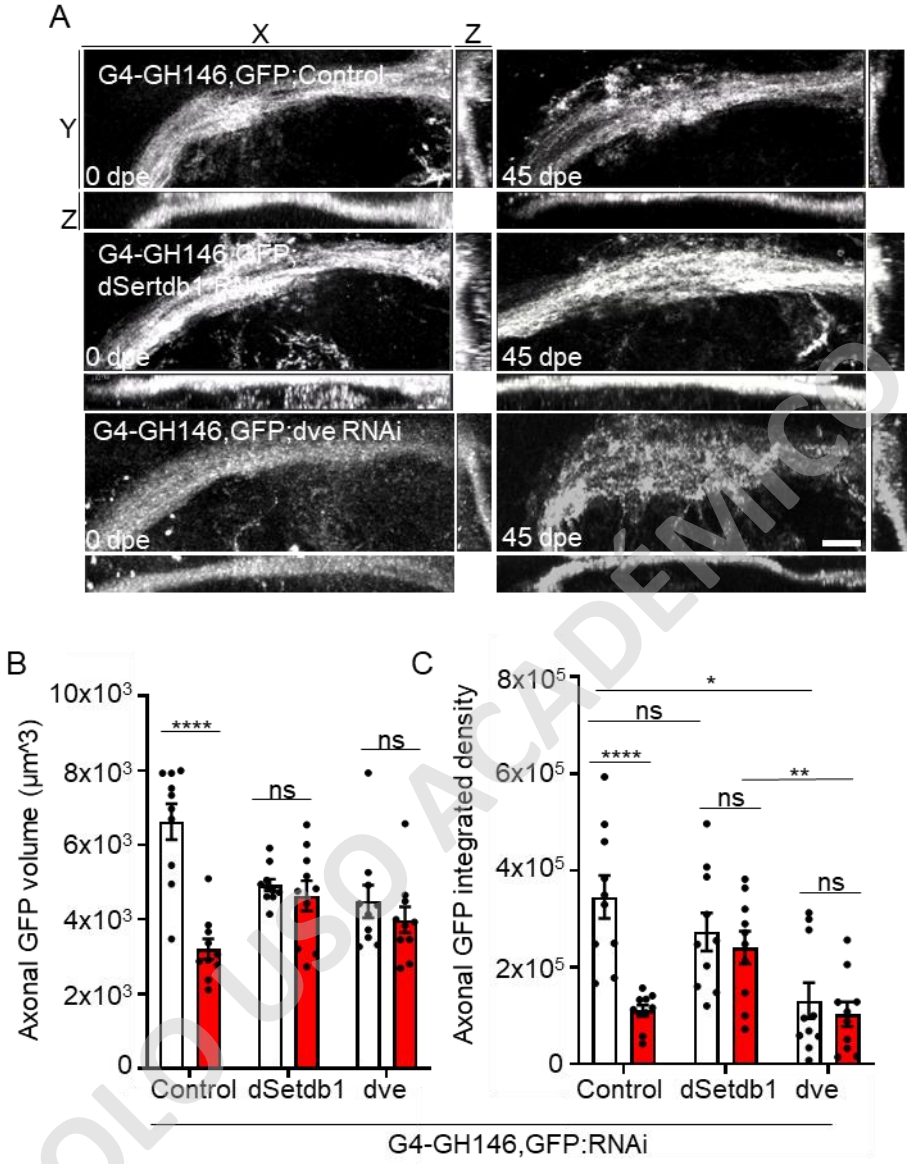

Figure 29. Downregulation of dSetdb1 inhibits the decrease in OPNs axonal GFP signal. A) Orthogonal view of the 3D reconstruction of the distal axonal tract of OPNs tagged with GFP. The panel shows axons from control flies and knockdown flies of dSetdb1 and dve. Images show the combination of axis Y and X, Z and X, and Z and Y. B) axonal volume in μm^3 of the axonal tract of D. C) Axonal integrated density of D. Scale Bar 5µm. Two-way ANOVA statistical analysis with Bonferroni's multiple comparisons. P-value: *** $p < 0.001$; ** $p < 0.01$, * $p<0.05$ and ns > 0.05 (Tables 54 and 55).

10.8 UPR^{MT} epigenetic regulation on the age-associated decrease of OPNs synapsis in LH.

It has been previously demonstrated that age-associated decline in olfactory function in *Drosophila* is tightly associated to the loss of OPNs synapses (Hussain et al., 2018). Thus, we focus on the lateral horn (LH), a region enriched in presynaptic connections of OPN neurons (Fig. 30A). Importantly, 45 dpe control flies do not show significant difference in LH GFP volume in comparison with 0 dpe control flies, but they do present a significant difference in LH OPN GFP signal at 45 dpe flies (Fig. 30A-C). Importantly, dSetdb1 knockdown in OPN led to an increased GFP volume in the LH compared to age-matched controls. In contrast, knockdown of dve in OPNs significantly reduced GFP volume in LH and integrated density of 0 dpe flies compared to age-matched controls and 0 dpe dSetdb1 knockdown flies (Fig. 30B). We observed that dSetdb1 reduced the lower LH GFP volume and integrated density in 45 dpe flies when compared to 0 dpe flies of the same genotype (Fig. 30C). This data suggests that downregulation of dSetdb1 in OPNs maintain neuronal integrity in GFP-labeled OPNs axonal terminals located in the presynaptic enriched zone, the LH.

In light of the apparent reduction in integrated density of GFP-tagged OPNs in the LH, we realized a quantitative analysis of presynaptic zones tagged with the presynaptic reporter, Brp::GFP(Wagh et al., 2006), under the control of GH146-Gal4 driver. Brp::GFP volume and punctae number analyses in the LH were performed using confocal imaging and 3D reconstruction (Fig. 31D). Control 45 dpe flies presented a reduction in Brp:GFP volume and punctae when compared to 0 dpe control flies (Fig. 31D-F). Importantly, downregulation of dSetdb1 in OPNs of 0 dpe flies presented no significant changes in Brp::GFP positive punctae and Brp::GFP integrated density in comparison to age-matched controls and when compared to 45 dpe dSetdb1 flies (Fig. 31F and G). These results demonstrate that the downregulation of dSetdb1 preserves neuronal integrity of GFP-labeled OPNs and the presynaptic densities labeled with Brp:GFP, which correlated with the inhibition of the age-associated increase of H3K9Me3, UPR^{MT} activation and preservation of olfactory function in 45 dpe flies.

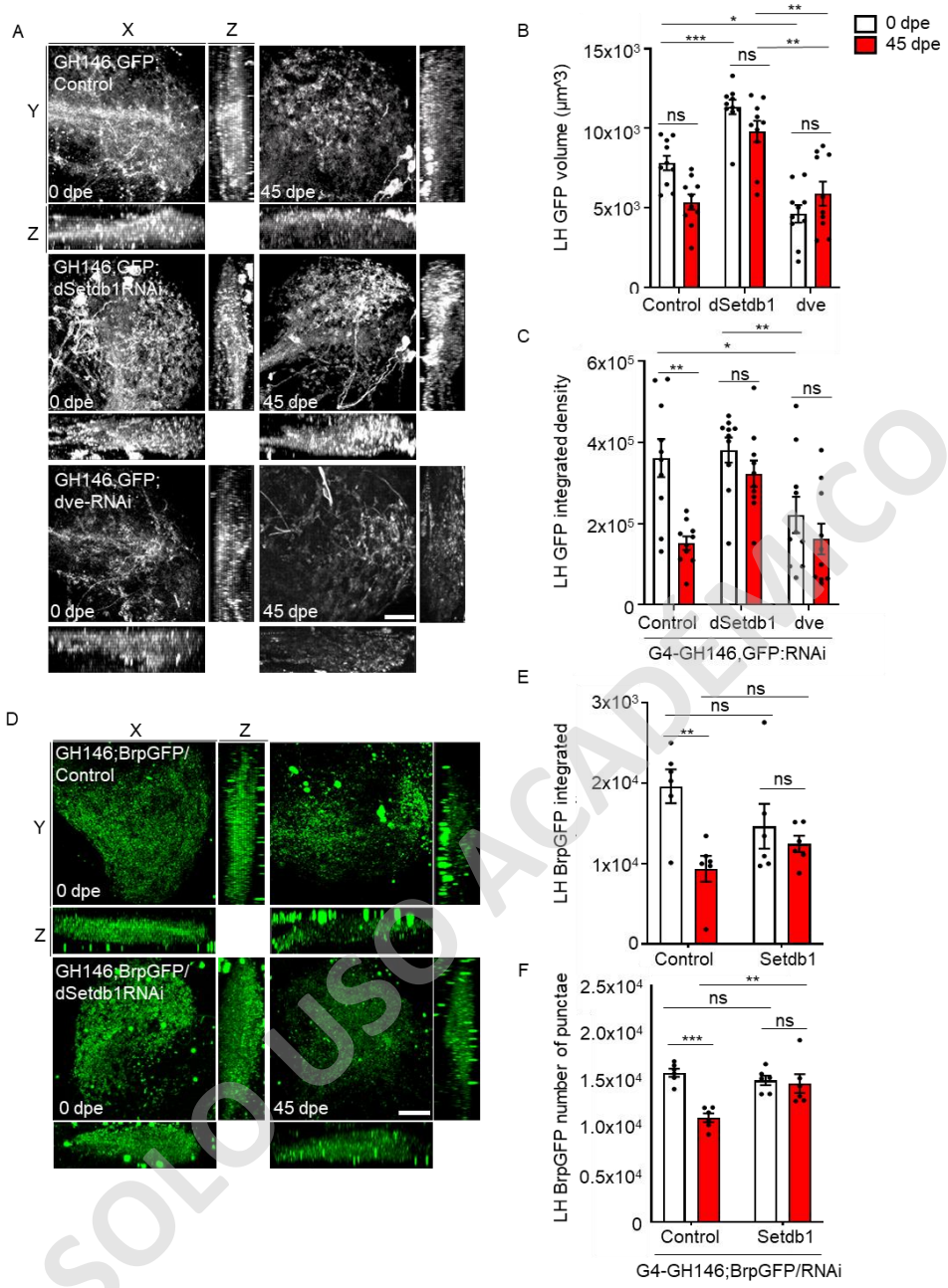

Figure 30. UPR^{MT} regulation of OPNs age-associated synaptic degeneration in LH of the *Drosophila* brain. A) Representative images of orthogonal view of the 3D reconstruction of LH of OPNs tagged with GFP. Images show the combination of axis Y and X, Z and X, and Z and Y. Panel shows LH from control flies and knockdown flies of *dSetdb1* and *dve*. B) LH volume of images shown in A. C) LH integrated density of images shown in A. D) Orthogonal view of representative 3D reconstruction images of presynaptic densities of LH labeled with BrpGFP of young and aged flies bearing the dSetdb1 GH146 knockdown. E) BrpGFP integrated density of images shown in D. F) Number of presynaptic densities labeled with BrpGFP in the LH of flies bearing the dSetdb1 knockdown. Scale Bar is 10µm. Two-way ANOVA statistical analysis with Bonferroni's multiple comparisons. P-value: *** $p < 0.001$; ** $p < 0.01$, * $p<0.05$ and ns > 0.05 (Tables 56 to 59).

Given all the data presented, we propose the following mechanism of UPR^{MT} regulation by methylation of H3K9 during aging in olfactory projection neurons (Fig. 31). In young animals (Left side of the panel), several stressors result in the accumulation of mitochondrial malfunction, leading to damage and activation of a retrograde response from the mitochondria to the nucleus. Ubl, crc, and DVE are translocated to the nucleus, where DVE maintains an open chromatin state to allow the binding of UPR^{MT} transcriptional modulators. This event selectively triggers the transcription of chaperones, proteases, and antioxidant enzymes to restore mitochondrial homeostasis and oxidation exclusively in a mono/demethylated state of H3K9. During aging (right side of the panel), trimethylation of H3K9 is a mark of heterochromatin associated with the repression of transcription. This trimethylated state of H3K9 does not allow the binding of the transcriptional modulators of UPR^{MT}, inhibiting the mitochondrial response to age-related stressors. Thus, mitochondrial function persists, increasing mitochondrial oxidation and contributing to aging phenotypes, such as neurodegeneration marked by the reduction of OPNs, axonal volume, and presynaptic connections (Fig. 31).

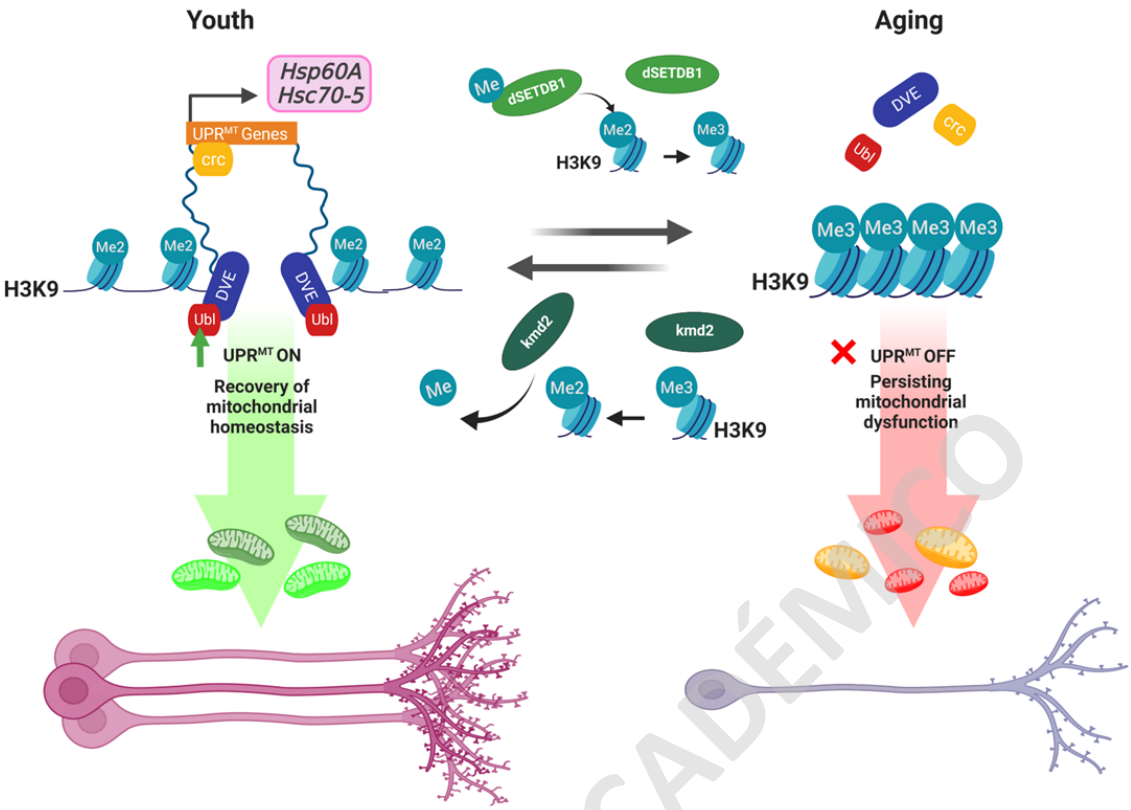

Figure 31. Mechanism of UPR^{MT} epigenetic regulation by methylation of H3K9 during aging in OPNs. In young organisms, mitochondria are challenged by various insults that lead to the accumulation of mitochondrial dysfunction, causing damage and activating a retrograde response from mitochondria to the nucleus. Ubl, crc and DVE are translocated to the nucleus, and DVE maintains an open chromatin state, allowing the binding of transcriptional modulators of the UPR^{MT}. This event activates the transcription of chaperones and proteases to recover mitochondrial homeostasis and oxidation exclusively on a mono/dimethylated state of H3K9. During aging, trimethylation of H3K9 is a mark of heterochromatin associated with the repression of transcription. This trimethylated state of H3K9 would not allow the binding of the transcriptional modulators of UPR^{MT,} inhibiting the mitochondrial response to aging-causing damage. Thus, mitochondrial function persists, increasing mitochondrial oxidation and contributing to aging phenotypes, such as neurodegeneration marked by the reduction of OPNs, axonal volume, and presynaptic connections. Figure created with BioRender.com.

11. Discussion.

11.1 Inhibition of H3K9Me3 reduces age-associated neurodegeneration of OPNs through UPR^{MT}.

Mitochondrial unfolded protein response (UPR^{MT}) responds to cellular stressors to prevent the accumulation of damage that disrupts mitochondrial homeostasis (Muñoz-Carvajal and Sanhueza, 2020). Existing evidence demonstrates an age-dependent effect of UPR^{MT} on longevity (Dillin et al., 2002; Durieux et al., 2011; Mouchiroud et al., 2013). The histone demethylases JMJD-1.2 and JMJD-3.1 partially mediate this extension since their overexpression is sufficient to lengthen the worms lifetime (Merkwirth et al., 2016). Reducing the expression of nuclear effectors ATFS-1, UBL-5, and DVE- 1 or demethylases JMJD-1.2 and JMJD-3.1 decreases lifetime extension (Durieux et al., 2011; Houtkooper et al., 2013; Merkwirth et al., 2016; Cooper et al., 2017; Lan et al., 2019). Recent research has demonstrated that the methyltransferase SET-6 and the neuronal epigenetic reader BAZ-2 mediate an age-dependent regulation of UPR^{MT} (Yuan et al., 2020), highlighting histone 3 methylation as a critical epigenetic mediator for UPR^{MT} throughout the lifespan (Merkwirth et al., 2016; Tian et al., 2016; Ono et al., 2017; Sobue et al., 2017). Changes in the activation capacity of the UPR^{MT} influence mitochondrial function and morphological parameters of this organelle (Merkwirth et al., 2016; Yuan et al., 2020; Ng et al., 2021; Zhou et al., 2022). Alterations in mitochondrial morphology are linked to neuron degeneration (Barrientos et al., 2011; Arrázola et al., 2019). Age-related neurodegeneration is usually associated to degeneration of specific compartments, such as synapses, are layer-specific which affects distinct functions and behaviors, including olfactory function (Dan et al.; Richard et al.). It has been well documented that olfactory function declines with age and a variety of features has been identified to be involved in this functional loss (Stevens et al., 1989; Cerf-ducastel and Murphy, 2003; Wang et al., 2017; Dweck et al., 2018; Xu et al., 2020). Nevertheless, the exact underlying cellular and molecular mechanisms remains unclear. Specifically, the effects of UPR^{MT} regulation by H3K9Me3 in aging associated olfactory dysfunction were not previously considered.

In this work, we have identified a mechanism in which dSetdb1 regulates H3K9Me3, whose repressive epigenetic regulation on UPR^{MT} during aging induces mitochondrial morphological abnormalities, increase in mitochondrial ROS, and contributes to the age-associated neurodegeneration of olfactory projection neurons (OPNs). Ultimately, this leads to the functional decline of the olfactory system, particularly affecting neuronal integrity and presynaptic connections on the LH in the *Drosophila* brain. Genetic inhibition of H3K9Me3 by dSetdb1 downregulation, specifically in OPNs, restored H3K9Me3 to youthful levels, allowing UPR^{MT} activation capacity to restore mitochondrial morphology and oxidation. This effect prevented age-associated olfactory projection neuron degeneration, highlighted by the conservation of AL OPNs number, axonal GFP signal, and presynaptic connections in the LH. Our data demonstrated that dSetdb1 contributes to the age-associated increase in H3K9Me3, which is responsible for the lack of UPR^{MT} activation in aging and contributes to the functional decline of olfactory function in *Drosophila*.

Importantly, our work argues in favor of the therapeutical potential for targeting repressive epigenetic regulation of UPR^{MT} and thus, recover of mitochondrial function. Indeed, age-associated olfactory loss of function is conserved in humans (Doty et al., 1984; Rawson et al., 2012; Pinto et al., 2015; Wang et al., 2017). The loss of sense of smell has a negative impact on the overall quality of life, and for humans, smell processing in the olfactory lobe is associated with experiencing emotions and memories through direct connection with the limbic system and cerebral cortex (Churchwell and Yurgelun-Todd, 2013; Dan et al., 2021). Olfactory dysfunction correlates with age-associated depression in 30% of the cases (Croy et al., 2014) and precedes the onset of neurodegenerative diseases associated to aging such as Alzheimer's disease (Vasavada et al., 2015; Zou et al., 2016) and Parkinson's diseases (Cecchini et al., 2019; Leonhardt et al., 2019). This suggests that understanding complicated but conserved behavioral neural networks may provide insights into countering neurodegeneration and functional decline in aging (Daramola and Becker, 2015; Marin et al., 2018).

Notably, neuronal loss may not be homogeneous along aging. In contrast, the loss of distinct neuronal compartments with age appears to be region-specific (Kraemer and Apfelbach, 2004; Dickstein et al., 2007; Burke and Barnes, 2010; Mandairon and Didier, 2010; Richard

et al., 2010; Arrázola et al., 2019). This raises the question about the specific differential epigenetic regulation of UPR^{MT} on different behaviors governed by different neuronal types. UPR^{MT} is regulated epigenetically by H3K9Me3, which in turn is finely regulated by an array of diverse demethylases such as JMJD 3.1, JMJD 1.3, and methyltransferases MET-2, SET6, and BAZ2 (Merkwirth et al., 2016; Tian et al., 2016; Yuan et al., 2020). Now we add dSetdb1 to this list, suggesting that heterogenous epigenetic regulation is, in fact, masking specific phenotypes to independent types of neurons.

This difference in epigenetic regulation can be explained, in part, when we observe the expression levels of H3K9Me3-regulating enzymes in different neurons, which variation suggests a differential epigenetic regulation of H3K9Me3, impacting mitochondrial function through UPR^{MT}. Indeed, previous studies have shown that H3K9Me3 levels are not homogeneous in the whole brain since different levels of trimethylated H3K9 differ depending on the brain zone or the neuronal type (Benayoun et al., 2015; Cao and Dang, 2018; Kane and Sinclair, 2019).

As the organism age, there are discernible modifications to both the global and specific histone mark patterns. The specific pattern of histone modifications varies among organisms, tissues of the same individual, and even in cells within the same tissue (Benayoun et al., 2015). H3K9me3 is a hallmark of heterochromatin and therefore, enriched in chromatin regions involving gene silencing. Concordantly with previous data (Wood et al., 2010 Schwörer et al., 2016), we found an increase of H3K9Me3 in the aged brains of flies. Suppression of methyltransferase SET-6 and epigenetic reader BAZ-2, enzymes normally upregulated along aging, worms live longer (Yuan et al., 2020) and mice treated with an H3K9Me3 inhibitor had less age-related cognitive impairment and more hippocampus but no cerebellum dendritic spines (Petrosyan et al., 2016). Heterochromatin protein 1 (HP-1) and mH2A, which bind to H3K9Me3, have been linked to senescent heterochromatin foci in aged primates and mice (Narita et al., 2003, 2006; Herbig et al., 2006). In some rare cases, H3K9Me3 is reduced under various aging conditions, including fibroblasts from HGPS patients (Shumaker et al., 2006). In the fibroblast of a progeria mouse model of Werner syndrome with defective DNA repair, levels of both H3K9me3 marks and the H3K9 methyltransferase SUV39H1 are decreased. However, we demonstrate that dSetdb1

contributes to the age-associated increase in H3K9Me3 and contributes to the lack of UPR^{MT} activation in aging in olfactory projection neurons of the AL in *Drosophila*, which correlates with the functional decline of olfactory function specifically. This data supports the previous studies that showed improved functions in aging by reducing the levels of H3K9Me3 (Merkwirth et al., 2016; Petrosyan et al., 2016; Yuan et al., 2020).

Mitochondrial dysfunction is a hallmark of pathological aging and neurodegeneration (López-Otín et al., 2013). Since UPR^{MT} activation improves mitochondrial function, additional pathway characterization will provide stronger clues for comprehending neuronal homeostasis and healthspan extension. Until now, UPR^{MT} activation has been partially modulated by the age-dependent methylation levels of Histone 3, which is not homogeneous in different brain regions. Indeed, the regulation of UPR^{MT} appears to vary between neuronal types. This duality of UPR^{MT} complicates therapeutic approaches, as systemic inhibition of UPR^{MT} may be advantageous for cell types with dysregulated UPR^{MT} activation, but deleterious for cell types that require UPR^{MT} activation. Consequently, the fine-tuning of UPR^{MT} in aging and various pathogenic contexts will be crucial in future research, which is essential for determining if either known neurodegeneration-causing genes are associated with UPR^{MT} components at initial or late, irreversible stages of the disease. The precise pharmaceutical control of the mitochondrial stress response could offer new possibilities for recovering damaged neuronal functions, thereby enhancing the quality of life for patients with neurodegenerative illnesses and the elderly.

For instance, related to Parkinson's Disease (PD) (Leng et al., 2021), Pink-1 and pdr-1 (Parkin ortholog) downregulation in worms activate UPR^{MT}, as dopaminergic neurons degenerate when inhibited (Cooper et al., 2017). PINK1 activates ERα target HTRA2, which has been associated with UPR^{MT} (Plun-Favreau et al., 2007). Importantly, mutations in HTRA2 have been linked to PD patients (Strauss et al., 2005). Another PD-associated mutated protein, α-synuclein A53T, accumulates in mitochondria and inhibits UPR^{MT}-regulator ClpP, while its overexpression reduces SynA53T pathology (Hu et al., 2019). From an epigenetic point of view, α-synuclein expression in *Drosophila* upregulated the dimethyltransferase EHMT2, causing H3K9 dimethylation (Sugeno et al., 2016). It would be interesting to see if H3K9Me2-linked chromatin remodeling modifies UPR^{MT} activation in

this PD model (Merkwirth et al., 2016; Tian et al., 2016). Post-mortem ALS samples have altered ETC activity (Bowling et al., 1993), and transgenic SOD1 overexpression causes dysregulation in mitochondrial metabolism (Mattiazzi et al., 2002a; Brookes, 2004) and activates two UPR^{MT} axes (Riar et al., 2017; Gomez and Germain, 2019). Recent reports show that UPR^{MT} activation precedes and increases with ALS (Pharaoh et al., 2019). Finally, UPR^{MT} and AD have been recently linked (Weidling and Swerdlow; Butterfield and Halliwell, 2019; Shen et al., 2020) as Aβ aggregates stimulate human and mouse UPR^{MT} (Shen et al., 2020). In *C.elegans*, resveratrol reduced Aβ aggregates and toxicity(Regitz et al., 2016), suggesting a link between the two UPR^{MT} axes and AD. Haga clic o pulse aquí para escribir texto.AD prefrontal cortex samples have high UPR^{MT} gene expression (S. Beck et al., 2016). It would be interesting to know if this increased expression is either a disease-progression-related early program or a mitochondrial dysfunction-related late response. Additionally, expression of the epigenetic regulators of UPR^{MT} EHMT1 and BAZ2B correlate positively with AD progression (Zhang et al., 2013; Yuan et al., 2020). Future research should determine if UPR^{MT} inhibition or persistent activation is linked to the degeneration of neurons in the context of disease. However, it has become clear that brain systems are also vulnerable to aging, even in the absence of disease.

12. Conclusion.

We conclude that dSetdb1 negatively regulates UPR^{MT}, since the loss of its function is sufficient to increase UPR^{MT} activation along aging. Pan-neuronal downregulation of dSetdb1 decreased H3K9Me3 levels in aging, resulting in an increase in healthspan and prevalence of olfactory function, but did not affect the aging-related reduction of locomotor or circadian spontaneous activity. In addition, increasing H3K9Me3 levels impaired olfactory function, locomotor activity, and spontaneous circadian activity. This finding supports prior research indicating that decreasing H3K9Me3 levels improves aging-related function (Merkwirth et al., 2016; Petrosyan et al., 2016; Yuan et al., 2020). In addition, it establishes that the aging-related increase in H3K9Me3 is responsible for the absence of UPR^{MT} activation in aging in OPNs, which contributes explicitly to the reduction in olfactory function and no other behaviors. Consequently, the olfactory system was the focus of this inquiry.

Remarkably, we discovered a pathway by which dSetdb1 regulates H3K9Me3, whose repressive epigenetic regulation on UPR^{MT} during aging causes mitochondrial morphological abnormalities and oxidation, which contributes to age-related neurodegeneration of OPNs and olfactory system functional loss. Significantly, genetic inhibition of H3K9Me3 by dSetdb1 downregulation, specifically in OPNs, restored Histone 3 methylation to youthful levels, allowing UPR^{MT} activation capacity to restore mitochondrial morphology and oxidation. This prevents age-associated olfactory projection neuron degeneration, as evidenced by maintaining the number of OPNs in the AL, axonal volume, and presynaptic connections in the LH. Our findings indicate that dSetdb1 negatively regulates UPR^{MT} in OPNs in the AL and that its downregulation has favorable impacts on the integrity and function of olfactory neurons as they age.

14. References.

Aldridge, J. E., Horibe, T., and Hoogenraad, N. J. (2007). Discovery of genes activated by the mitochondrial Unfolded Protein Response (mtUPR) and cognate promoter elements. *PLoS One* 2. doi: 10.1371/journal.pone.0000874.

Anderson, C. J., Bredvik, K., Burstein, S. R., Davis, C., Meadows, S. M., Dash, J., et al. (2019). ALS/FTD mutant CHCHD10 mice reveal a tissue-specific toxic gain-of-function and mitochondrial stress response. *Acta Neuropathol* 138, 103–121. doi: 10.1007/s00401-019-01989-y.

Arrázola, M. S., Saquel, C., Catalán, R. J., Barrientos, S. A., Hernandez, D. E., Martínez, N. W., et al. (2019). Axonal degeneration is mediated by necroptosis activation. *Journal of Neuroscience* 39, 3832–3844. doi: 10.1523/JNEUROSCI.0881-18.2019.

Bárcena, C., Mayoral, P., and Quirós, P. M. (2018). Mitohormesis, an Antiaging Paradigm. *Int Rev Cell Mol Biol* 340, 35–77. doi: 10.1016/bs.ircmb.2018.05.002.

Barrientos, S. A., Martinez, N. W., Yoo, S., Jara, J. S., Zamorano, S., Hetz, C., et al. (2011). Axonal degeneration is mediated by the mitochondrial permeability transition pore. *J Neurosci* 31, 966–978. doi: 31/3/966 [pii]\r10.1523/JNEUROSCI.4065-10.2011.

Beal, M. F. (2003). Mitochondria, oxidative damage, and inflammation in Parkinson's disease. *Ann N Y Acad Sci* 991, 120–131. doi: 10.1111/j.1749-6632.2003.tb07470.x.

Beal, M. F. (2005). Mitochondria take center stage in aging and neurodegeneration. *Ann Neurol* 58, 495–505. doi: 10.1002/ana.20624.

Benayoun, B. A., Pollina, E. A., and Brunet, A. (2015). Epigenetic regulation of ageing: Linking environmental inputs to genomic stability. *Nat Rev Mol Cell Biol* 16, 593–610. doi: 10.1038/nrm4048.

Bender, A., Krishnan, K. J., Morris, C. M., Taylor, G. A., Reeve, A. K., Perry, R. H., et al. (2006). High levels of mitochondrial DNA deletions in substantia nigra neurons in aging and Parkinson disease. *Nat Genet* 38, 515–517. doi: 10.1038/ng1769.

Benedetti, C., Haynes, C. M., Yang, Y., Harding, H. P., and Ron, D. (2006). Ubiquitin-like protein 5 positively regulates chaperone gene expression in the mitochondrial unfolded protein response. *Genetics* 174, 229–239. doi: 10.1534/genetics.106.061580.

Borrás, C., Gambini, J., López-Grueso, R., Pallardó, F. V., and Viña, J. (2010). Direct antioxidant and protective effect of estradiol on isolated mitochondria. *Biochim Biophys Acta Mol Basis Dis* 1802, 205–211. doi: 10.1016/j.bbadis.2009.09.007.

Borrás, C., Sastre, J., García-Sala, D., Lloret, A., Pallardó, F. V., and Viña, J. (2003). Mitochondria from females exhibit higher antioxidant gene expression and lower oxidative damage than males. *Free Radic Biol Med* 34, 546–552. doi: 10.1016/S0891-5849(02)01356-4.

Bowling, A. C., Schulz, J. B., Brown, R. H., and Beal, M. F. (1993a). Superoxide Dismutase Activity, Oxidative Damage, and Mitochondrial Energy Metabolism in Familial and Sporadic Amyotrophic Lateral Sclerosis. *J Neurochem* 61, 2322–2325. doi: 10.1111/j.1471-4159.1993.tb07478.x.

Brookes, P. S. (2004). Calcium, ATP, and ROS: a mitochondrial love-hate triangle. *AJP: Cell Physiology* 287, C817–C833. doi: 10.1152/ajpcell.00139.2004.

Burbulla, L. F., Fitzgerald, J. C., Stegen, K., Westermeier, J., Thost, A. K., Kato, H., et al. (2014). Mitochondrial proteolytic stress induced by loss of mortalin function is rescued by Parkin and PINK1. *Cell Death Dis* 5, 1–19. doi: 10.1038/cddis.2014.103.

Burke, S. N., and Barnes, C. A. (2010). Senescent synapses and hippocampal circuit dynamics. *Trends Neurosci* 33, 153–161. doi: 10.1016/J.TINS.2009.12.003.

Butterfield, D. A., and Halliwell, B. (2019). Oxidative stress, dysfunctional glucose metabolism and Alzheimer disease. *Nat Rev Neurosci* 20, 148–160. doi: 10.1038/s41583-019-0132-6.

Cao, X., and Dang, W. (2018). *Histone Modification Changes During Aging*. Elsevier Inc. doi: 10.1016/B978-0-12-811060-7.00015-2.

Casley, C. S., Canevari, L., Land, J. M., Clark, J. B., and Sharpe, M. a (2002). Beta-amyloid inhibits integrated mitochondrial respiration and key enzyme activities. *J Neurochem* 80, 91–100. doi: 10.1046/j.0022-3042.2001.00681.x.

Cecchini, M. P., Federico, A., Zanini, A., Mantovani, E., Masala, C., Tinazzi, M., et al. (2019). Olfaction and taste in Parkinson's disease: The association with mild cognitive impairment and the single cognitive domain dysfunction. *J Neural Transm* 126, 585–595. doi: 10.1007/s00702-019-01996-z.

Cerf-ducastel, B., and Murphy, C. (2003). F MRI brain activation in response to odors is reduced in primary olfactory areas of elderly subjects. 986, 39–53.

Chen, C., Turnbull, D. M., and Reeve, A. K. (2019). Mitochondrial dysfunction in Parkinson's disease—cause or consequence? *Biology (Basel)* 8, 1–26. doi: 10.3390/biology8020038.

Chen, Y., Zhang, J., Lin, Y., Lei, Q., Guan, K. L., Zhao, S., et al. (2011). Tumour suppressor SIRT3 deacetylates and activates manganese superoxide dismutase to scavenge ROS. *EMBO Rep* 12, 534–541. doi: 10.1038/embor.2011.65.

Chistiakov, D. A., Sobenin, I. A., Revin, V. V., Orekhov, A. N., and Bobryshev, Y. V. (2014). Mitochondrial aging and age-related dysfunction of mitochondria. *Biomed Res Int* 2014. doi: 10.1155/2014/238463.

Choi, S. J., Panhelainen, A., Schmitz, Y., Larsen, K. E., Kanter, E., Wu, M., et al. (2015). Changes in neuronal dopamine homeostasis following 1-methyl-4-phenylpyridinium (MPP+) exposure. *Journal of Biological Chemistry* 290, 6799–6809. doi: 10.1074/jbc.M114.631556.

Chu, D., and Tao, Y. (2018). A protein isolation method for western blot to study histones with an internal control protein. *Journal of Advanced Biotechnology and Experimental Therapeutics* 1, 25. doi: 10.5455/jabet.d4.

Churchwell, J. C., and Yurgelun-Todd, D. A. (2013). Age-related changes in insula cortical thickness and impulsivity: Significance for emotional development and decision-making. *Dev Cogn Neurosci* 6, 80–86. doi: 10.1016/J.DCN.2013.07.001.

Clough, E., Tedeschi, T., and Hazelrigg, T. (2014). Epigenetic regulation of oogenesis and germ stem cell maintenance by the Drosophila histone methyltransferase Eggless/dSetDB1. *Dev Biol* 388, 181–191. doi: 10.1016/j.ydbio.2014.01.014.

Cooper, J. F., Machiela, E., Dues, D. J., Spielbauer, K. K., Senchuk, M. M., and van Raamsdonk, J. M. (2017). Activation of the mitochondrial unfolded protein response promotes longevity and dopamine neuron survival in Parkinson's disease models. *Sci Rep* 7, 1–16. doi: 10.1038/s41598-017-16637-2.

Copeland, J. M., Cho, J., Lo, T., Hur, J. H., Bahadorani, S., Arabyan, T., et al. (2009). Extension of Drosophila Life Span by RNAi of the Mitochondrial Respiratory Chain. *Current Biology* 19, 1591–1598. doi: 10.1016/j.cub.2009.08.016.

Court, F. A., and Coleman, M. P. (2012). Mitochondria as a central sensor for axonal degenerative stimuli. *Trends Neurosci* 35, 364–372. doi: 10.1016/j.tins.2012.04.001.

Couvillion, M. T., Soto, I. C., Shipkovenska, G., and Churchman, L. S. (2016). Synchronized mitochondrial and cytosolic translation programs. *Nature* 533, 499–503. doi: 10.1038/nature18015.

Creed, R. B., and Goldberg, M. S. (2018). New Developments in Genetic rat models of Parkinson's Disease. *Movement Disorders* 33, 717–729. doi: 10.1002/mds.27296.

Croy, I., Nordin, S., and Hummel, T. (2014). Olfactory Disorders and Quality of Life-An Updated Review. *Chem. Senses* 39, 185–194. doi: 10.1093/chemse/bjt072.

Cui, L., Jeong, H., Borovecki, F., Parkhurst, C. N., Tanese, N., and Krainc, D. (2006). Transcriptional Repression of PGC-1α by Mutant Huntingtin Leads to Mitochondrial Dysfunction and Neurodegeneration. *Cell* 127, 59–69. doi: 10.1016/j.cell.2006.09.015.

Dan, X., Wechter, N., Gray, S., Mohanty, J. G., Croteau, D. L., and Bohr, V. A. (2021). Olfactory dysfunction in aging and neurodegenerative diseases. *Ageing Res Rev* 70. doi: 10.1016/J.ARR.2021.101416.

Dan, X., Wechter, N., Gray, S., Mohanty, J. G., Croteau, D. L., and Bohr, V. A. Olfactory dysfunction in aging and neurodegenerative diseases. doi: 10.1016/j.arr.2021.101416.

Daramola, O. O., and Becker, S. S. (2015). An algorithmic approach to the evaluation and treatment of olfactory disorders. *Curr Opin Otolaryngol Head Neck Surg* 23, 8–14. doi: 10.1097/MOO.0000000000000118.

de Nobrega, A. K., and Lyons, L. C. (2020). Aging and the clock: Perspective from flies to humans. *European Journal of Neuroscience* 51, 454–481. doi: 10.1111/ejn.14176.

Deng, P., and Haynes, C. M. (2017). Mitochondrial dysfunction in cancer: Potential roles of ATF5 and the mitochondrial UPR. *Semin Cancer Biol* 47, 43–49. doi: 10.1016/j.semcancer.2017.05.002.

Dickstein, D. L., Kabaso, D., Rocher, A. B., Luebke, J. I., Wearne, S. L., and Hof, P. R. (2007). Changes in the structural complexity of the aged brain. *Aging Cell* 6, 275–284. doi: 10.1111/J.1474-9726.2007.00289.X.

Dillin, A., Hsu, A., Arantes-oliveira, N., Lehrer-graiwer, J., Hsin, H., Fraser, A. G., et al. (2002a). Rates of Behavior and Aging Specified by Mitochondrial Function During Development. *Science (1979)* 298, 2398–2402. doi: 10.1126/science.1077780.

Doty, R. L., Shaman, P., Applebaum, S. L., Giberson, R., Siksorski, L., and Rosenberg, L. (1984). Smell identification ability: Changes with age. *Science (1979)* 226, 1441–1443. doi: 10.1126/science.6505700.

Durieux, J., Wolff, S., and Dillin, A. (2011a). The cell-non-autonomous nature of electron transport chain-mediated longevity. *Cell* 144, 79–91. doi: 10.1016/j.cell.2010.12.016.

Dweck, H. K. M., Ebrahim, S. A. M., Retzke, T., Grabe, V., Weißflog, J., Svatoš, A., et al. (2018). The Olfactory Logic behind Fruit Odor Preferences in Larval and Adult Drosophila. *Cell Rep* 23, 2524–2531. doi: 10.1016/j.celrep.2018.04.085.

Federico, A., Cardaioli, E., Da Pozzo, P., Formichi, P., Gallus, G. N., and Radi, E. (2012). Mitochondria, oxidative stress and neurodegeneration. *J Neurol Sci* 322, 254–262. doi: 10.1016/j.jns.2012.05.030.

Fiorese, C. J., Schulz, A. M., Lin, Y. F., Rosin, N., Pellegrino, M. W., and Haynes, C. M. (2015). The Transcription Factor ATF5 Mediates a Mammalian Mitochondrial UPR. *Current Biology* 26, 1–7. doi: 10.1016/j.cub.2016.06.002.

Fiorese, C. J., Schulz, A. M., Lin, Y. F., Rosin, N., Pellegrino, M. W., and Haynes, C. M. (2016). The Transcription Factor ATF5 Mediates a Mammalian Mitochondrial UPR. *Current Biology* 26, 1–7. doi: 10.1016/j.cub.2016.06.002.

Franco-Iborra, S., Vila, M., and Perier, C. (2018). Mitochondrial quality control in neurodegenerative diseases: Focus on Parkinson's disease and Huntington's disease. *Front Neurosci* 12, 1–25. doi: 10.3389/fnins.2018.00342.

Gilestro, G. F., and Cirelli, C. (2009). PySolo: A complete suite for sleep analysis in Drosophila. *Bioinformatics* 25, 1466–1467. doi: 10.1093/bioinformatics/btp237.

Gomez, M., and Germain, D. (2019a). Cross talk between SOD1 and the mitochondrial UPR in cancer and neurodegeneration. *Molecular and Cellular Neuroscience* 98, 12–18. doi: 10.1016/j.mcn.2019.04.003.

Gur, R. C., Mozley, P. D., Resnick, S. M., Gottlieb, G. L., Kohn, M., Zimmerman, R., et al. (1991). Gender differences in age effect on brain atrophy measured by magnetic resonance imaging. *Proceedings of the National Academy of Sciences* 88, 2845–2849. doi: 10.1073/pnas.88.7.2845.

Hartl, M., Loschek, L. F., Stephan, D., Siju, K. P., Knappmeyer, C., and Kadow, I. C. G. (2011). A new prospero and microRNA-279 pathway restricts CO 2 receptor neuron formation. *Journal of Neuroscience* 31, 15660–15673. doi: 10.1523/JNEUROSCI.2592-11.2011.

Haug, G. (1978). Neuroradiologv. 204, 201–202.

Haynes, C. M., Petrova, K., Benedetti, C., Yang, Y., and Ron, D. (2007). ClpP Mediates Activation of a Mitochondrial Unfolded Protein Response in C. elegans. *Dev Cell* 13, 467–480. doi: 10.1016/j.devcel.2007.07.016.

Haynes, C. M., and Ron, D. (2010). The mitochondrial UPR - protecting organelle protein homeostasis. *J Cell Sci* 123, 3849–3855. doi: 10.1242/jcs.075119.

Herbig, U., Ferreira, M., Condel, L., Carey, D., and Sedivy, J. M. (2006). Cellular senescence in aging primates. *Science (1979)* 311, 1257. doi: 10.1126/science.1122446.

Hernandez, G., Thornton, C., Stotland, A., Lui, D., Sin, J., Ramil, J., et al. (2013). MitoTimer. *Autophagy* 9, 1852–1861. doi: 10.4161/auto.26501.

Herz, H. M., Madden, L. D., Chen, Z., Bolduc, C., Buff, E., Gupta, R., et al. (2010). The H3K27me3 Demethylase dUTX Is a Suppressor of Notch- and Rb-Dependent Tumors in Drosophila. *Mol Cell Biol* 30, 2485–2497. doi: 10.1128/mcb.01633-09.

Horibe, T., and Hoogenraad, N. J. (2007). The Chop gene contains an element for the positive regulation of the mitochondrial unfolded protein response. *PLoS One* 2. doi: 10.1371/journal.pone.0000835.

Houtkooper, R. H., Mouchiroud, L., Ryu, D., Moullan, N., Katsyuba, E., Knott, G., et al. (2013a). Mitonuclear protein imbalance as a conserved longevity mechanism. *Nature* 497, 451–457. doi: 10.1038/nature12188.
Hu, D., Sun, X., Liao, X., Zhang, X., Zarabi, S., Schimmer, A., et al. (2019). Alpha-synuclein suppresses mitochondrial protease ClpP to trigger mitochondrial oxidative damage and neurotoxicity. *Acta Neuropathol*, 939–960. doi: 10.1007/s00401-019-01993-2.

Huang, Y., and Mucke, L. (2013). Alzheimer Mechanisms and Therapeutic Strategies. *Cell* 148, 1204–1222. doi: 10.1016/j.cell.2012.02.040.Alzheimer.

Hussain, A., Pooryasin, A., Zhang, M., Loschek, L. F., la Fortezza, M., Friedrich, A. B., et al. (2018). Inhibition of oxidative stress in cholinergic projection neurons fully rescues aging-associated olfactory circuit degeneration in drosophila. *Elife* 7, 1–20. doi: 10.7554/eLife.32018.

Jellinger, K. A. (2010). Basic mechanisms of neurodegeneration: A critical update. *J Cell Mol Med* 14, 457–487. doi: 10.1111/j.1582-4934.2010.01010.x.

Jensen, M. B., Qi, Y., Riley, R., Rabkina, L., and Jasper, H. (2017). PGAM5 promotes lasting FoxO activation after developmental mitochondrial stress and extends lifespan in Drosophila. *Elife* 6, 1–22. doi: 10.7554/eLife.26952.

Ji, T., Zhang, X., Xin, Z., Xu, B., Jin, Z., Wu, J., et al. (2020). Does perturbation in the mitochondrial protein folding pave the way for neurodegeneration diseases? *Ageing Res Rev* 57, 100997. doi: 10.1016/j.arr.2019.100997.

Jin, S. M., and Youle, R. J. (2013). The accumulation of misfolded proteins in the mitochondrial matrix is sensed by PINK1 to induce PARK2/Parkin-mediated mitophagy of polarized mitochondria. *Autophagy* 9, 1750–1757. doi: 10.4161/auto.26122.

Kaarniranta, K., Kajdanek, J., Morawiec, J., Pawlowska, E., and Blasiak, J. (2018). PGC-1α protects RPE cells of the aging retina against oxidative stress-induced degeneration through the regulation of senescence and mitochondrial quality control. The significance for AMD pathogenesis. *Int J Mol Sci* 19, 1–20. doi: 10.3390/ijms19082317.

Kane, A. E., and Sinclair, D. A. (2019). Epigenetic changes during aging and their reprogramming potential. *Crit Rev Biochem Mol Biol* 54, 61–83. doi: 10.1080/10409238.2019.1570075.

Kenny, T. C., and Germain, D. (2017). From discovery of the CHOP axis and targeting ClpP to the identification of additional axes of the UPRmt driven by the estrogen receptor and SIRT3. *J Bioenerg Biomembr* 49, 297–305. doi: 10.1007/s10863-017-9722-z.

Kenny, T. T., Hart, P., Ragazzi, M., Sersinghe, M., Chipuk, J., Sagar, M. A. K., et al. (2017). Selected mitochondrial DNA landscapes activate the SIRT3 axis of the UPRmt to promote metastasis. *Oncogene* 36, 4393–4404. doi: 10.1038/onc.2017.52.

Kim, Y., Zheng, X., Ansari, Z., Bunnell, M. C., Herdy, J. R., Traxler, L., et al. (2018). Mitochondrial Aging Defects Emerge in Directly Reprogrammed Human Neurons due to Their Metabolic Profile. *Cell Rep* 23, 2550–2558. doi: 10.1016/j.celrep.2018.04.105.

Kirkwood, T. B. L., and Kowald, Axel. (2000). Accumulation of Defective Mitochondria through Delayed Degradation of Damaged Organelles and Its Possible Role in the Ageing of Post-mitotic and Dividing Cells. *J Theor Biol*, 145–160.

Kraemer, S., and Apfelbach, R. (2004). Olfactory sensitivity, learning and cognition in young adult and aged male Wistar rats. *Physiol Behav* 81, 435–442. doi: 10.1016/J.PHYSBEH.2004.01.012.

Laker, R. C., Xu, P., Ryall, K. A., Sujkowski, A., Kenwood, B. M., Chain, K. H., et al. (2014). A novel mitotimer reporter gene for mitochondrial content, structure, stress, and damage in vivo. *Journal of Biological Chemistry* 289, 12005–12015. doi: 10.1074/jbc.M113.530527.

Lan, J., Rollins, J. A., Zang, X., Wu, D., Zou, L., Wang, Z., et al. (2019a). Translational Regulation of Non-autonomous Mitochondrial Stress Response Promotes Longevity. *Cell Rep* 28, 1050-1062.e6. doi: 10.1016/j.celrep.2019.06.078.

Larsen, S., Hanss, Z., and Krüger, R. (2017). The genetic architecture of mitochondrial dysfunction in Parkinson's disease. *Cell Tissue Res*, 21–37. doi: 10.1007/s00441-017-2768-8.

Leng, K., Li, E., Eser, R., Piergies, A., Sit, R., Tan, M., et al. (2021). Molecular characterization of selectively vulnerable neurons in Alzheimer's disease. *Nat Neurosci* 24, 276–287. doi: 10.1038/s41593-020-00764-7.

Leonhardt, B., Tahmasebi, R., Jagsch, R., Pirker, W., and Lehrner, J. (2019). Awareness of olfactory dysfunction in Parkinson's disease. *Neuropsychology* 33, 633–641. doi: 10.1037/NEU0000544.

Levenson, R. W., Sturm, V. E., and Haase, C. M. (2014). Emotional and behavioral symptoms in neurodegenerative disease: A model for studying the neural bases of psychopathology. *Annu Rev Clin Psychol* 10, 581–606. doi: 10.1146/annurev-clinpsy-032813-153653.

Lin, Y. F., and Haynes, C. M. (2016). Metabolism and the UPRmt. *Mol Cell* 61, 677–682. doi: 10.1016/j.molcel.2016.02.004.

Lin, Y. F., Schulz, A. M., Pellegrino, M. W., Lu, Y., Shaham, S., and Haynes, C. M. (2016). Maintenance and propagation of a deleterious mitochondrial genome by the mitochondrial unfolded protein response. *Nature* 533, 416–419. doi: 10.1038/nature17989.

López-Otín, C., Blasco, M. A., Partridge, L., Serrano, M., and Kroemer, G. (2013a). The hallmarks of aging. *Cell* 153. doi: 10.1016/j.cell.2013.05.039.

Lores-Arnaiz, S., and Bustamante, J. (2011). Age-related alterations in mitochondrial physiological parameters and nitric oxide production in synaptic and non-synaptic brain cortex mitochondria. *Neuroscience* 188, 117–124. doi: 10.1016/j.neuroscience.2011.04.060.

Lores-Arnaiz, S., Lombardi, P., Karadayian, A. G., Orgambide, F., Cicerchia, D., and Bustamante, J. (2016a). Brain cortex mitochondrial bioenergetics in synaptosomes and non-synaptic mitochondria during aging. *Neurochem Res* 41, 353–363. doi: 10.1007/s11064-015-1817-5.

Lucas-Sánchez, A., Almaida-Pagán, P. F., Tocher, D. R., Mendiola, P., and De Costa, J. (2014). Age-Related Changes in Mitochondrial Membrane Composition of Nothobranchius rachovii. *Journals of Gerontology: BIOLOGICAL SCIENCES Cite journal as J Gerontol A Biol Sci Med Sci* 69, 142–151. doi: 10.1093/gerona/glt066.

Mandairon, N., and Didier, A. (2010). The brain's fight against aging. *Proc Natl Acad Sci U S A* 107, 15316–15317. doi: 10.1073/PNAS.1010574107.

Marin, C., Vilas, D., Langdon, C., Alobid, I., López-Chacón, M., Haehner, A., et al. (2018). Olfactory Dysfunction in Neurodegenerative Diseases. *Curr Allergy Asthma Rep* 18. doi: 10.1007/s11882-018-0796-4.

Martinez, B. A., Petersen, D. A., Gaeta, A. L., Stanley, S. P., Caldwell, G. A., and Caldwell, K. A. (2017). Dysregulation of the mitochondrial unfolded protein response

induces non-apoptotic dopaminergic neurodegeneration in *C. elegans* models of Parkinson's disease. *The Journal of Neuroscience* 37, 1294–17. doi: 10.1523/JNEUROSCI.1294-17.2017.

Martinus, R. D., Garth, G. P., Webster, T. L., Cartwright, P., Naylor, D. J., Høj, P. B., et al. (1996). Selective induction of mitochondrial chaperones in response to loss of the mitochondrial genome. *Eur J Biochem* 240, 98–103. doi: 10.1111/j.1432-1033.1996.0098h.x.

Matilainen, O., Quirós, P. M., and Auwerx, J. (2017). Mitochondria and Epigenetics – Crosstalk in Homeostasis and Stress. *Trends Cell Biol* 27, 453–463. doi: 10.1016/j.tcb.2017.02.004.

Mattiazzi, M., D'Aurelio, M., Gajewski, C. D., Martushova, K., Kiaei, M., Flint Beal, M., et al. (2002a). Mutated human SOD1 causes dysfunction of oxidative phosphorylation in mitochondria of transgenic mice. *Journal of Biological Chemistry* 277, 29626–29633. doi: 10.1074/jbc.M203065200.

Mattson, M. R. (2007). Calcium and neurodegeneration. *Aging Cell* 6, 337–350. doi: 10.1111/j.1474-9726.2007.00275.x.

Merkwirth, C., Jovaisaite, V., Durieux, J., Matilainen, O., Jordan, S. D., Quiros, P. M., et al. (2016a). Two Conserved Histone Demethylases Regulate Mitochondrial Stress-Induced Longevity. *Cell* 165, 1209–1223. doi: 10.1016/j.cell.2016.04.012.

Misgeld, T., and Schwarz, T. L. (2017). Mitostasis in Neurons: Maintaining Mitochondria in an Extended Cellular Architecture. *Neuron* 96, 651–666. doi: 10.1016/j.neuron.2017.09.055.

Moisoi, N., Fedele, V., Edwards, J., and Martins, L. M. (2014). Loss of PINK1 enhances neurodegeneration in a mouse model of Parkinson's disease triggered by mitochondrial stress. *Neuropharmacology* 77, 350–357. doi: 10.1016/j.neuropharm.2013.10.009.

Mouchiroud, L., Houtkooper, R. H., Moullan, N., Katsyuba, E., Ryu, D., Cant??, C., et al. (2013a). XThe NAD+/sirtuin pathway modulates longevity through activation of mitochondrial UPR and FOXO signaling. *Cell* 154, 430. doi: 10.1016/j.cell.2013.06.016.

Muñoz-Carvajal, F., and Sanhueza, M. (2020). The Mitochondrial Unfolded Protein Response: A Hinge Between Healthy and Pathological Aging. *Front Aging Neurosci* 12. doi: 10.3389/fnagi.2020.581849.

Nargund, A. M., Fiorese, C. J., Pellegrino, M. W., Deng, P., and Haynes, C. M. (2015). Mitochondrial and nuclear accumulation of the transcription factor ATFS-1 promotes OXPHOS recovery during the UPRmt. *Mol Cell* 58, 123–133. doi: 10.1016/j.molcel.2015.02.008.

Nargund, A. M., Pellegrino, M. W., Fiorese, C. J., Baker, B. M., and Haynes, C. M. (2012). Mitochondrial import efficiency of ATFS-1 regulates mitochondrial UPR activation. *Science (1979)* 337, 587–590. doi: science.1223560 [pii]\r10.1126/science.1223560.

Narita, M., Narita, M., Krizhanovsky, V., Nuñez, S., Chicas, A., Hearn, S. A., et al. (2006). A Novel Role for High-Mobility Group A Proteins in Cellular Senescence and Heterochromatin Formation. *Cell* 126, 503–514. doi: 10.1016/j.cell.2006.05.052.

Narita, M., Nũnez, S., Heard, E., Narita, M., Lin, A. W., Hearn, S. A., et al. (2003). Rb-mediated heterochromatin formation and silencing of E2F target genes during cellular senescence. *Cell* 113, 703–716. doi: 10.1016/S0092-8674(03)00401-X.

Newman, L. E., and Shadel, G. S. (2018). Pink1/Parkin link inflammation, mitochondrial stress, and neurodegeneration. *J Cell Biol* 217, 3327–3329. doi: 10.1083/jcb.201808118.

Ng, M. Y. W., Wai, T., and Simonsen, A. (2021). Quality control of the mitochondrion. *Dev Cell* 56, 881–905. doi: 10.1016/j.devcel.2021.02.009.

Niemann, J., Johne, C., Schröder, S., Koch, F., Ibrahim, S. M., Schultz, J., et al. (2017). An mtDNA mutation accelerates liver aging by interfering with the ROS response and mitochondrial life cycle. *Free Radic Biol Med* 102, 174–187. doi: 10.1016/j.freeradbiomed.2016.11.035.

Nunnari, J., and Suomalainen, A. (2012). Mitochondria: In sickness and in health. *Cell* 148, 1145–1159. doi: 10.1016/j.cell.2012.02.035.

Obashi, K., and Okabe, S. (2013). Regulation of mitochondrial dynamics and distribution by synapse position and neuronal activity in the axon. *European Journal of Neuroscience* 38, 2350–2363. doi: 10.1111/ejn.12263.

Ono, T., Kamimura, N., Matsuhashi, T., Nagai, T., Nishiyama, T., Endo, J., et al. (2017a). The histone 3 lysine 9 methyltransferase inhibitor chaetocin improves prognosis in a rat model of high salt diet-induced heart failure. *Sci Rep* 7, 1–11. doi: 10.1038/srep39752.

Owusu-Ansah, E., Song, W., and Perrimon, N. (2013). XMuscle mitohormesis promotes longevity via systemic repression of insulin signaling. *Cell* 155, 699–712. doi: 10.1016/j.cell.2013.09.021.

Papa, L., and Germain, D. (2011). Estrogen receptor mediates a distinct mitochondrial unfolded protein response. *J Cell Sci* 124, 1396–1402. doi: 10.1242/jcs.078220.

Papa, L., and Germain, D. (2014). SirT3 Regulates the Mitochondrial Unfolded Protein Response. *Mol Cell Biol* 34, 699–710. doi: 10.1128/MCB.01337-13.

Pérez, M. J., Ivanyuk, D., Panagiotakopoulou, V., Napoli, G. D. G. D., Brunetti, D., Al-Shaana, R., et al. (2020). Loss of function of the mitochondrial peptidase PITRM1 induces proteotoxic stress and Alzheimer's disease-like pathology in human cerebral organoids. *bioRxiv*, 2020.01.27.919522. doi: 10.1101/2020.01.27.919522.

Pessin, J. E., Epel, E. S., Campisi, J., Rando, T. A., Wyss-Coray, T., Kennedy, B. K., et al. (2014). Geroscience: Linking Aging to Chronic Disease. *Cell* 159, 709–713. doi: 10.1016/j.cell.2014.10.039.

Petrosyan, A., Loertscher, B. M., Dieskau, A. P., Snigdha, S., Cotman, C. W., Overman, L. E., et al. (2016a). H3K9me3 Inhibition Improves Memory, Promotes Spine Formation, and Increases BDNF Levels in the Aged Hippocampus. *Journal of Neuroscience* 36, 3611–3622. doi: 10.1523/jneurosci.2693-15.2016.

Pfeiffenberger, C., Lear, B. C., Keegan, K. P., and Allada, R. (2010). Locomotor activity level monitoring using the Drosophila activity monitoring (DAM) system. *Cold Spring Harb Protoc* 5. doi: 10.1101/pdb.prot5518.

Pharaoh, G., Sataranatarajan, K., Street, K., Hill, S., Gregston, J., Ahn, B., et al. (2019a). Metabolic and stress response changes precede disease onset in the spinal cord of mutant SOD1 ALS mice. *Front Neurosci* 13, 1–19. doi: 10.3389/fnins.2019.00487.

Pimenta de Castro, I., Costa, a C., Lam, D., Tufi, R., Fedele, V., Moisoi, N., et al. (2012). Genetic analysis of mitochondrial protein misfolding in Drosophila melanogaster. *Cell Death Differ* 19, 1308–1316. doi: 10.1038/cdd.2012.5.

Pinto, J. M., Wroblewski, K. E., Kern, D. W., Schumm, L. P., and McClintock, M. K. (2015). The Rate of Age-Related Olfactory Decline Among the General Population of Older U.S. Adults. *Journals of Gerontology - Series A Biological Sciences and Medical Sciences* 70, 1435–1441. doi: 10.1093/gerona/glv072.

Plun-Favreau, H., Klupsch, K., Moisoi, N., Gandhi, S., Kjaer, S., Frith, D., et al. (2007a). The mitochondrial protease HtrA2 is regulated by Parkinson's disease-associated kinase PINK1. *Nat Cell Biol* 9, 1243–1252. doi: 10.1038/ncb1644.

Poewe, W., Seppi, K., Tanner, C. M., Halliday, G. M., Brundin, P., Volkmann, J., et al. (2017). Parkinson disease. *Nat Rev Dis Primers* 3, 1–21. doi: 10.1038/nrdp.2017.13.

Quirós, P. M., Mottis, A., and Auwerx, J. (2016). Mitonuclear communication in homeostasis and stress. *Nat Rev Mol Cell Biol* 17, 213–226. doi: 10.1038/nrm.2016.23.

Qureshi, M. A. M. H., Haynes, C. M., and Pellegrino, M. W. (2017). The mitochondrial unfolded protein response: signaling from the powerhouse. *Journal of Biological Chemistry*, jbc.R117.791061. doi: 10.1074/jbc.R117.791061.

Rawson, N. E., Gomez, G., Cowart, B. J., Kriete, A., Pribitkin, E., and Restrepo, D. (2012). Age-associated loss of selectivity in human olfactory sensory neurons. *Neurobiol Aging* 33, 1913–1919. doi: 10.1016/j.neurobiolaging.2011.09.036.

Regitz, C., Fitzenberger, E., Mahn, F. L., Dußling, L. M., and Wenzel, U. (2016a). Resveratrol reduces amyloid-beta (Aβ1–42)-induced paralysis through targeting proteostasis in an Alzheimer model of Caenorhabditis elegans. *Eur J Nutr* 55, 741–747. doi: 10.1007/s00394-015-0894-1.

Rhodenizer, D., Martin, I., Bhandari, P., Pletcher, S. D., and Grotewiel, M. (2008). Genetic and environmental factors impact age-related impairment of negative geotaxis in Drosophila by altering age-dependent climbing speed. *Exp Gerontol* 43, 739–748. doi: 10.1016/J.EXGER.2008.04.011.

Riar, A. K., Burstein, S. R., Palomo, G. M., Arreguin, A., Manfredi, G., and Germain, D. (2017a). Sex specific activation of the ERα axis of the mitochondrial UPR (UPRmt) in the G93A-SOD1 mouse model of familial ALS. *Hum Mol Genet* 26, 1318–1327. doi: 10.1093/hmg/ddx049.

Richard, M. B., Taylor, S. R., and Greer, C. A. (2010). Age-induced disruption of selective olfactory bulb synaptic circuits. *Proc Natl Acad Sci U S A* 107, 15613–15618. doi: 10.1073/PNAS.1007931107/SUPPL_FILE/PNAS.201007931SI.PDF.

Ristow, M., and Zarse, K. (2010). How increased oxidative stress promotes longevity and metabolic health: The concept of mitochondrial hormesis (mitohormesis). *Exp Gerontol* 45, 410–418. doi: 10.1016/j.exger.2010.03.014.

Rosen, D. R., Siddique, T., Patterson, D., Figlewicz, D. A., Sapp, P., Hentati, A., et al. (1993). Mutations in Cu/Zn superoxide dismutase gene are associated with familial amyotrophic lateral sclerosis. *Nature* 362, 59–62. doi: 10.1038/362059a0.

Rottenberg, H., and Hoek, J. B. (2021). The mitochondrial permeability transition: Nexus of aging, disease and longevity. *Cells* 10, 1–23. doi: 10.3390/cells10010079.

Runkel, E. D., Liu, S., Baumeister, R., and Schulze, E. (2013). Surveillance-Activated Defenses Block the ROS-Induced Mitochondrial Unfolded Protein Response. *PLoS Genet* 9. doi: 10.1371/journal.pgen.1003346.

S. Beck, J., J. Mufson, E., and E. Counts, S. (2016). Evidence for Mitochondrial UPR Gene Activation in Familial and Sporadic Alzheimer's Disease. *Curr Alzheimer Res* 13, 610–614. doi: 10.2174/1567205013666151221145445.

Salvadores, N., Sanhueza, M., Manque, P., and Court, F. A. (2017a). Axonal degeneration during aging and its functional role in neurodegenerative disorders. *Front Neurosci* 11. doi: 10.3389/fnins.2017.00451.

Sastre, J., Millan, A., De La Asuncion, J. G., Pla, R., Juan, G., Pallardo, F. V., et al. (1998). A ginkgo biloba extract (EGb 761) prevents mitochondrial aging by protecting against oxidative stress. *Free Radic Biol Med* 24, 298–304. doi: 10.1016/S0891-5849(97)00228-1.

Schapira, A. H. (2008). Mitochondria in the aetiology and pathogenesis of Parkinson's disease. *Lancet Neurol* 7, 97–109. doi: 10.1016/S1474-4422(07)70327-7.

Schroeder, D. H., and Salthouse, T. A. (2004). Age-related effects on cognition between 20 and 50 years of age. *Pers Individ Dif* 36, 393–404. doi: 10.1016/S0191-8869(03)00104-1.

Schulz, A. M., and Haynes, C. M. (2015). UPRmt-mediated cytoprotection and organismal aging. *Biochimica et Biophysica Acta (BBA) - Bioenergetics* 1847, 1448–1456. doi: 10.1016/j.bbabio.2015.03.008.

Shen, Y., Ding, M., Xie, Z., Liu, X., Yang, H., Jin, S., et al. (2020a). Activation of Mitochondrial Unfolded Protein Response in SHSY5Y Expressing APP Cells and APP/PS1 Mice. *Front Cell Neurosci* 13, 1–12. doi: 10.3389/fncel.2019.00568.

Shumaker, D. K., Dechat, T., Kohlmaier, A., Adam, S. A., Bozovsky, M. R., Erdos, M. R., et al. (2006). Mutant nuclear lamin A leads to progressive alterations of epigenetic control in premature aging. *Proc Natl Acad Sci U S A* 103, 8703–8708. doi: 10.1073/PNAS.0602569103.

Sobue, S., Inoue, C., Hori, F., Qiao, S., Murate, T., and Ichihara, M. (2017a). Molecular hydrogen modulates gene expression via histone modification and induces the mitochondrial unfolded protein response. *Biochem Biophys Res Commun* 493, 318–324. doi: 10.1016/j.bbrc.2017.09.024.

Sonntag, K.-C., Ryu, W.-I., Amirault, K. M., Healy, R. A., Siegel, A. J., McPhie, D. L., et al. (2017). Late-onset Alzheimer's disease is associated with inherent changes in bioenergetics profiles. *Sci Rep* 7, 14038. doi: 10.1038/s41598-017-14420-x.

Stevens, J. C., Cain, W. S., Schiet, F. T., and Oatley, M. W. (1989). Olfactory adaptation and recovery in old age. *Perception* 18, 265–276. doi: 10.1068/p180265.

Strauss, K. M., Martins, L. M., Plun-Favreau, H., Marx, F. P., Kautzmann, S., Berg, D., et al. (2005). Loss of function mutations in the gene encoding Omi/HtrA2 in Parkinson's disease. *Hum Mol Genet* 14, 2099–2111. doi: 10.1093/hmg/ddi215.

Sugeno, N., Jäckel, S., Voigt, A., Wassouf, Z., Schulze-Hentrich, J., and Kahle, P. J. (2016a). α-Synuclein enhances histone H3 lysine-9 dimethylation and H3K9me2-dependent transcriptional responses. *Sci Rep* 6, 1–11. doi: 10.1038/srep36328.

Terman, A., Kurz, T., Navratil, M., Arriaga, E. A., and Brunk, U. T. (2009). Mitochondrial Turnover and Aging of Long-Lived Postmitotic Cells: The Mitochondrial–Lysosomal Axis Theory of Aging. *Antioxid Redox Signal* 12, 503–535. doi: 10.1089/ars.2009.2598.

Teske, B. F., Fusakio, M. E., Zhou, D., Shan, J., McClintick, J. N., Kilberg, M. S., et al. (2013). CHOP induces activating transcription factor 5 (ATF5) to trigger apoptosis in response to perturbations in protein homeostasis. *Mol Biol Cell* 24, 2477–2490. doi: 10.1091/mbc.E13-01-0067.

Tian, Y., Garcia, G., Bian, Q., Steffen, K. K., Joe, L., Wolff, S., et al. (2016a). Mitochondrial Stress Induces Chromatin Reorganization to Promote Longevity and UPRmt. *Cell* 165, 1197–1208. doi: 10.1016/j.cell.2016.04.011.

Tönnies, E., and Trushina, E. (2017). Oxidative Stress, Synaptic Dysfunction, and Alzheimer's Disease. *Journal of Alzheimer's Disease* 57, 1105–1121. doi: 10.3233/JAD-161088.

Tramutola, A., Lanzillotta, C., Perluigi, M., and Butterfield, D. A. (2017). Oxidative stress, protein modification and Alzheimer disease. *Brain Res Bull* 133, 88–96. doi: 10.1016/j.brainresbull.2016.06.005.

Tufi, R., Gandhi, S., de Castro, I. P., Lehmann, S., Angelova, P. R., Dinsdale, D., et al. (2014). Enhancing nucleotide metabolism protects against mitochondrial dysfunction and neurodegeneration in a PINK1 model of Parkinson's disease. *Nat Cell Biol* 16, 157–166. doi: 10.1038/ncb2901.

Vasavada, M. M., Wang, J., Eslinger, P. J., Gill, D. J., Sun, X., Karunanayaka, P., et al. (2015). Olfactory Cortex Degeneration in Alzheimer's Disease and Mild Cognitive Impairment. *Journal of Alzheimer's Disease* 45, 947–958. doi: 10.3233/JAD-141947.

Vijayvergiya, C. (2005). Mutant Superoxide Dismutase 1 Forms Aggregates in the Brain Mitochondrial Matrix of Amyotrophic Lateral Sclerosis Mice. *Journal of Neuroscience* 25, 2463–2470. doi: 10.1523/JNEUROSCI.4385-04.2005.

Wagh, D. A., Rasse, T. M., Asan, E., Hofbauer, A., Schwenkert, I., Dürrbeck, H., et al. (2006). Bruchpilot, a protein with homology to ELKS/CAST, is required for structural integrity and function of synaptic active zones in Drosophila. *Neuron* 49, 833–844. doi: 10.1016/j.neuron.2006.02.008.

Wallace, D. C., Chalkia, D., Schwarz, T. L., Stojanovski, D., and Bohnert, M. (2014). Mitochondrial DNA Genetics and the Heteroplasmy Conundrum in Evolution and Disease. 1–48. doi: 10.1101/cshperspect.a021220.

Wang, J., Sun, X., and Yang, Q. X. (2017a). Early Aging Effect on the Function of the Human Central Olfactory System. *Journals of Gerontology - Series A Biological Sciences and Medical Sciences* 72, 1007–1014. doi: 10.1093/gerona/glw104.

Wang, P., Deng, J., Dong, J., Liu, J., Bigio, E. H., Mesulam, M., et al. (2019). *TDP-43 induces mitochondrial damage and activates the mitochondrial unfolded protein response*. doi: 10.1371/journal.pgen.1007947.

Weidling, I. W., and Swerdlow, R. H. Mitochondria in Alzheimer's disease and their potential role in Alzheimer's proteostasis. *Exp. Neurol* 330, 113321. doi: 10.1016/j.expneurol.2020.113321.

Wood, J. G., Hillenmeyer, S., Lawrence, C., Chang, C., Hosier, S., Lightfoot, W., et al. (2010a). Chromatin remodeling in the aging genome of Drosophila. *Aging Cell* 9, 971–978. doi: 10.1111/j.1474-9726.2010.00624.x.

Wu, J. S., and Luo, L. (2006). A protocol for dissecting Drosophila melanogaster brains for live imaging or immunostaining. *Nat Protoc* 1, 2110–2115. doi: 10.1038/nprot.2006.336.

Xu, L., Liu, J., Wroblewski, K. E., Mcclintock, M. K., and Pinto, J. M. (2020). Odor Sensitivity Versus Odor Identification in Older US Adults: Associations With Cognition, Age, Gender, and Race. *Chem Senses* 45, 321–330. doi: 10.1093/chemse/bjaa018.

Yoneda, T., Benedetti, C., Urano, F., Clark, S. G., Harding, H. P., and Ron, D. (2004). Compartment-specific perturbation of protein handling activates genes encoding mitochondrial chaperones. doi: 10.1242/jcs.01275.

Yuan, J., Chang, S. Y., Yin, S. G., Liu, Z. Y., Cheng, X., Liu, X. J., et al. (2020a). Two conserved epigenetic regulators prevent healthy ageing. *Nature* 579, 118–122. doi: 10.1038/s41586-020-2037-y.

Zhang, B., Gaiteri, C., Bodea, L. G., Wang, Z., McElwee, J., Podtelezhnikov, A. A., et al. (2013). Integrated systems approach identifies genetic nodes and networks in late-onset Alzheimer's disease. *Cell* 153, 707–720. doi: 10.1016/j.cell.2013.03.030.

Zhao, Q., Wang, J., Levichkin, I. V., Stasinopoulos, S., Ryan, M. T., and Hoogenraad, N. J. (2002a). A mitochondrial specific stress response in mammalian cells. *EMBO Journal* 21, 4411–4419. doi: 10.1093/emboj/cdf445.

Zhou, Z., Fan, Y., Zong, R., and Tan, K. (2022). The mitochondrial unfolded protein response : A multitasking giant in the fight against human diseases ☆. *Ageing Res Rev* 81, 101702. doi: 10.1016/j.arr.2022.101702.

Zhu, J. Y., Vereshchagina, N., Sreekumar, V., Burbulla, L. F., Costa, A. C., Daub, K. J., et al. (2013). Knockdown of Hsc70-5/mortalin induces loss of synaptic mitochondria in a Drosophila Parkinson's disease model. *PLoS One* 8. doi: 10.1371/journal.pone.0083714.

Zou, Y. M., Lu, D., Liu, L. P., Zhang, H. H., and Zhou, Y. Y. (2016). Olfactory dysfunction in Alzheimer's disease. *Neuropsychiatr Dis Treat* 12, 869–875. doi: 10.2147/NDT.S104886.

15. Products generated.

Muñoz-Carvajal, F., and Sanhueza, M (2020). The Mitochondrial Unfolded Protein Response: A Hinge Between Healthy and Pathological Aging. *Front. Aging Neurosci.* 12. doi:10.3389/fnagi.2020.581849.